GEMS & GEMOLOGY

FALL 2013
VOLUME XLIX

THE QUARTERLY JOURNAL OF THE GEMOLOGICAL INSTITUTE OF AMERICA

The Cheapside Hoard: An Extraordinary Collection of Jewels

Digit Patterns in Opal

Agate from Morocco

Field Report on Oregon Sunstone

GEMS & GEMOLOGY

Fall 2013
VOLUME 49, No. 3

pg. 129

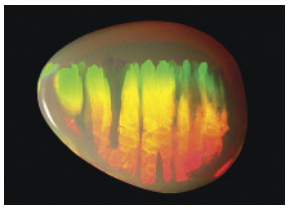

pg. 143

pg. 162

GEMS & GEMOLOGY

gia.edu/gems-gemology

Subscriptions
Copies of the current issue may be purchased for $29.95 plus shipping. Subscriptions are $79.99 for one year (4 issues) in the U.S. and $99.99 elsewhere. Canadian subscribers should add GST. Discounts are available for group subscriptions, GIA alumni, and current GIA students. For institutional rates, contact Customer Service.

To purchase print subscriptions, visit store.gia.edu or contact Customer Service.

Database Coverage
Gems & Gemology is abstracted in Thomson Reuters products (Current Contents: Physical, Chemical & Earth Sciences and Science Citation Index—Expanded, including the Web of Knowledge) and other databases. For a complete list of sources abstracting *G&G*, go to gia.edu/gems-gemology.

Manuscript Submissions
Gems & Gemology welcomes the submission of articles on all aspects of the field. Please see the Guidelines for Authors at gia.edu/gandg or contact the Managing Editor. Letters on articles published in *Gems & Gemology* are also welcome.

Gems & Gemology is published quarterly by the Gemological Institute of America, a nonprofit educational organization for the gem and jewelry industry.

Postmaster: Return undeliverable copies of *Gems & Gemology* to GIA, The Robert Mouawad Campus, 5345 Armada Drive, Carlsbad, CA 92008.

Our Canadian goods and service registration number is 126142892RT.

About the Cover

Measuring an estimated 42 mm deep × 20 mm wide, this Colombian emerald pocket watch is one of the most notable items from the Cheapside Hoard collection, on full display for the first time since its discovery more than 100 years ago. Dating back to the 16th century, the treasure's nearly 500 antique pieces comprise gems from around the world, each telling a unique story of the time (see article on page 126). Courtesy of the Museum of London; photo by Robert Weldon.

Printing is by L+L Printers, Carlsbad, CA.
GIA World Headquarters The Robert Mouawad Campus 5345 Armada Drive Carlsbad, CA 92008 USA

ISSN 0016-626X

STRIVING FOR TIMELINESS AND SYNERGY

We hope you enjoy the Fall 2013 *Gems & Gemology*. For this issue, we present two fascinating papers from European authors, one on Moroccan agate and one on columnar growth patterns in natural opal from Ethiopia. This second paper outlines a persuasive model of formation for the distinctive "digit" patterns characteristic of some gems from this source.

We also feature articles from GIA authors on diverse topics ranging from a practical indication of heat treatment to Oregon sunstone to our lead article on the Museum of London's fabulous Cheapside Hoard.

In August, GIA's Robert Weldon received an invitation to view this astonishing collection, lost for almost 300 years until a chance discovery in 1912 during a demolition near London's famous St. Paul's Cathedral.

As it was such a rare opportunity—this cache of jewels represents both a tantalizing window into trade patterns of the 1600s *and* a great story in itself—we accepted the invitation and traveled to the UK to document it. This trip also gave the impetus to produce an article in time for the Fall 2013 *G&G*, which will coincide with the very first major exhibition of the jewels. In other words, we had an opportunity to be timely and produce what we hope will be the definitive paper on this extraordinary collection. In London, GIA was able to record video interviews with the museum's staff and a tour of the hoard, which we will make available on our website.

The field report, which chronicles a GIA expedition to a gem-producing or processing area and may even stand as a statement of intent for future lines of research and publication...

In this issue, we're also introducing a new article category to *G&G*: the field report, which chronicles a GIA expedition to a gem-producing or processing area and may even stand as a statement of intent for future lines of research and publication. Field reports will also serve as anchors on the GIA website for video and images acquired on these trips. Our first field report documents three sunstone feldspar occurrences in Oregon. Readers will find slideshows plus videos of mining processes and interviews with miners at www.gia.edu/gems-gemology. This rich media allows us to offer a far more comprehensive and engaging picture of a topic than we've been able to in the past.

This synergy with the GIA website gives us the ability to quickly post articles and news stories online rather than waiting three months for the next print issue. And we can provide supporting resources for our regular print articles that enrich the user experience. We trust we've been able to deliver this with the Fall issue and invite you to explore the associated online media for the Cheapside Hoard and Oregon sunstone articles.

Let me also take this opportunity to thank all the authors who have submitted manuscripts to *G&G* for review. We truly value your contributions.

Duncan Pay | Editor-in-Chief | dpay@gia.edu

The Museum of London's Extraordinary Cheapside Hoard

Robert Weldon and Cathleen Jonathan

An astonishing collection of jewels, discovered by chance in 1912 after centuries of concealment, is on display at the Museum of London. Nearly 500 pieces, including jewelry, loose gems, and functional items, offer a unique glimpse into the global trade and use of gems in the 1600s.

Just over a century ago, in the summer of 1912, a workman's pickaxe struck through the floor of an old tenement house in Cheapside, a commercial district near the renowned St. Paul's Cathedral in London. A trio of adjoining houses there was scheduled for demolition. In a brick-lined cellar under a chalk floor, the workman cleared the debris and saw what appeared to be a decayed wooden box or casket containing a hidden treasure of several hundred gleaming jewels (Museum of London, 1928). Shock and curiosity, perhaps mingled with apprehension and greed, must have overcome the man, though his own story is not recorded. In this dank, long-forgotten cellar, the gems spilled onto the muddy floor and experienced their first light of day after nearly 300 years of concealment.

Fellow workmen are said to have immediately lined their pockets with the precious loot (figure 1; Forsyth, 2013), and much of the treasure buried in the cellar would have been lost to history were it not for a quirk of fate. An antiquities trader and pawnbroker named George Fabian Lawrence (1861–1939; figure 2) had established a shrewd arrangement with demolition workers. "Stony Jack," as he was known, would pay them in cash or pints of beer for interesting finds made in the course of their work.

"I taught them that every scrap of metal, pottery, glass, or leather that has been lying under London may have a story to tell the archaeologist, and is worth saving," Lawrence told the *Daily Herald* in 1937, toward the end of his life (Forsyth, 2003).

Lawrence's success in antiquities, and his connections with the crews, paid off in 1912 when he became the inspector of excavations for the newly established London Museum. In the acquisition of archaeological finds, his accomplishments were

Figure 1. This iconic jewel is a scent bottle, or pomander, from the Cheapside Hoard. The bejeweled handle implies that it was hung from a chain. This gold bottle with white enamel is set with milky chalcedony carvings of leaves, rubies, pink sapphires, spinels, and diamonds. The bottle would have contained musk oils combined with essential oils, ambergris, and other substances to prolong the perfume. Courtesy of the Museum of London; photo by Robert Weldon/GIA.

See end of article for About the Authors and Acknowledgments.
Gems & Gemology, Vol. 49, No. 3, pp. 126–137,
http://dx.doi.org/10.5741/GEMS.49.3.126.

Figure 2. G.F. "Stony Jack" Lawrence was appointed inspector of excavations at the London Museum in 1912, the year the treasure was found. Courtesy of the Museum of London.

remarkable—during his career he reportedly obtained 15,000 artifacts (Gosling, 1995), some of which were traded with museums around the world. In his first six months of employment with the museum, he sourced a total of 1,600 pieces (Macdonald, 1996).

The discovery on June 18, 1912, at the intersection of Cheapside and Friday streets (figure 3) was to become Lawrence's most significant procurement. Over the ensuing weeks, parcels and handkerchiefs of jewelry from the hoard showed up at his office, and an astonishing collection began to accumulate. This treasure of mostly Elizabethan and Jacobean jewelry eventually constituted almost 500 pieces. Over the past century, items purportedly from the hoard have continued to trickle in. Mr. Lawrence's own son presented two fancy-cut amethysts to museum officials in 1927. The stones were not documented, but it is quite possible they are the two amethysts pictured in figure 4.

After the discovery, pieces from the collection were held by three museums. The British Museum received 20 items in 1914, but the bulk of the treasure was split between the London Museum (now the Museum of London) and the Guildhall Museum in 1916 (H. Forsyth, pers. comm., 2013). Collectively the items became known as the Cheapside Hoard.

"The Guildhall Museum and the Museum of London came together in 1976, so we were really formed from two museums," said Sharon Ament, director of the Museum of London. "Each of these museums had part of the Cheapside Hoard, and when they came together the hoard also came together."

Most of the collection now resides permanently at the Museum of London. Its pieces continue to draw acclaim for their diversity, their enormous chronological range, and their relatively pristine condition. "This collection is unique in the world," explained Hazel Forsyth, the museum's senior curator of medieval and post-medieval collections. "It is the largest hoard of its kind, dating from the very late 16th to the early 17th century. Part of the reason why it's so important is that jewelry tends to be broken up, refashioned, reworked, and so therefore doesn't

Figure 3. These two images of London's Cheapside district show the area where the Cheapside Hoard was found. The first, taken around the time of its discovery, highlights the tenement house under which the hoard was buried. This house stood just a few steps from the St. Mary Le Bow Church, near St. Paul's Cathedral. The second, from approximately the same angle in 2013, shows a busy shopping area. The photo on the left is courtesy of the Museum of London. The photo on the right is by Robert Weldon/GIA.

Figure 4. These two amethysts, shown face-up and from the side, feature surprisingly contemporary fancy cutting styles. Rather than a large table facet, the stones have a domed, faceted configuration. In the 1600s, amethysts were sourced from Russia or Brazil. Courtesy of the Museum of London; photo by Robert Weldon/GIA.

Figure 6. This rose-cut sapphire and diamond cross pendant would have been worn with enameled chains during the Elizabethan era. The back of the pendant (right) showcases highly skilled enameling and delicate metalsmithing. Courtesy of the Museum of London; photos by Robert Weldon/GIA.

survive. Because this was buried and lay undisturbed for the better part of 300 years, it survived in the condition that it has. And it covers a huge spectrum of jewelry designs and types, but also gem material from many parts of the world, which really underlines London's role in the international gem and jewelry trade in this period."

For experts such as Forsyth, numerous unanswered questions surround this extraordinary find (figure 5). Who was the owner? Why did he hide the treasure, and when? Why was it never claimed? In seeking answers to those questions, close examination of the pieces elicits a form of intimacy with the onetime owner's tastes and predilections, almost as if an image of the person could be conjured up through time. These found jewels also provide a snapshot of time and place, aligning themselves with historical events and filling gaps in our knowledge about how gems were cut and jewelry was fabricated and enjoyed in eras past (figure 6).

Figure 5. This chain demonstrates incredible enameling skill from the Elizabethan and Jacobean eras. Although precious few chains of this delicate nature have survived the centuries, 30 of them were well preserved within the Cheapside Hoard. Comprising mostly floral motifs, they include gem materials such as turquoise, beryl, amethyst, corundum, and spinel. Courtesy of the Museum of London.

A picture of those eras emerges more clearly upon visiting London's Victoria & Albert Museum and National Portrait Gallery. Both museums house magnificent portraits from the 16th through 18th centuries, often depicting European aristocracy wearing jewelry. In many cases they mirror the jewels found in the hoard and offer a tantalizing glimpse into how the jewels were actually used (figure 7).

In the summer of 2013, GIA was given the rare privilege of photographing several important items from the Cheapside Hoard at the Museum of London. This took place as the museum prepared for its first major exhibition of the collection, opening in October. The hoard was initially displayed in a small glass case in 1914, coinciding with the museum's inauguration. In 1928, a richly illustrated catalogue describing some of the items was published. Over the years, some pieces have been shown in smaller ex-

Figure 7. The miniature portrait on the left of Queen Anne of Denmark (1574–1619) is not from the Cheapside Hoard, but it shows a jewel in her hair that is remarkably similar to the blue sapphire and spinel pendant on the right. These gems from the hoard indicate trade with far-off Asia, including modern day Sri Lanka, India, and Myanmar. Only one of the pearls from the original design survived. The portrait photo on the left is © Victoria & Albert Museum. The pendant on the right is courtesy of the Museum of London; photo by Robert Weldon/GIA.

hibits. Now, nearly a century after the museum's original exhibit, this new high-tech, interactive multimedia event features all of the known pieces from the hoard. This includes its wealth of rare enameled long chains, which were being painstakingly prepared for display at the time of our visit.

CONCEALMENT OF THE CHEAPSIDE HOARD

Scholars have concluded that the hoard was likely stashed for safekeeping by someone who expected to recover it at a later date. Forsyth said that newspaper accounts from 1914 describe a wooden box or casket. She and a colleague found possible evidence of soil contamination in some pieces, suggesting that the container disintegrated and its contents were gradually enveloped by the surrounding soil. "The other thing that is clear is how many pearls are missing," Forsyth said. "I have worked out from the empty settings that there were probably 4,000 originally, or perhaps more in loose form, that rotted away in the soil."

The location of the hoard is also telling. In the late 1500s, Cheapside and Friday streets in London's West End were at the heart of a bustling jewelry manufacturing district, mostly concentrated along Goldsmith's Row. By 1625, other businesses had entered the area, diminishing its luster. The properties where the hoard was located, tenement houses 30–32, were owned by the Goldsmiths' Company. Because of subleasing and sub-subleasing to foreign workers, though, it is difficult to reconstruct the buildings' inhabitants or determine who may have buried the hoard (Forsyth, 2002; Mitchell, 2013).

THEORIES ABOUT THE HOARD

Nonetheless, the condition and contents of the hoard offer potential insights. Forsyth describes it as a mixture of finished jewels of the latest fashion and design (figure 8), alongside other pieces that may have already been in circulation for centuries. Some of the stones had been removed from their settings, possibly for a jeweler to repair or repurpose. Forsyth believes the collection was most likely owned by a jeweler or syndicate of jewelers, but the extent and diversity of its

Figure 8. These front and back images show a delicately carved cameo inspired by the Aesop fable "The Dog and His Reflection." This rare gem shows the degree of skill in carving banded agate, where the darker sublayer adds depth and dimension to the portrait. Courtesy of the Museum of London; photo by Robert Weldon/GIA.

contents also suggest the possibility that a wealthy collector or even a fence for stolen property could have owned it.

The hiding of the treasure occurred at a time before commercial banks were available to preserve valuables, so it may have been secreted away for safekeeping. "It could be that the jeweler did this regularly—that he had a hole in the floor where he kept his stock in trade," Forsyth said. "It could also be that he was facing a calamity or emergency that required him to take desperate action. Possibly he planned to go abroad for a period of time. We know that almost 60% of the jeweler goldsmiths in London were immigrant craftsmen, and that they traveled." Whatever the case, the owner of the hoard never reclaimed it.

Certainly it was a calamitous time in England. The outbreak of civil war in 1642 ultimately resulted in an overthrow of the monarchy and the execution of King Charles I in 1649. Unrest and political upheaval may have caused the hoard's owner to hide his prized possessions, as many jewelers took up arms to fight. More uncertainty followed, including the restoration of the monarchy in 1660 and the return from exile of Charles II, son of the former king. Over the centuries, the bubonic plague had swept through Europe and Britain in waves, culminating in 1665–1666 with the Great Plague of London, which killed about 15% of the population. Those who had the means fled the city to avoid the deadly epidemic.

In 1666, a fire that started in a bakery spread quickly through the city. In less than three days it consumed more than 13,000 buildings, including St. Paul's Cathedral, about a block away from the hoard. The Great Fire of London, as it came to be known, destroyed most of the city's wooden structures, including those above the site of the treasure. Evidence of fire damage found during the Cheapside excavations led experts to conclude that the jewels were buried no later than 1666. It is unlikely that the owner of the hoard perished in the fire, as very few casualties were actually recorded.

Following the Great Fire of London and the rebuilding of the city, new structures were erected in the Cheapside district around 1670. This time, brick and mortar structures rose above the forgotten cellars, sealing the Cheapside Hoard for two and a half centuries.

Despite the enormous historical expanse of the collection, several clues have allowed experts to pinpoint the stashing of the hoard within a few years' range. According to Forsyth, comparing the pieces with contemporaneous portraits helps date the collection. For example, the style of dress in a cameo of Elizabeth I (figure 9, right) suggests it was most likely carved after 1575, toward the end of her reign (Forsyth, 2003; H. Forsyth, pers. comm., 2013). In fact, the cameo closely resembles the Armada Jewel (figure 9, left), a gold locket featuring an image of Elizabeth I fashioned by Nicholas Hilliard. The jewel was bestowed on Sir Thomas Heneage in 1588 to commemorate Britain's resounding defeat of the Spanish Armada that year.

Forsyth and her museum colleagues believe that an intaglio from the collection, only recently identified, establishes a possible time frame for the hoard's burial. In 1640, William Howard received the title of Viscount Stafford upon his marriage to Mary Stafford. A chipped, unassuming carnelian intaglio from the Cheapside Hoard (figure 10) exhibits his newly appointed heraldic badge, narrowing the concealment date between 1640 and the time of the Great Fire of

Figure 9. Queen Elizabeth I (1533–1603) is portrayed in the Armada Jewel (left) and the agate cameo (right). The gold locket was created in 1588 to commemorate the defeat of the Spanish Armada. Such representations of historical events help date some of the hoard's items. Photos courtesy of the Victoria & Albert Museum (left) and the Museum of London (right).

Figure 10. This small, chipped carnelian intaglio shows the unique heraldic badge of Viscount Stafford. Because the viscount received his title in 1640, experts are able to narrow down the concealment date of the Cheapside Hoard. Courtesy of the Museum of London; photo by Robert Weldon/GIA.

Figure 11. One of the imitation gems from the Cheapside Hoard is a quench-crackled and dyed quartz made to resemble spinel. A genuine spinel of this size would have sold for hundreds, if not thousands, of pounds in the 1600s. Courtesy of the Museum of London; photo by Robert Weldon/GIA.

London in 1666. Once again, the diversity of the collection and the presence of this flawed, inconspicuous jewel suggest that this was the working stock of a professional gem merchant or jeweler who received gems in trade, took in items for repair, or traveled extensively.

CURIOSITIES IN THE CHEAPSIDE HOARD

Furthering the theory that a working jeweler owned the hoard is the presence of an imitation gem that raises some thought-provoking possibilities. In 1610, the Goldsmiths' Company investigated one of its own members, a goldsmith-jeweler who was making fake "balas rubies" (an old misnomer for spinel). Pendant spinel drops were extremely popular and extraordinarily expensive (H. Forsyth, pers. comm., 2013). The counterfeiter used an old recipe for quench-crackling inexpensive rock crystal quartz and infusing the surface-reaching fissures with a red dye—possibly cochineal, an insect-based dye—to produce a very realistic imitation of spinel (Nassau, 1994). Three and a half centuries later, the dye has faded to a pale pinkish orange (figure 11).

"We know rather a lot about who made this particular piece," said Forsyth. "This was made by, or at the instigation of, Thomas Simpson, a goldsmith jeweler who was quite prominent in Cheapside. He would make models in clay or lead, take them to his acquaintances, and say, 'Here are your models. Please cut the rock crystal in this fashion of a balas ruby.' Other jewelers and setters then [drilled] the rock crystal through, and made clasps for the top and bottom. These were then fashioned in pendant style, with claws of white and black enamel."

Forsyth noted that many such fakes were sold. Some even made it back to India and Africa, eventually bringing enormous discredit to the British East India Company, which was sourcing gems and jewels for the crown. That the quench-crackled quartz pendant ended up in the Cheapside Hoard casts another oblique, uncertain light on who might have owned the collection.

One of the jewels was carved long before the 1600s. It is a banded agate cameo of a Ptolemaic queen, likely Cleopatra, the last pharaoh of ancient Egypt (figure 12). She is depicted in the guise of the goddess Isis, wearing a vulture headdress. It is unquestionably Egyptian in origin (H. Forsyth, pers. comm., 2013). Both the Roman conquest of Britain,

Figure 12. This agate cameo is likely a representation of Cleopatra (69–30 BC), the last pharaoh of ancient Egypt. Curators believe it is the oldest item in the Cheapside Hoard. Courtesy of the Museum of London; photo by Robert Weldon/GIA.

and Cleopatra's relationship with Julius Caesar, raise tantalizing possibilities as to how it surfaced in 17th century Britain, as well as its possible origin. Egyptian and Greek carved gems were highly collectible in Renaissance Europe, and were sometimes reused in jewelry during this time.

TRADING PARTNERSHIPS AND GLOBALIZATION

The profusion of loose and mounted gems in the collection includes, among others: diamonds from India or Borneo; emeralds from Colombia; natural pearls from the Persian (Arabian) Gulf, Scotland, or possibly the Caribbean or Comoros; sapphires, rubies, spinel, and other gems from Sri Lanka and Burma; garnets from European sources or India; peridot from Egypt (figure 13); turquoise from Persia; and opal from an unknown source (figure 14). This global snapshot indicates that London's gem merchants and jewelers enjoyed a wide array of commercial choices. It also underscores the rising significance of the Cheapside district as a trading center. England's global outlook at the time clearly stemmed from the colonial impulses of Queen Elizabeth I. She sent explorers—Sir Francis Drake and Sir Walter Raleigh, among others—on expeditions around the world, with an eye toward establishing colonies and new sources of raw materials. For England, it was a global competition for power with other European countries, particularly Spain (Sinkankas, 1981). We photographed some very interesting and important examples of these gems during our visit to the Museum of London.

Figure 13. This small wedge-shaped peridot cabochon is from the Egyptian island of Zabargad, also known as St. John's Island. Courtesy of the Museum of London; photo by Robert Weldon/GIA.

Figure 14. Because opal is prone to damage by heat, the condition of this gold and enameled opal hat pin demonstrates that the treasure was well protected. The opal clearly withstood the Great Fire of London in 1666, which obliterated the wooden structure above the cellar. Courtesy of the Museum of London; photo by Robert Weldon/GIA.

Corundum. Corundum was first recognized in Europe by the Greek Theophrastus and later by Pliny the Elder, as evidenced in their writings. Two important blue sapphires from the Cheapside Hoard were made available to photograph. Both are well cut, with a square outline, and paired with spinel in a pendant (see figure 7, right). The sapphires are likely Sri Lankan or Burmese in origin and contain visible rutile silk inclusions.

Following the initial classification efforts of Belgian mineralogist Anselmus Boetius de Boodt (1609), Europeans began to understand gem materials much more clearly, including the relationship between sapphires and rubies, and how to differentiate them from gems of similar color. Red gems, for example, had once been known collectively as "carbuncles" (Hughes, 1997). Thomas Nichols, an English naturalist at the time the Cheapside Hoard was hidden, furthered the leap forward in gemological knowledge. In 1652, he clearly described gem treatments as well as the sources for ruby and sapphire and other gem materials: "The best of these [rubies] are found in the island of Zeilan [Ceylon, modern-day Sri Lanka]. . . . there are excellent ones found in the [Burmese] river Pegu, the inhabitants there try them with their mouth and tongues: the colder and harder they are,

the better they are," he wrote, adding that the same deposits often carried sapphires. Nichols (1652) also reported other producers of sapphires, including India, and even some European sources such as Silesia (a region on the Oder River, mostly in modern-day Poland). Most of the rubies we viewed from this collection were smaller stones, many of them adorning an enameled perfume bottle (see figure 1). One large, mostly opaque ruby from the hoard was in cabochon form.

Diamonds. After expeditions led by Alexander the Great (356–323 BC) opened trade with the East, diamonds began to appear in Europe. The Indian mines at Golconda were the only known source at that time, and many centuries would pass before diamonds attained the status of ruby and sapphire. Around 1500, the discovery of a sea route around Africa's Cape of Good Hope increased the supply of high-quality rough from India to satisfy Europe's growing demand for diamonds (Lenzen, 1970).

Polished diamonds initially appeared in Europe in the 1380s. The earliest cut, the point cut, remained popular into the 15th century. It closely followed the rough diamond's octahedral shape. The late 1400s saw the recutting of point cuts into a new style, the table cut. This was produced by removing the top point to create a square polished facet. Often the lower point was also removed to create a smaller square facet. Thus the table cut resembled a square within a square, which appealed to European interest in classical proportions during the Renaissance. Because table-cut diamonds were more brilliant than point-cut gems, they remained popular throughout the 1500s and 1600s (Tillander, 1995).

The gold ring with white enamel in figure 15 dates from the late 16th or early 17th century. It is set with a table-cut diamond that measures 8.4 mm × 8.0 mm and weighs an estimated 3 to 4 ct. With its table-cut crown and modified "scissor-cut" pavilion, it is an extraordinary survivor, as most were recut by about 1700. India is the likely source of this diamond (Jobbins, 1991; Gosling, 1995).

Emeralds. The hoard's largest and arguably most striking item is a pocket watch set in a massive polished hexagonal emerald crystal from Colombia (figure 16). It measures an estimated 42 mm deep × 20 mm wide (Jobbins, 1991). Aside from its inherent beauty and craftsmanship, the piece serves as a fitting metaphor that says much about the time and place of the Cheapside Hoard. Emeralds from Colombia began to enter the European trade in the mid-1500s. Although Hernando Cortez had received emeralds as a gift from Montezuma in the early 1500s, an actual South American source for the gem remained elusive. But in 1537 Spanish conquistador Jimenez de Quezada seized areas of Colombia that included the emerald-rich Somondoco Valley (Sinkankas, 1981). Emeralds and gold from Nueva Granada, as Colombia was then called, were soon being exported to Spain. The Spaniards regarded emeralds as a commodity and readily traded them. By the late 1500s, these gems from the New World were making their way across Europe. The beauty, size, and intense color of the Colombian material overshadowed the meager supply from the so-called Cleopatra Mines in southern Egypt.

Invented in the late 1400s, pocket watches had improved significantly by the mid-1500s. The combina-

Figure 15. Three views of an enameled gold ring set with a table-cut diamond, an evolutionary cut developed in the mid-1400s. The diamond is estimated to weigh between 3 and 4 ct, and it likely originated from the Golconda mines. Courtesy of the Museum of London; photos by Robert Weldon/GIA.

Figure 16. One of the most important items from the Cheapside Hoard is this large Colombian emerald pocket watch, circa 1600. Watches first appeared in England around 1540, and Colombian emeralds reached Europe by the late 1500s. Taking advantage of the crystal's hexagonal shape, the maker removed a slice for the cover, cut out a central section for the movement, and used that gem material to embellish the metalwork. Green enamel decorates various parts of the watch. The artistry and meticulous engineering indicate this timepiece was intended for nobility. Courtesy of the Museum of London; photos by Robert Weldon/GIA.

tion of new technology and this spectacular emerald must have proven irresistible for the watchmaker. The champlevé style of enameling, where recessed areas are carved into the metal and filled with enamel, at the center of the dial adds to the splendor of the timepiece. Forsyth believes this watch dates to the 1600s, and that the skill and craftsmanship required to manufacture this elaborate jewel suggest it was made for nobility.

A salamander hat pin, also containing Colombian cabochon emeralds, is one of the hoard's most iconic

Figure 17. This enameled gold hat ornament in the form of a salamander is one of the Cheapside Hoard's most iconic pieces. The enameling on the front shows an open mouth with tiny black flecks resembling teeth. The pin is decorated with cabochon emeralds from Colombia, and the tail contains table-cut diamonds. The underside of the pin shows the quality of enamelwork during the late 1500s and early 1600s. Notice the complex curved pins that allow the wearer to twist the salamander into place on the hat. Courtesy of the Museum of London; photos by Robert Weldon/GIA.

Figure 18. Some "mystery jewels" were also found in the Cheapside Hoard. This gold piece with white enamel and Colombian emeralds is thought to be a fan holder. Large feathers for a fan could be attached on the flared side, and the holder could be attached to a chain on the other end. Courtesy of the Museum of London; photo by Robert Weldon/GIA.

and recognizable jewels (figure 17). It compares in style to another item in the collection, an apparent fan holder in gold and white enamel with Colombian emeralds (Scarisbrick, 1995; figure 18). Together the pieces underscore the European demand for Colombian emeralds in the late 1500s and early 1600s.

Pearls. The primary source for pearls in the 1600s was the Persian (Arabian) Gulf, where they had been traded for thousands of years (Dirlam and Weldon, 2013). These popular organic gems were also being sourced from the Gulf of Manaar, between Sri Lanka and India (Tavernier, 1676). In his description of the hoard, gem expert Alan Jobbins (1991) attributed the decomposition of the organic conchiolin to exposure to the elements. He also described the beauty revealed in the breakdown of some of the concentric layers of nacre, which is clearly evident in a pendant featuring a large pearl paired with a pale blue sapphire (H. Forsyth, pers. comm., 2013). The carving dates to the Byzantine period and depicts the incredulity of Saint Thomas, with exquisite green and white enamel detail on the reverse (figure 19). As noted, many jewels that would have contained pearls were empty due to their presumed decomposition.

Figure 19. This pendant jewel contains a pale blue sapphire cameo from the Byzantine era. The enameled gold back features a floral motif. The pendant is hung from a large pearl, likely from the Persian (Arabian) Gulf, one of the few surviving pearl specimens in the hoard. Courtesy of the Museum of London; photos by Robert Weldon/GIA.

Spinel ("Balas Ruby"). One of the most misunderstood yet coveted gems during the Renaissance was spinel. For its subtle differences with ruby, red spinel was known as "balas ruby." The name was derived from a source in the Pamir Mountains of modern-day Tajikistan, where they were known as *Laal-Bedashan*. Marco Polo, who traveled through the area in the 13th century, used the term in his notes (Hughes, 1997).

Spinels were long thought of as rubies, perhaps because they were often intermingled with actual corundum in the alluvial gem gravels. Interestingly, spinels were much in demand—as evidenced by the counterfeit "balas ruby" contained in the hoard and the high prices fetched by these goods. One historical example of a mistaken spinel is the Black Prince's Ruby, the most important colored gemstone in the British Imperial State Crown. This spinel was believed to be a ruby for many centuries.

Toadstone. Though virtually unknown today, this unusual gem enjoyed considerable prestige at the time the hoard was assembled. Toadstone was con-

Figure 20. Loose gemstones found in the Cheapside Hoard include banded agate, sard, and carnelian, garnet (left), ruby (right), and unusual gem materials such as toadstone (top) and fibrolite (bottom). Courtesy of the Museum of London; photo by Robert Weldon/GIA.

sidered an antidote for poisons and also thought to warn of their presence by becoming hot (Kunz, 1915). Shakespeare (1564–1616), writing during this time, mentioned toadstone in *As You Like It*:

> Sweet are the uses of adversity,
> Which like the toad, ugly and venomous,
> Wears yet a precious jewel in his head.

Three centuries later, American mineralogist George Frederick Kunz (1915) wrote:

> While it is quite possible that some of the so-called toadstones may really have been concretions found in the head of the toad, by far the greater part were probably small pebbles sold as "toad-stones" to those who believed in the magic virtues of such a stone and were willing to pay a good price for one.

Many toadstones are actually fossilized teeth, approximately 150 million years old, from a species of fish called *Lipodotus maximus* (Forsyth, 2003). Fourteen toadstones were among the loose gems found in the hoard (figure 20). They would have been set in rings and worn as amulets for protection or to bring good fortune and prosperity (Kunz, 1913; Kunz, 1915).

CONCLUSION

Because of its centuries of concealment and the context in which it was found, the Cheapside Hoard is a supremely important collection of jewels. This unique assemblage encompassing a wide variety of gems from around the world shows fine examples of 16th and 17th century jewelry, including rings, chains, necklaces, pendants, buttons, brooches, hat or cloak pins, and watches. Functional items are also represented: tankards, vessels, utensils, a scent bottle, and even a few mystery objects. From this treasure we can glean valuable insight into the global trade and use of gems in the 1600s (figure 21).

"London has always been a trading port," said Sharon Ament. "Even from the early Roman days it has been a place of many different cultures. The Cheapside Hoard and the history of London really come together in this museum."

Undisturbed in a cellar in the Cheapside district of London, the gems and jewelry worn nearly 400 years ago emerged relatively unscathed. Now they are once again in the spotlight, and the world will have the opportunity to see this remarkable collection at the Museum of London from October 11, 2013, through April 27, 2014.

Figure 21. Another notable artifact is this chalcedony cameo. The Medici family of Florence commissioned similar cameos, and this likeness suggests the profile of Mary de Medici. Courtesy of the Museum of London; photo by Robert Weldon/GIA.

REFERENCES

Boodt A. de (1609) *Gemmarum et Lapidum Historia: Qua Non Solum Ortus, Natura, Vis & Precium, Sed Etiam Moduasquo Exiis, Olea, Salia, Tincturæ, Effentiæ, Arcana & Magisteria Arte Chymica Confici Possint, Stenditur. Opus Principibus, Medicis, Chymicis, Physicis, Aeliberaliorbus Ingeniis Vtilissimum*. Typis Wechelianis apud Claudium Marnium & Heredes Joannis Aubrii, Hanover, Germany.

Dirlam D.M., Weldon R., Eds. (2013) *Splendor & Science of Pearls*. GIA (Gemological Institute of America), Carlsbad, CA.

Emerald: The Most Valuable Beryl, the Most Precious Gemstone (2002) *extraLapis English No. 2*. Lapis International, East Hampton, CT.

Evans J. (1922) *Magical Jewels of the Middle Ages and the Renaissance, Particularly in England*. Clarendon Press, Oxford.

Forsyth H. (2002) The Cheapside Hoard. *Goldsmiths' Review 2001/2002*. The Worshipful Company of Goldsmiths, London.

——— (2003) *The Cheapside Hoard*. Museum of London, London.

——— (2013) *London's Lost Jewels: The Cheapside Hoard*. Philip Wilson Publishers, London.

Gosling J.G. (1995) The Cheapside confusion. *Journal of Gemmology*, Vol. 24, No. 6, pp. 395–400.

Hughes R.W. (1997) *Ruby & Sapphire*. RWH Publishing, Boulder, CO.

Jobbins A.E. (1991) The Gemmology of the Cheapside Hoard. *Goldsmiths Technical Digest* 1990/91. The Worshipful Company of Goldsmiths, London, pp. 22–25.

Kunz G.F. (1913) *The Curious Lore of Precious Stones: Being a Description of Their Sentiments and Folk Lore, Superstitions, Symbolism, Mysticism, Use in Medicine, Protection, Prevention, Religion, and Divination, Crystal Gazing, Birthstones, Lucky Stones and Talismans, Astral, Zodiacal and Planetary*. J. B. Lippincott Co., Philadelphia, PA.

——— (1915) *The Magic of Jewels and Charms*. J. B. Lippincott Co., Philadelphia, PA.

Lenzen G. (1970) *The History of Diamond Production and the Diamond Trade*. Praeger Publishers, New York.

Macdonald J. (1996) Stony Jack's Roman London. In J. Bird, M. Hassall, and H. Sheldon, *Interpreting Roman London*, Oxbow Monograph 58.

Lesley P. (1968) *Renaissance Jewels and Jeweled Objects: From the Melvin Gutman Collection*. The Baltimore Museum of Art, Baltimore, MD.

London Museum (1928) *The Cheapside Hoard of Elizabethan and Jacobean Jewelry*. London Museum Catalogues, No. 2.

Mitchell D. (2013) Divers riche and costlye Jewells… The Cheapside Hoard. *Goldsmiths' Review 2012/2013*. The Worshipful Company of Goldsmiths, London, pp.18–19.

Nassau K. (1994) *Gemstone Enhancement: History, Science and State of the Art*. Butterworth-Heinemann, Oxford.

Nichols T. (1652) *A Lapidary, or, the History of Pretious Stones: with Cautions for the Undeceiving of All Those That Deal with Pretious Stones*. Thomas Buck, Cambridge.

Scarisbrick D. (1995) *Tudor and Jacobean Jewellery*. Tate Publishing, London.

Sinkankas J. (1981) *Emerald and Other Beryls*. Chilton Book Company, Radnor, PA.

Tavernier J.B. (1676–77) *Le Six Voyages de Jean Baptiste Tavernier, Ecuyer Baron d'Aubonne*. Gervais Clouzier...et Claude Barbin, Paris.

Tillander H. (1995) *Diamond Cuts in Historic Jewellery 1381–1910*. Art Books International, London.

ABOUT THE AUTHORS

Mr. Weldon (rweldon@gia.edu) is manager of photography and visual communications, and Ms. Jonathan is a research librarian, at GIA in Carlsbad, California.

ACKNOWLEDGMENTS

The authors would like to thank Sharon Ament, director of the Museum of London, for her gracious interview and for opening the doors for us to see and photograph some of the most remarkable items in the Cheapside Hoard. Hazel Forsyth, senior curator of medieval and post-medieval collections at the Museum of London, offered gifted insights into the mysteries that surround the hoard, as well as contagious enthusiasm about its story. Antony Robbins, director of communications at the Museum of London, provided flawless guidance though the museum's magnificent exhibits and vast knowledge of London's storied history. We also thank Kevin Schumacher, digital resources specialist at GIA, for his expertise in videotaping interviews and several treasures from the Cheapside Hoard. We are grateful to the GIA Library staff for their support and for access to the rare book collection.

On the Origin of Digit Patterns in Gem Opal

Benjamin Rondeau, Jean-Pierre Gauthier, Francesco Mazzero, Emmanuel Fritsch, Yves Bodeur, and Boris Chauviré

Some natural opals, mostly from Ethiopia, show a macroscopic finger-like structure called a *digit* pattern. This pattern consists of vertical columns that are more or less parallel, separated by a homogeneous matrix of different color, transparency, or play-of-color. This study proposes that digits develop through: (1) the deposition of a homogeneous opal layer and subsequent polygonization in the form of vertical columns; (2) preferential alteration of this layer at the vertical grain and sub-grain boundaries, creating the digit shape; (3) precipitation of a new silica gel in the space between the digits; and (4) the drying and solidification of the opal. Although polygonization in the form of vertical columns is a growth process typical of synthetic opal, the post-growth alteration of these columns into digits and the deposition of matrix are observed only in natural opal.

Opal is a poorly crystallized or amorphous hydrated silica formed through the solidification of a silica gel (Jones and Segnit, 1971). The most valuable variety is "precious opal," which displays play-of-color: patches of pure spectral colors from violet to red flashing over the stone as it is tilted. Precious opals are mined in many parts of the world, most notably in Australia, Brazil, Mexico, and Ethiopia. Other sources include the United States, Honduras, and Java. Ethiopia has been a major producer since the 2008 discovery of abundant opal at Wegel Tena, in the northeastern Wollo Province (Rondeau et al., 2009, 2010; Mazzero et al., 2009, 2010).

Play-of-color arises from the diffraction of visible light on monosized, well-ordered silica spheres in opal-A (Sanders 1964; Darragh and Sanders, 1965), and lepispheres in opal-CT (Flörke et al., 1976) of appropriate diameter. Most often, play-of-color involves several juxtaposed patches of various diffraction colors. In rare cases, a network of silica spheres is distributed over the whole stone, so that the color patches move in unison. Such samples are considered natural "photonic" crystals. Whereas a crystal *sensu stricto* diffracts X-rays, a photonic crystal diffracts wavelengths in the visible range of the spectrum, giving rise to visible play-of-color. The diffraction colors in precious opal can be arranged in a variety of patterns, including intense specks (pinfire), flames, bands, and juxtaposed polygons (harlequin opal). Straight black lines or bands often cross the patches, and these are due to polysynthetic or mechanical twin planes of the photonic crystal, merging at the surface of the gem (Kinder, 1969; Gauthier, 1985). Unlike precious opal, common opals do not display play-of-color, usually because the silica spheres lack regular packing (Gaillou et al., 2008).

Although some rare opals are colorless, most specimens present a bodycolor: white, black, gray, brown, yellow to orange (as in fire opal), red, pink, blue, green, or violet. These colors are typically due to minute mineral inclusions colored by transition metal ions that absorb part of the visible spectrum of light. These include iron for yellow to orange to brown (fire opal), copper for a saturated blue ("Peruvian opal"), and nickel for green (chrysopal; Fritsch et al., 1999). Other causes of color in the inclusions are color centers (purple fluorite inclusions) and organic compounds (quinones in pink opals; Mathey and Luckins, 1998; Fritsch et al., 2004).

In this article, we document an optical feature encountered in some gem opals: Viewed in one di-

See end of article for About the Authors and Acknowledgments.
Gems & Gemology, Vol. 49, No. 3, pp. 138–146,
http://dx.doi.org/10.5741/GEMS.49.3.138.

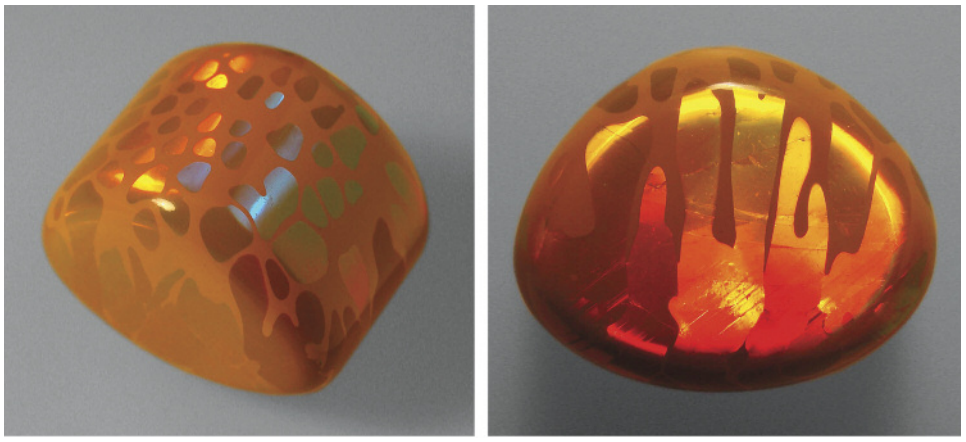

Figure 1. Digits in an Ethiopian opal from Mezezo, in Ethiopia's Shewa Province. Digits are rounded, finger-like columns of opal embedded in a matrix of opal with a different appearance. This 1.5 cm stone shows rounded patches on one side (left) and columns on the other side (right). Photos by F. Mazzero.

rection, the surface shows a mosaic of polygonal to rounded patches of opal, separated by a homogeneous matrix of distinctly different opal. When viewed from the perpendicular direction, these patches appear more elongated and parallel, like columns, that are rounded at one end (figure 1). Each column represents a grain made up of a homogeneous network of silica spheres. The resulting three-dimensional feature's resemblance to fingers (at the millimeter scale), inspired us to call them *digits* (Gauthier et al., 2004; Rondeau et al., 2010). This feature has also been described by other gemologists (Hainschwang, 2006; Choudhary, 2008). Digits are most spectacular when the rounded columns possess play-of-color and the matrix is common opal, as shown in figure 1.

Figure 2. A rare observation of digits in Australian common opal (potch) from Coober Pedy. The sample is 3 cm across. Photo by E. Fritsch.

Digits are so frequently observed in Ethiopian opals, either from Wegel Tena in Wollo Province (Rondeau et al., 2010) or from Mezezo in Shewa Province (Johnson et al., 1996; Mazzero, 2003) that they have become the industry's unofficial identifier for Ethiopian opal. Examples have occasionally been reported from other deposits, such as Virgin Valley, Nevada (Gübelin and Koivula, 2005; Gaber, 2007). Digits have been reported in only one Australian sample (figure 2). This paper aims to provide further documentation on digit patterns by proposing a model for their formation.

MATERIALS AND METHODS

All Ethiopian samples were rough or cabochon opals collected in the gem market at Addis Ababa, Ethiopia, between 2008 and 2011. Their digit patterns were observable with the unaided eye at the millimeter or centimeter scale (again, see figure 1). From thousands of samples examined, more than 10% of them showed digit patterns. We documented those that showed spectacular or interesting features before they were sold. The specimen from Honduras was photographed during the 2011 Sainte-Marie-aux-Mines gem and mineral show (see figure 14). The specimen from Australia (figure 2) was photographed at the Coober Pedy mine.

We photographed the specimens using a camera equipped with either a macro objective lens or a binocular microscope with up to 50× magnification.

RESULTS: OPTICAL PROPERTIES OF DIGIT PATTERNS

As defined earlier, digits are characterized by their shape and revealed by the optical contrast between the columns and the matrix. This section provides observations and interpretation useful for establishing a formation model.

Figure 3. The patches of play-of-color are rounded and separated by a continuous network of matrix in the upper part of this opal, but the matrix diminishes toward the lower right as the patches become more polygonal. This 32 × 28 mm Ethiopian sample is from Mezezo, Shewa Province. Photo by F. Mazzero.

Variation in the Appearance of the Digits. In samples that contain abundant matrix and few play-of-color patches, the digits are clearly rounded at the ends (again, see figure 1). In samples that contain less matrix and abundant patches, the digit ends are less rounded and more polygonal (figure 3). Some samples display juxtaposed, polygonal columns with no matrix at all in between. In this last case, the digit pattern is no longer visible, and such stones show, in a transversal section, juxtaposed polygonal columns of play-of-color opal (as in the lower right part of figure 3). This is somewhat similar to the harlequin opal.

When digits are polygonal or nearly polygonal (with no matrix or little matrix, respectively), one can observe their cross-sections; these are usually pentagonal or hexagonal. That is, each cross-section is generally five- or six-sided and neighbored by five or six others (again, see figure 3). In only one sample did we encounter polygonal digits with matrix in between with irregular, angular shapes instead of rounded ones (figure 4).

Digits are most pronounced in play-of-color opal, though they also exist very rarely in common opal (again, see figure 2). These digits can be displayed in opals with various bodycolors—from white to gray to brown—and a range of transparencies. The matrix typically has a similar hue but is less transparent, though this is not always the case: Figure 5 shows a sample with colorless to whitish digits embedded in a brownish orange common opal matrix.

Play-of-Color Network Preceding the Formation of Digits. When digits are composed of precious opal, the play-of-color network is usually continuous from one patch to another. In some cases, the whole sample consists of a single network of diffracting opal, subdivided into digits (figure 6). We also observed that twin planes are continuous from one digit to its neighbors (figure 7). These observations indicate that some digits may result from the cross-section partitioning of a larger, preexisting opal. Digit patterns that are not continuous, but display very similar diffraction colors from one patch to the next, may be the result of slight misorientation in the silica sphere network (figure 8).

In Brief

- Finger-like digit patterns are commonly observed in natural opals from Ethiopia.
- A multi-step mechanism for digit formation is proposed.
- Digits form vertically, and their rounded ends face upward.
- The rounded ends are thought to result from "remobilization of the silica spheres," specifically the erosion of polygonal boundaries by an influx of water.

Figure 4. In this unusual 23.83 ct opal from Wollo, Ethiopia, play-of-color patches are not rounded but irregular, though the matrix is abundant. Photo by B. Rondeau.

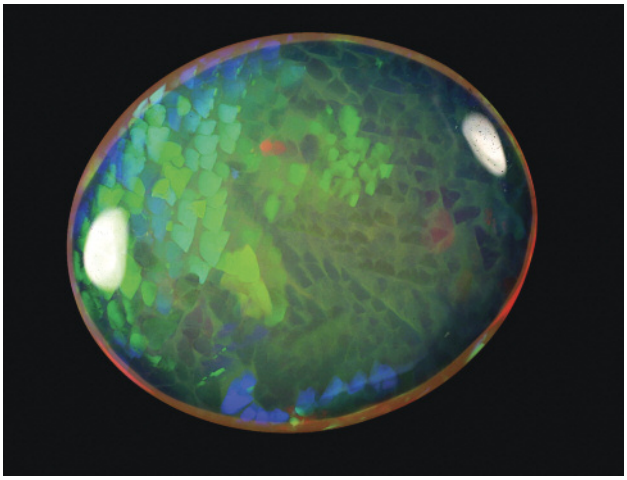

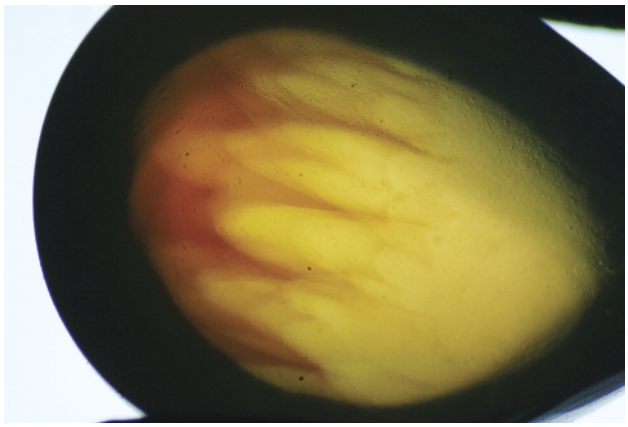

Figure 5. Some samples, such as this 1.29 ct Ethiopian opal from Wollo, show colorless to whitish digits in a matrix that appears brownish in transmitted light. Such contrast in bodycolor is rare. Photo by B. Rondeau.

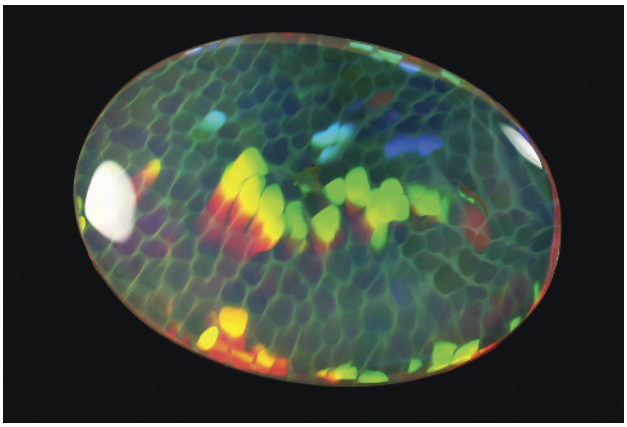

Figure 6. All adjacent patches show a single diffraction color for a given viewing position. Hence, the silica spheres are packed to form a single regular, continuous network throughout the whole sample. This 14.84 ct sample is from Wollo, Ethiopia. Photo by B. Rondeau.

Digits Developing Vertically. Many opal deposits in the world provide samples that show parallel layers of opal that contrast in both color and transparency. These banded opals formed by successive deposition of opal layers, each layer varying slightly in composition. The layering plane is parallel with the surface (e.g., Escard, 1914). When such samples contain digits, the digits are always perpendicular to the banding, indicating that they developed vertically (figure 9). We observed digits in dozens of banded opal samples, all showing the same orientation.

Digits with Rounded Ends Facing Upward. Two rough banded samples showed a flat surface that represents the last horizontal layer deposited. This has been clearly established by our many field observations (e.g., figure 10) and documented in several other deposits (e.g., Escard, 1914). This happens when the silica gel does not entirely fill the cavity where the opal is forming. When samples contain digits, their rounded ends always point upward (figure 11).

Some digit-bearing samples showed a layering of play-of-color. The diffraction colors progressively

Figure 7. In this opal from Wollo, the striations corresponding to twinning planes are continuous from one digit to the next, indicating that the digits originated from the same photonic crystal. Field of view: 5 mm. Photo by J.-P. Gauthier.

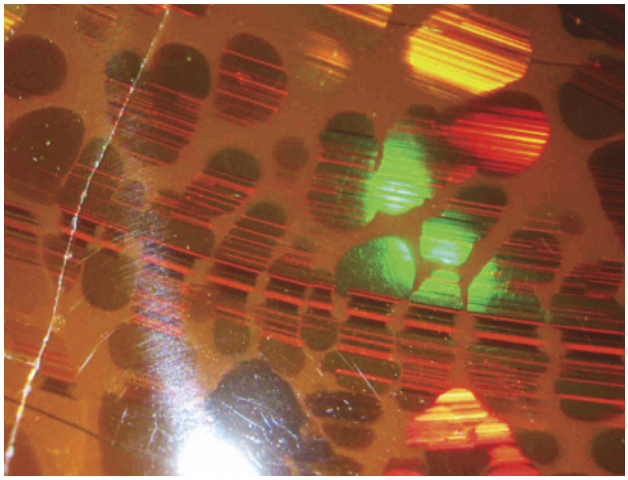

Figure 8. Due to slight changes in the angle of refraction from one sub-grain to the next, the diffraction color changes in this sample from Mezezo. Photo by J.-P. Gauthier.

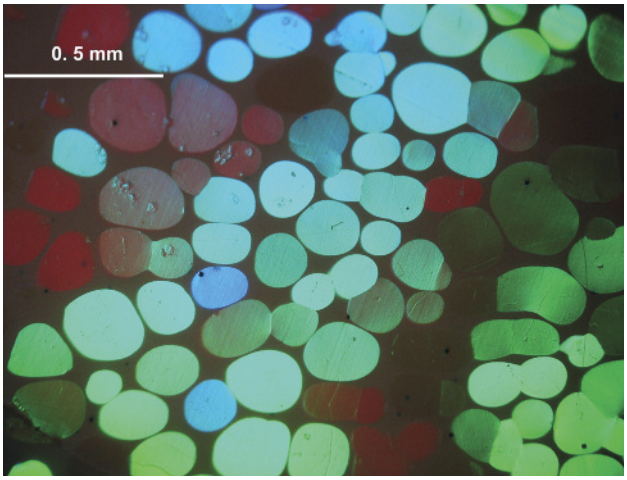

Figure 9. This 18.68 ct specimen from Wollo shows several different layers of opal, revealing several influxes of silica gel during the formation of the opal and its digits. Note that the digits are perpendicular to the banding. Photo by Robert Weldon, © GIA.

shifted from red to yellow to green in a given position of observation (figure 12). This indicates that the silica spheres' diameter progressively diminishes from larger (red diffraction) to smaller (green diffraction); see Sanders (1964) and Darragh and Sanders (1965). In specimens where the top and bottom are known,

Figure 10. Sometimes opal observed in the field only partially fills cavities. In such cases, the top surface of the opal is usually flat and horizontal, with the top of the cavity remaining empty. This specimen is shown in a weathered ignimbritic host rock in Ethiopia. The arrow points upward. Picture width: 2 cm. Photo by B. Rondeau.

this layering has been observed as horizontal, with the red layer corresponding to the bottom and the green layer to the top. Such a distribution is controlled by gravity during the sedimentation of the silica spheres: larger spheres sediment first, followed by progressively smaller spheres. Again, in samples we examined that showed this color zoning, the digits were perpendicular to the horizontal layering, their rounded ends pointing upward (figure 12).

DISCUSSION

A Model for Digit Formation. Based on the previous observations, we propose a step-by-step model for digit formation, illustrated in figure 13. This model

Figure 11. The cavity where this opal from Wollo formed was only partially filled during formation, leaving a free horizontal surface on top. The bottom horizontal layer shows digit patterns that developed vertically, the rounded ends pointing upward. Photographed in transmitted light (top) and reflected light (bottom). Field of view 1.5 cm. Photos by B. Rondeau.

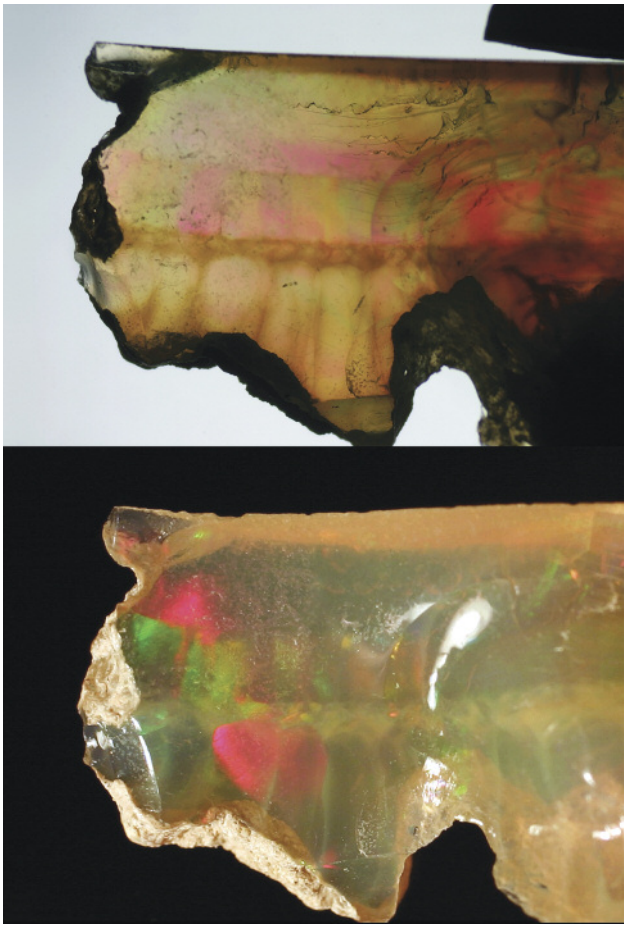

Figure 12. The shift from red (bottom) to green (top) diffraction colors indicates a regular size gradation of the spheres: larger spheres at the bottom, smaller spheres at the top. This 3.90 ct sample from Wollo is shown in the same position as when the spheres were deposited, with the rounded ends of the digits pointing upward. Photo by D. Goubert.

deals specifically with the development of digits in play-of-color opal.

- *Step 1: Formation of Play-of-Color Opal in Silica Gel*. Hydrated spheres of silica combine to form either a single large, homogeneous photonic crystal or several juxtaposed ones, forming prismatic, vertical columns.
- *Step 2: Polygonization of the Crystals.* Photonic crystals split into juxtaposed columns, polygonal in cross-section (which we refer to as sub-grains). Each column generally has five to six faces per prism, but may have four or seven in rare cases.
- *Step 3: Remobilization of the Photonic Crystal by a New Fluid with Opal Etching Properties*. Alteration of the photonic crystal by remobilization of the silica spheres occurs preferentially at the grain and sub-grain boundaries, which offer more available surface. Individual columns (either grains or sub-grains) then acquire their rounded shape, forming true digits.
- *Step 4: Deposition of Common Opal*. Changes in local chemical conditions lead to deposition in the remaining spaces between digits. When step 3 is more pronounced, so is step 4.
- *Step 5: Additional Deposition*. Additional horizontal layers of opal of any variety may also be deposited.
- *Step 6: Solidification*. Through dehydration and cementation, this silica gel forms a solid opal.

We encountered digits much less frequently in common opal (again, see figure 2), possibly because they are much less conspicuous than digits in play-of-color opal. Digits in common opal form according to a very similar model. In this case, step 1 produces a homogeneous layer of common opal, while step 2 gives rise to the columns, presumably through shrinkage during compaction. The rest of the process is identical.

How Does Polygonization Occur? Polygonization (step 2) also occurs in synthetic opal. It happens after the silica spheres are deposited and while the silica gel is drying (Nassau, 1980). Polygonization may be due to the bonding forces between the gel and the walls of the cavity that contains the gel. Alternatively, it may occur because of the expulsion of the

Figure 13. Our model of digit formation contains four basic steps: (1) sedimentation of silica spheres, taking on a columnar structure after dehydration; (2) polygonization of the color patches; (3) influx of water, altering the columns by progressive erosion along the polygonal boundaries; and (4) settling of new interstitial silica-rich filler, formation of silica lepispheres, and dehydration.

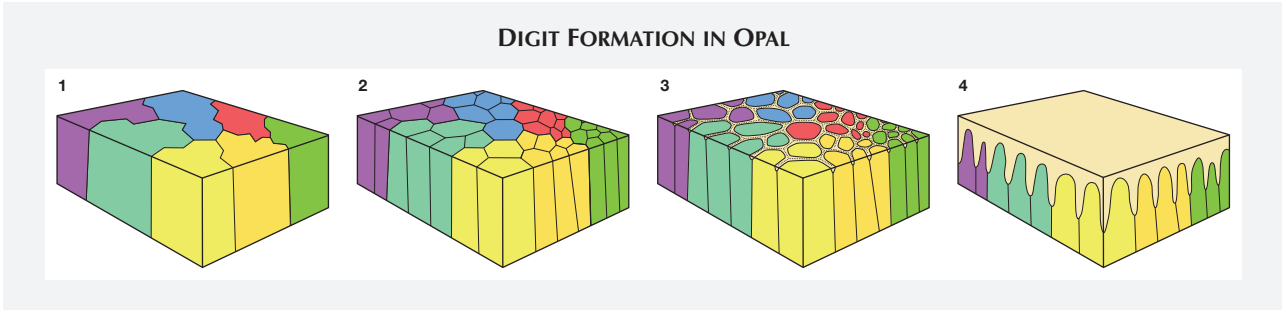

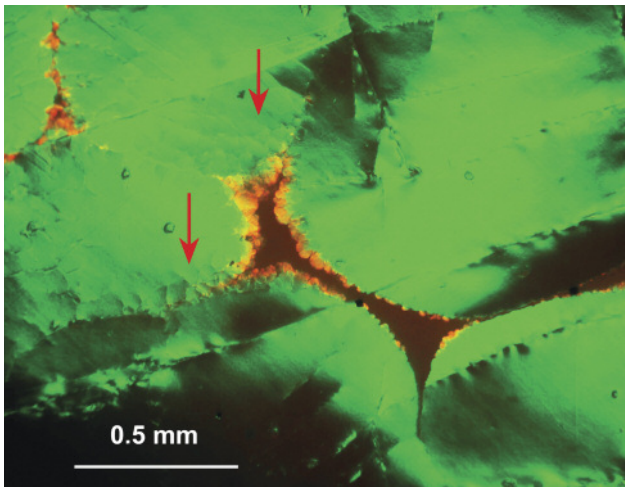

Figure 14. Some digits show different play-of-color (here, orange) at their boundaries, possibly as a result of progressive water impregnation from the matrix toward the digits. The opal patches at the red arrows show secondary re-polygonization. This sample is from Wollo, Ethiopia. Photo by J.-P. Gauthier.

liquid from the silica gel (dehydration), producing a contraction effect, a phenomenon known as *syneresis*. Syneresis should create some space between the columns, but this was not observed in our samples. In either case, columns are vertical because there is a free horizontal surface at the top of the gel. Polygonal columns in opal evoke the basaltic prism that forms due to shrinkage during magma cooling.

There can be several orders of polygonization. Sub-grains produced by polygonization can in turn polygonize (as indicated by the red arrows in figure 14). Multiple generations of polygonization are responsible for the "lizard-skin" optical effect typical of synthetic opal (Nassau, 1980; Gauthier, 2004) and rarely observed in natural opal.

How Does Remobilization (Step 3) Occur? Similar rounded shapes are found in many crystals in nature, such as beryl or diamond. Those are generated by dissolution processes (Sunagawa, 2005). This happens when the growth medium turns unfavorable due to changes in temperature, pressure, oxygen fugacity, redox conditions, chemical potential, or other variables. In the case of opal, remobilization of the silica spheres is enough to cause erosion of the photonic crystal, rather than true dissolution. This may occur when an influx of water with a lower silica content leads to the remobilization of the previously deposited silica. In samples that are well separated by abundant matrix, and have thus undergone more significant alteration, the digits show a more rounded shape.

Variations on the Model. All these steps can occur in a single sample, in particular when alteration (step 3) only affects the upper part of the columns. More often, some steps are not seen because the sample was cut or broken during mining. For example, the stone in figure 3 shows only steps 2 (polygons of play-of-color opal) through 4 (rounded patches separated by some matrix). Likewise, figure 11 shows the result of steps 4 and 5 only. Patterns formed by only steps 1 and 2 are common in opals from many deposits, including Australia (Pecover, 2010), and those in thin fractures in basalts from Honduras (figure 15). Such samples show a "honeycomb" structure (Maddison, 1992) somewhat similar to that observed in synthetic opal, in which case digits did not develop because no remobilization stage occurred.

In one case we observed that remobilization can disrupt the digits' play-of-color. In figure 14, most of the digits diffract a green light, while orange diffraction occurs between the digits and matrix. The orange diffraction may be the result of higher water content between the silica spheres at this contact point (as described in Gauthier, 2004). This may indicate that remobilization sometimes happens pro-

Figure 15. Opals found in thin fractures in basalt from Honduras commonly show pronounced banding that marks the horizontal level. Play-of-color bands have a vertical, columnar shape that corresponds to steps 1 and 2 of digit pattern development. Field of view: 6 cm. Photo by B. Rondeau.

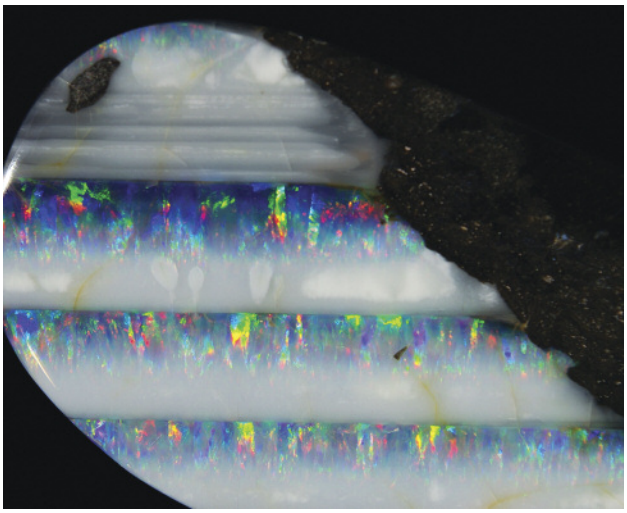

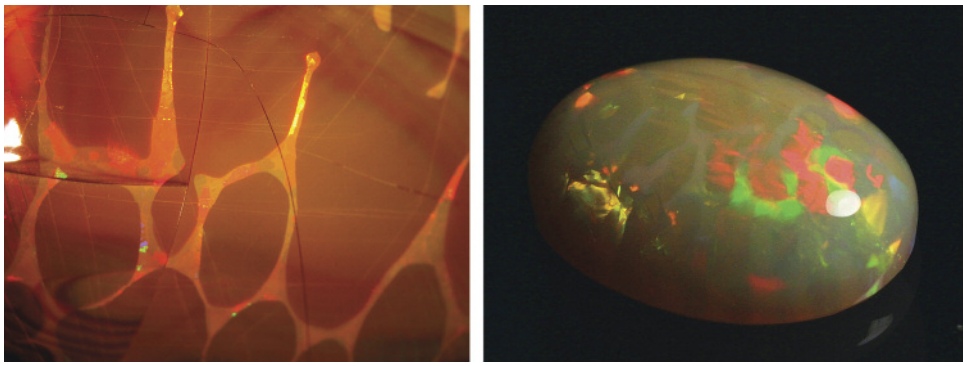

Figure 16. Some rare samples show a play-of-color matrix around play-of-color digits with a different diffraction color. These samples are from Mezezo (left) and Wollo (right). Photos by B. Rondeau.

gressively, and not always abruptly. Alternatively, this feature may result from the overgrowth of a higher-water-content layer at the early stage of binder formation.

Two samples also showed play-of-color in the matrix around the digits, but with a different orientation of diffraction (figure 16). Another one showed features that resembled digits, but with angular shapes (e.g., figure 4) or non-parallel digits. This can be explained by additional local forces or parameters that perturb the "regular" model. For example, we propose that non-vertical digits developed when the cavity was totally filled with silica gel, as opposed to the normal free, horizontal surface in a partially filled cavity, producing a different strain distribution. Such variations may be worth investigating further.

Confusion with Synthetics. Ethiopian opals showing the "lizard-skin" effect are not uncommon, as in the bottom right area of the stone in figure 3. This may cause confusion with synthetic opals (e.g., Choudhary, 2008). The presence of a matrix between the columns may therefore be the first step in identifying a natural opal. When no matrix is present, other indicators are inclusions typical of Ethiopian opals, such as opaque black octahedra, pyrite cubes, or rootlet fossils (Gauthier et al., 2013).

CONCLUSION

This study has documented the macroscopic characteristics of digits, distinct aesthetic features observed in many natural opals from Ethiopia but rarely seen in specimens from other regions. We propose that these columns form vertically with their rounded ends pointing upward, and that larger patches of color formed before the matrix. The first step in our model is the deposition of a homogeneous layer of opal with juxtaposed vertical columns. Next, polygonization of the columns occurs. Then, an influx of fluid (probably less rich in silica) remobilizes this layer. The remobilization is most efficient at grain boundaries, separating the columns and rounding their edges. Finally, opal precipitates again between the partially dissolved columns, cementing them into a matrix of either common or play-of-color opal.

Among the open questions remaining, we emphasize that the process by which remobilization occurs remains unclear: Is this a true dissolution process, in which silica spheres dissolve into water, or do the spheres remain intact but dispersed into the gel? Also, the combination of geological conditions necessary for digits to form have been encountered in Ethiopia but are uncommon in other localities: What makes this combination so rare?

REFERENCES

Choudhary G. (2008) Gem News International: An interesting opal. *G&G*, Vol. 44, No. 2, pp. 172–174.

Darragh P.J., Sanders J.V. (1965) The origin of color in opal based on electron microscopy. *G&G*, Vol. 11, No. 10, pp. 291–298.

Escard J. (1914) *Les Pierres Précieuses*. H. Dunod & E. Pinat Ed., Paris, 520 pp.

Flörke O.W., Hollmann R., von Rad U.V., Rösch H. (1976) Intergrowth and twinning in opal-CT lepispheres. *Contributions to Mineralogy and Petrology*, Vol. 58, No. 3, pp. 235–242.

Fritsch E., Rondeau B., Ostrooumov M., Lasnier B., Marie A.-M., Barreau A., Wery J., Connoué J., Lefrant S. (1999) Découvertes récentes sur l'opale. *Revue de Gemmologie a.f.g.*, Vol. 138/139, pp. 34–40.

Fritsch E., Gaillou E., Ostroumov M., Rondeau B., Barreau A. (2004) Relationship between nanostructure and optical absorption in fibrous pink opals from Mexico and Peru. *European Journal of Mineralogy*, Vol. 16, pp. 743–752, http://dx.doi.org/10.1127/0935-1221/2004/0016-0743.

Gaber C.J. (2007) Opal in the United States and Canada. In *Opal, the Phenomenal Gemstone*, Lithographie, LLC, East Hampton,

CT, 82 pp.
Gaillou E., Fritsch E., Aguilar-Reyes B., Rondeau B., Post J., Barreau A., Ostroumov M. (2008) Common gem opal: An investigation of micro- to nano-structure. *American Mineralogist*, Vol. 93, No. 11–12, pp. 1865–1873, http://dx.doi.org/10.2138/am.2008.2518.
Gauthier J.-P. (1985) Observation directe par microscopie électronique à transmission de diverses variétés d'opale I. Opales nobles. *Journal de Microscopie et Spectroscopie Electronique*, Vol. 10, No. 2, pp. 117–128.
——— (2004) L'opale de synthèse. *Revue de Gemmologie a.f.g.*, Vol. 149, pp. 24–26.
Gauthier J.P., Mazzero F., Mandaba Y., Fritsch E. (2004) L'opale d'Ethiopie: Gemmologie ordinaire et caractéristiques exceptionnelles. *Revue de Gemmologie a.f.g.*, Vol. 149, pp. 15–23.
Gauthier J.-P., Mazzero F., Rondeau B., Fritsch E. (2013) De l'originalité des opales éthiopiennes. *Revue de Gemmologie a.f.g.*, Vol. 184, pp. 11–16.
Gübelin E., Koivula J.I. (2005) *Photoatlas of Inclusions in Gemstones Volume 2*. Opinio Verlag, Basel, Switzerland. 829 pp.
Hainschwang T. (2006) Gem News International: A large phenomenal fire opal with possible uranium-related luminescence. *G&G*, Vol. 42, No. 4, pp. 276–277.
Johnson M.L., Kammerling R.C., DeGhionno D.G., Koivula J.I. (1996) Opal from Shewa Province, Ethiopia. *G&G*, Vol. 32, No. 2, pp. 112–120, http://dx.doi.org/10.5741/GEMS.32.2.112.
Jones J.B., Segnit E.R. (1971) The nature of opal; I. Nomenclature and constituent phases. *Journal of the Geological Society of Australia*, Vol. 18, No. 1, pp. 57–68.
Kinder E. (1969) Elektronenmikroskopische Untersuchungen an Edelopalen. *Zeitschrift für Physik*, Vol. 224, No. 1–3, pp. 74–84.
Maddison P. (1992) Gem Trade Lab Notes: Opal, with natural cellular structure. *G&G*, Vol. 28, No. 1, pp. 55–56.
Mathey A., Luckins P. (1998) Spatial distribution of perylenequinones in lichens and quincyite (rock) using confocal fluorescence microscopy. *Focus on Microscopy 1998,* Sydney, Australia.
Mazzero F. (2003) A la découverte des gisements d'opale du Shewa, relation de voyage en Ethiopie. *Revue de Gemmologie a.f.g.*, Vol. 148, pp. 27–31.
Mazzero F., Gauthier J.P., Rondeau B., Fritsch E., Bekele E. (2009) Nouveau gisement d'opales d'Ethiopie dans la Province du Welo: Premières informations. *Revue de Gemmologie a.f.g.*, Vol. 167, pp. 4–5.
Mazzero F., Désagulier C., Rondeau B., Ayalew D., Ezezew G., Cenki T., Bekele E. (2010) L'opale du Wollo, Ethiopie: des mines de gisements. *Revue de gemmologie a.f.g.*, Vol. 174, pp. 14–20.
Nassau K. (1980) *Gems Made By Man*. Chilton Book Company, Radnor, PA, 364 pp.
Pecover S.R. (2010) Fluid flow and brittle fracture textures in opal veins: Clues to the origin of opal in the Great Australian Basin. *13th Quadrennial IAGOD Symposium*, Adelaide, Australia.
Rondeau B., Mazzero F., Bekele E., Gauthier J.P., Fritsch E. (2009) Gem News International: New play-of-color opal from Welo, Ethiopia. *G&G*, Vol. 45, No. 1, pp. 59–60.
Rondeau B., Fritsch E., Gauthier J.P., Mazzero F., Cenki-Tok B., Bekele E., Gaillou E. (2010) Play-of-color opal from Wegel Tena, Wollo Province, Ethiopia. *G&G*, Vol. 46, No. 2, pp. 90–105, http://dx.doi.org/10.5741/GEMS.46.2.90.
Sanders J.V. (1964) Colour of precious opal. *Nature*, Vol. 204, No. 4964, pp. 1151–1153.
Sunagawa, I. (2005) *Crystals-Morphology, Growth and Perfection*. Cambridge University Press, Cambridge, UK, 295 pp.

ABOUT THE AUTHORS

Dr. Rondeau (benjamin.rondeau@univ-nantes.fr) is assistant professor, Dr. Bodeur is a geologist, and Chauviré is a Ph.D. student at the University of Nantes, Laboratoire de Planétologie et Géodynamique, UMR-CNRS 6112. Jean-Pierre Gauthier is a gemologist at Centre de Recherches Gemmologiques in Nantes. Francesco Mazzero is manager of Opalinda in Paris. Dr. Fritsch is professor of physics at University of Nantes, Institut des Matériaux Jean Rouxel, UMR-CNRS 6205.

ACKNOWLEDGMENTS

We wish to thank Drs. Mary Johnson and Ahmadjan Abduriyim for reviewing and improving this article. We also thank Eyassu Bekele (Eyaopal, Addis Ababa, Ethiopia) and Thomas Cenki (Opalinda, Paris) who captured many samples of interest for this study, and the numerous miners in Ethiopia and Australia who provided useful information regarding the mode of occurrence of opal in the field.

This year, hundreds of readers participated in the 2013 *Gems & Gemology* Challenge. Entries arrived from around the world, as readers tested their gemological knowledge by answering questions listed in the Spring 2013 issue. Those who earned a score of 75% or better received a GIA Letter of Completion recognizing their achievement. The participants who scored a perfect 100% are listed below.

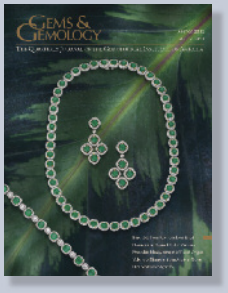

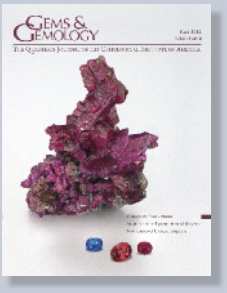


G&G Challenge Winners

Australia
Barbara Wodecki

Belarus
Dmitry Stepanenko

Belgium
Guy Lalous

Hong Kong
Cristina O. Piercey-O'Brien

Italy
Guiseppe Guidi
Chiara Piussi
Gabriele Tralli

Kenya
Marvin Wambua

Spain
Luis E. Ochando-Gomez

Switzerland
Eva Mettler

United Kingdom
Francesca Lawley
Giulia Nisoli

United States
Andrea Blake
Beverly Brannan
Giselle Chiechi
Susan DiGeorgio
Elaine Fosmire
Eloïse Gaillou
Edward A. Goodman
Brenda Harwick
Bruce Hoffmann
Sarah Horst
Stephen Kientop
Thaïs Anne Lumpp-Lamkie
James Markides
Daniel Novak
Abba Steinfeld
Andy Stevens
Ric Taylor
Kate Trunnell
Colleen Walsh
Flora Walters
Thomas Wendt

Answers

See pages 42–43 of the Spring 2013 issue for the questions.

1 (b or d)*, 2 (a), 3 (a), 4 (c), 5 (c), 6 (c), 7 (a), 8 (d), 9 (b), 10 (c), 11 (b), 12 (b), 13 (c), 14 (b), 15 (a), 16 (c), 17 (d), 18 (b), 19 (b), 20 (c), 21 (a), 22 (a), 23 (b), 24 (d), 25 (c)

* Review of the question showed that either answer is acceptable.

AGATES FROM SIDI RAHAL, IN THE ATLAS MOUNTAINS OF MOROCCO: GEMOLOGICAL CHARACTERISTICS AND PROPOSED ORIGIN

Magdalena Dumańska-Słowik, Lucyna Natkaniec-Nowak, Aleksandra Wesełucha-Birczyńska, Adam Gaweł, Marek Lankosz, and Paweł Wróbel

Moroccan agates from Sidi Rahal occur within Triassic basaltoids as lens-shaped specimens in sizes up to 25 cm. Their coloration and internal structure are quite specific and characteristic for this region. The pink outer rim is composed of opal-CT. The layer within it, usually red or red-brown, contains a significant concentration of Fe compounds (hematite and goethite) that are responsible for this zone's color. The nodules' interior, usually blue-gray or white-gray, is formed of fibrous low-α quartz (a low-temperature polymorph of quartz) with minor amounts of moganite. The presence of moganite and Fe compound inclusions suggests that the agate's formation was induced by Fe^{3+} activity in silica-rich fluids. Other solid inclusions such as Cu sulfides, Ti oxides, calcite, and an organic substance were incorporated during post-magmatic, hydrothermal, or hypogenic conditions.

Agate is a unique natural wonder, with no two identical specimens: Each has a different pattern and color. It occurs in various volcanic and sedimentary rocks in nearly all countries on earth, with the most famous gems found in Brazil, India, and Madagascar (e.g., Ball and Burns, 1975; Breiter and Pasava, 1984; Priester, 1999; Moxon et al., 2006; Strieder and Heemann, 2006; Cross, 2008; Götze et al., 2009). Agates consist mainly of fibrous microcrystalline low-α quartz—i.e., macroscopic banded chalcedony (Götze, 2000). Graetsch et al. (1987), Heaney and Post (1992), and Heaney (1995) noted that in agates and other microcrystalline silica phases, low-α quartz commonly forms intergrowths with moganite, a monoclinic silica phase first described by Flörke et al. (1976, 1984) and approved as a new mineral by the International Mineralogical Association in 1999 (Grice and Ferraris, 2000).

Agates are a microcrystalline variety of silica, generally defined as banded chalcedony, but they also contain a variety of other silica polymorphs (Götze et al., 2001). The mechanism of rhythmic bands that produces agate is still not completely understood (Beaster, 2005). A number of explanations have been proposed for this banded texture and the rhythmic segregation of the silica polymorphs (see French et al., 2013). The prevailing hypothesis is that voids in volcanic rock are filled in cycles, from the rim to the center. Silica-rich fluids are believed to have penetrated the rocks through microfissures or infiltration canals. The shape and width of the zones and the general pattern of the agate all depend on the concentration of silica in the fluids, as well as the temperature, pressure, and timing of the fluid influxes. Other elements found in the fluids (Fe, Ti, Mn, and others) affect only the coloration of the agate zones. At the final stage of formation, mainly in the center of the void, idiomorphic quartz of different colors—brown, smoky quartz, amethyst, and rock crystal—can crystallize, sometimes accompanied by calcite, hematite, goethite, barite, and other minerals (Heaney, 1993; Götze et al., 2001; Moxon and Rios, 2004; French et al., 2013).

Moroccan agates from the Atlas Mountains were first described in the 1940s (Jahn et al., 2003), but only recently have they drawn the interest of collectors worldwide. The specimens are commonly white-gray, blue-gray, red-gray, and brown-gray, and are found in sizes up to 25 cm in diameter (Zenz, 2005a). The scientific literature has dealt mainly with the geology of the deposits (e.g., Jahn et al., 2003; Zenz, 2005b, 2009; Gottschaller, 2012; Mayer, 2012; Mohr, 2012; Schwarz, 2012). This paper focuses instead on the gemological characteristics of these agates.

The town of Sidi Rahal is located about 60 km east of Marrakesh. The agate outcrops occur nearby in an

See end of article for About the Authors and Acknowledgments.
GEMS & GEMOLOGY, Vol. 49, No. 3, pp. 148–159,
http://dx.doi.org/10.5741/GEMS.49.3.148.

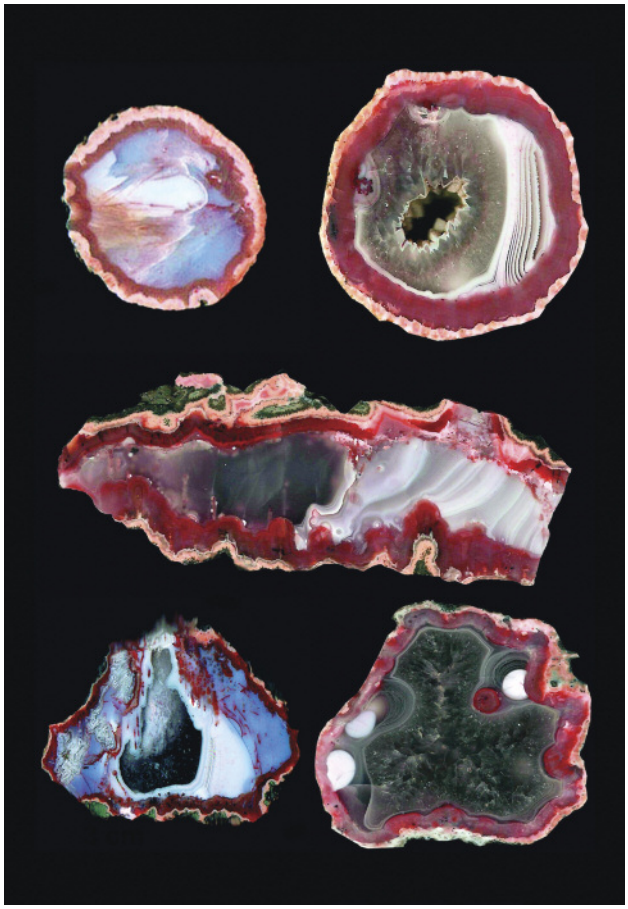

Figure 1. The Moroccan agate nodules investigated in this study showed a wide variety of patterns, including landscape, stalactite, and pipe forms. These samples range from 4 to 15 cm wide. Photo by Małgorzata Klimek.

area approximately 40–50 km long and 5 km wide. Although the region is abundant with these gems, it is not being worked on a commercial scale. Every day locals look for agate to sell to gem collectors from around the world. The most spectacular specimens are used for carvings and cabochons.

In the present study, we investigate the distribution of different silica phases within agate from Sidi Rahal and provide initial characterization of solid inclusions found in the colored zones. Observations of the samples' microtextures, and chemical and mineralogical analysis of the solid inclusions found in the matrix, are considered with regard to how the agates formed.

GEOLOGICAL SETTING

Morocco's largest agate deposits are found in Tizi-n-Tichka, Asni, and Sidi Rahal, in the northwestern part of the Atlas Mountains; detailed geological maps of this region are presented by Jahn et al. (2003). The Atlas Mountains consist mainly of Paleozoic crystalline schists, quartzites, limestones, and Paleogene volcanic rocks associated with Alpine orogenic tectonic movements (Babault et al., 2013). The upper part of the mountains is covered with folded Jurassic and Cretaceous limestone and lower Paleogene flysch rocks (schists-sandstone).

Triassic basaltoids as thick as 3 km outcrop in the vicinity of Sidi Rahal. This semicircular volcanic outcropping covers a 110 × 70 km area. The basaltoids frequently contain spherical or lens-shaped geodes filled with SiO_2 minerals (Verdier, 1971). Agates from Sidi Rahal are mainly gray-white or red-gray, with a red-orange or pink external rim. In the inner part of the geode, white-gray chalcedony coexists with colorless quartz. Cutting and polishing reveal landscape, stalactite, or pipe-shaped patterns (figure 1). Yet some are also monocentric (see the classification proposed by Campos-Venuti, 2012), with a void in the center or filled with the youngest generation of silica polymorph.

MATERIALS AND METHODS

Ten agate samples were provided by Polish gem collectors Jacek Szczerba and Remigiusz Molenda, who personally gathered the nodules in 2010 and 2011. Mineralogical characterization of selected nodules was carried out with a transmission microscope, a scanning electron microscope (SEM-EDS and SEM-CL), X-ray fluorescence (XRF) microspectroscopy, and Raman microspectroscopy.

The specimens were examined with an Olympus BX 51 polarizing microscope with a magnification range of 40× to 400×. Backscattered electron observations were performed on polished, carbon-coated sections using an FEI Quanta 200 field emission gun scanning electron microscope equipped with energy-dispersive spectroscopy and cathodoluminescence detectors. The system was operated at 20 kV accelerating voltage in high-vacuum mode. Scanning electron microscopy provides information on the quantity of solid inclusions and their general chemical composition. Combined with Raman spectroscopy, it enables the user to identify all mineral and organic phases found within an agate's matrix.

Raman spectra of silica phases and solid inclusions were recorded with a Renishaw InVia Raman microspectrometer coupled with a Leica microscope featuring 20×, 50×, and 100× magnification objectives. Two selected samples were excited with a 785 nm high-power near-infrared (HP NIR) laser. The laser

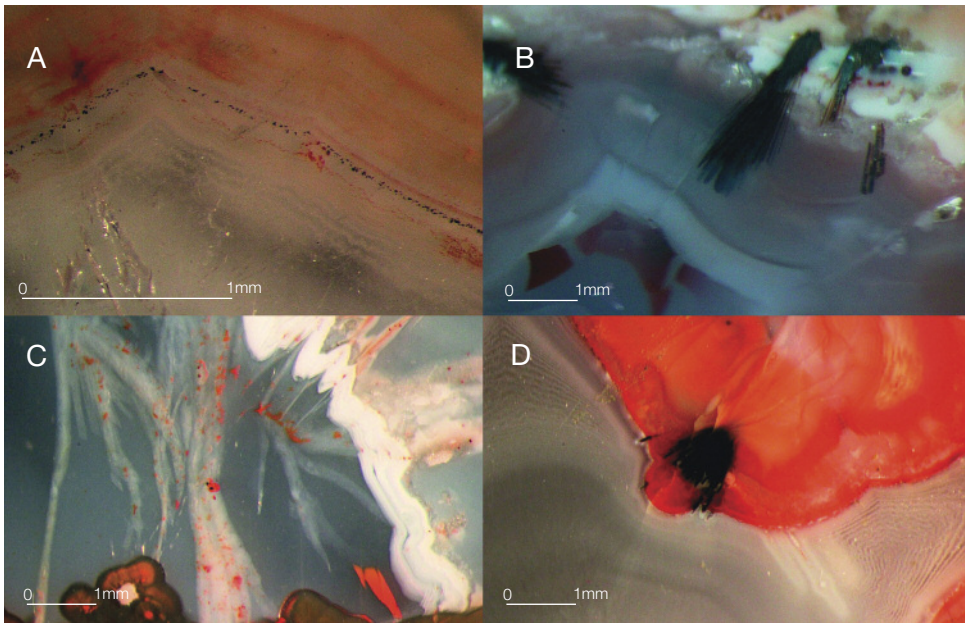

Figure 2. Solid inclusions of Fe compounds found in the agates can form tiny laminae (A), needle-like inclusions (B, D) or euhedral crystals irregularly scattered within silica (C, D). Photomicrographs by Tomasz Toboła.

power and excitation time were optimized to the optic character of the samples. The laser focus diameter was approximately 1–2 µm. It should be noted that almost no sample preparation was performed. The two samples were broken with a geological hammer, and the fractured surface was cleaned carefully with distilled water and acetone before measurements were made to avoid any contamination.

Raman maps were recorded with a Thermo Scientific DXR Raman microscope on selected areas (190 × 150 µm), using a step size of 3 µm. The agate sample was excited with a 780 nm laser. We recorded the most intense bands for quartz (460 cm^{-1}), opal (412 cm^{-1}), and moganite (501 cm^{-1}) in each point of the analytical grid.

Two-dimensional maps of elemental abundance were created with a laboratory setup consisting of a low-power X-ray tube with a molybdenum anode and a silicon drift detector, or SDD (Wróbel et al., 2012). The measurements were performed in typical 45°/45° geometry, where the angles between impinging beam, sample normal, and detector axis equaled 45°. The X-ray tube voltage and current were 50 kV and 1 mA, respectively. Primary radiation from the X-ray tube was focused with a polycapillary lens into a Gaussian-shaped beam with a spot size of at least 16.4 µm full width at half maximum (FWHM). The sample surface was placed out of focus of the primary radiation beam, which had an effective size of approximately 50 µm FWHM. The samples were mounted between two 2.5 µm thick Mylar films stretched across a plastic holder. Mounting the holder onto a motorized stage allowed the sample to be rotated in three directions with micrometer resolution.

For the mapping of agate samples 1 and 2, the step size (pixel size) equaled 150 µm in the horizontal and vertical directions. The first map measured 128 × 134 pixels, equal to 19.05 × 19.95 mm^2. The second map was 108 × 134 pixels, or 16.05 × 19.95 mm^2. The sample acquisition times were 2 seconds per pixel and 3 seconds per pixel, respectively.

The net intensities of the characteristic lines were calculated with AXIL-QXAS software using nonlinear least-squares fitting for peak deconvolution. Due to the number of measured points, we evaluated the spectra automatically using batch mode. Using our own LabVIEW scripts, we reconstructed maps of characteristic line intensities.

RESULTS

The vast majority of agate from Sidi Rahal exhibits two rim layers: pink-orange (outer) and red-brown (inner). Their thickness ranges from 0.1 to 1.0 cm. The color of the inner zone likely results from fine Fe-bearing pigments such as oxides and hydroxides scattered within the silica matrix (figures 2A, 2C, and 2D). Internally, the nodules are mostly gray-blue or white. Sometimes these regions are intersected by coarse groups of thin needle-like inclusions, either red-brown or black, that we initially attributed to Fe compounds (figures 2B and 2D). Within each zone, numerous infiltration canals called *osculum* were observed with the unaided eye.

Under the polarizing microscope in transmitted

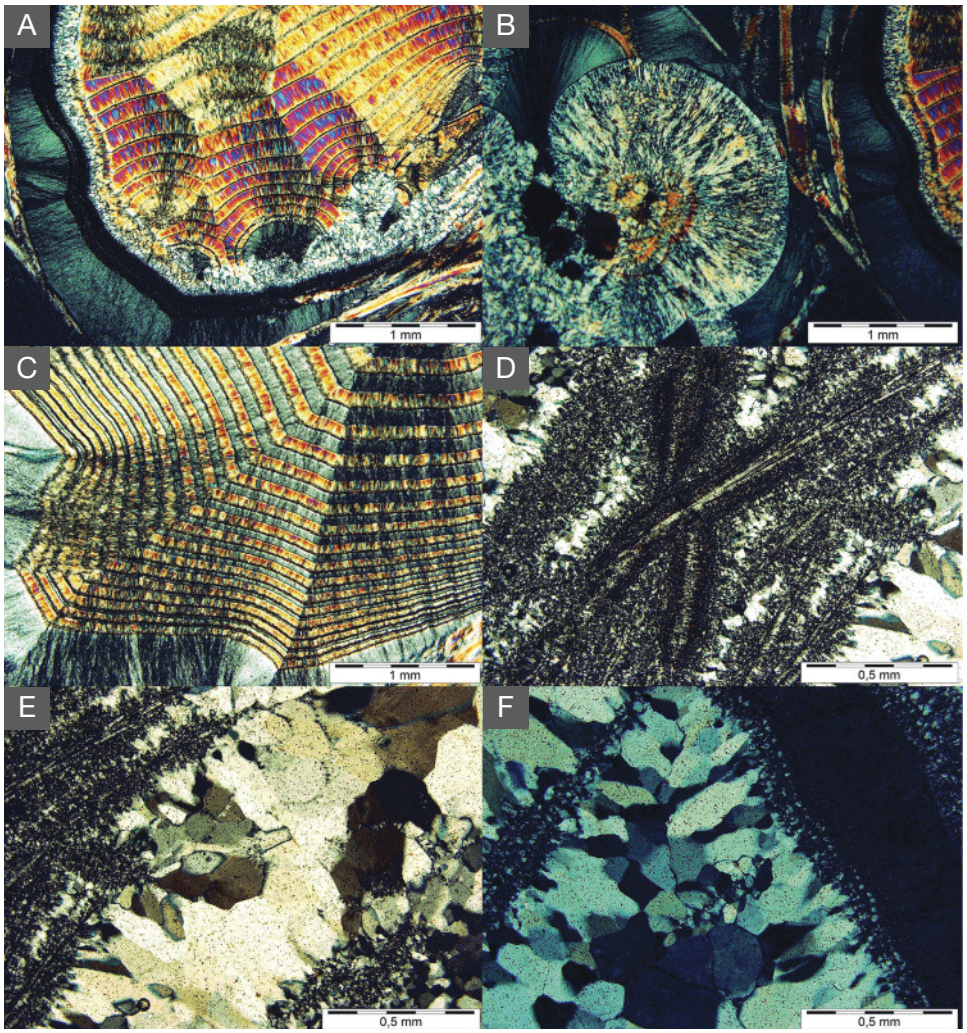

Figure 3. Between crossed polarizers, microtextures can be observed in the agates' various zones: external (A, B), middle (C, D), and internal (E, F). Photos by Małgorzata Klimek.

light, the gray-blue region inside the nodule appeared to be composed of a microcrystalline silica phase, while the internal white crustal zones contained idiomorphic quartz crystals. The microcrystalline silica phase crystallized as twisted crystals forming fibrous radial and fan-like (spherulitic) microtextures (figure 3). In the external part of the agates, the distinct boundaries between the microlayers were emphasized by thin laminae of nontransparent phases. Internally, the boundaries were almost invisible, indicating a continuous and even supply of silica-bearing water solutions. The dark brown zigzag-like inclusions consisted of an organic substance that luminesced under a long-wave UV lamp (figure 4).

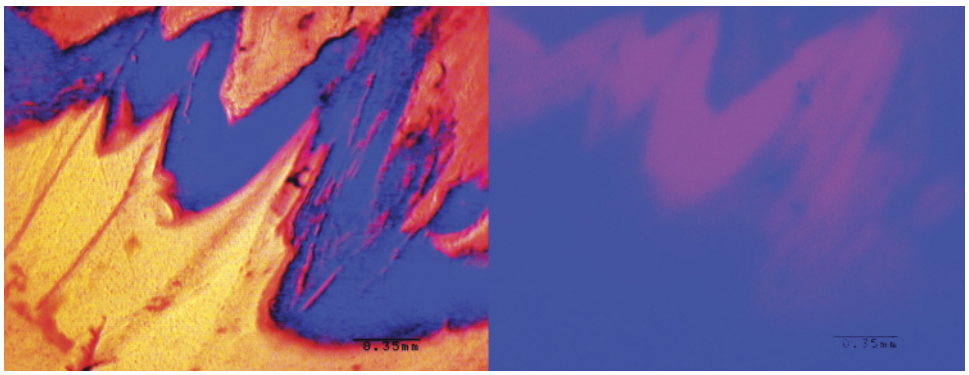

Figure 4. This agate shows organic matter in its middle region between crossed polarizers (left) and characteristic fluorescence under UV light (right). Photomicrographs by Tomasz Toboła.

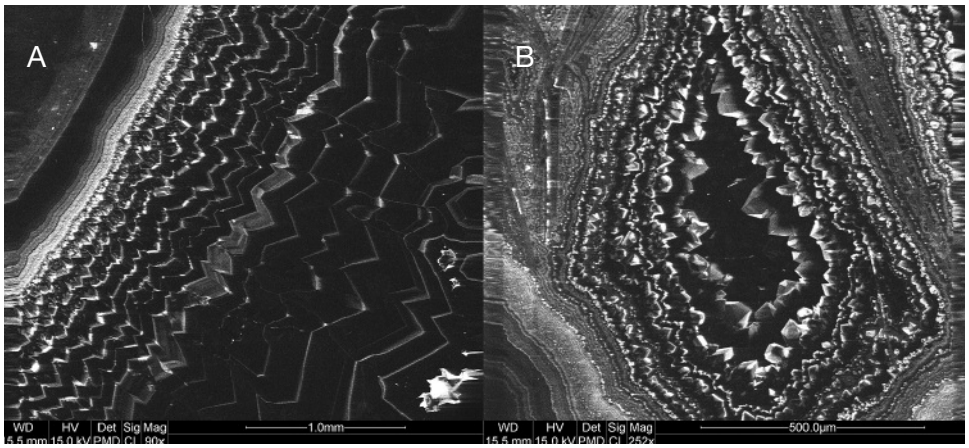

Figure 5. These SEM-CL images of agate from Sidi Rahal show the crystals' growth direction: outward from left to right (A) and inward to the center (B).

Using SEM-EDS and SEM-CL, we easily observed the various silica generations forming mosaic microtextures with different luminescence colors. The SEM-CL images revealed not only the sequence of the silica phases but also the growth direction of the crystals from the rim to the center of the agate void (figure 5). Solid mineral inclusions found in the silica matrix were comprised mainly of (1) pyroxene, typically occurring in the contact zone between the agate and the basaltoid host rock; (2) Fe compounds forming regular round crystals arranged into thin layers between silica zones; or (3) xenomorphic heterogeneous crystals scattered randomly within the matrix. Some Fe compounds, possibly hydroxides, also formed needle-like inclusions. In the central part of the nodule, tiny single crystals of Cu sulfides were accompanied by idiomorphic quartz (figure 6).

In Brief

- Agates from Sidi Rahal have a specific coloration, with a pink rim and a blue-gray core.
- They are composed of three silica phases: opal-CT, low-α quartz, and moganite.
- The main solid inclusions found within agate matrix include goethite, hematite, Ti- and Cu compounds, plagioclase, and carbonaceous matter.

The Raman spectra of different silica polymorphs, measured from selected areas of the agates, are presented in figure 7. Band assignments and comparisons with references are listed in table 1. The distinctive 460 and 501 cm^{-1} marker bands are related to symmetric stretching-bending vibrations of low-α quartz and moganite, respectively (Götze et al., 1998). The interior of the agate nodules from Sidi Rahal is a mix-

TABLE 1. Raman band positions (cm^{-1}) and assignments of agate from Sidi Rahal, Morocco.

Point 1: Opal-CT	Point 2: Low quartz + moganite	Point 3: Low quartz + moganite	Point 4: Low quartz + moganite	Point 5: Low quartz + moganite	Mode symmetry (Kingma and Hemley, 1994; Götze et al., 1998)	Interpretation
	122	121	123	126	$E_{(LO+TO)}$	Quartz/moganite
	199	197	200	207	A1	Low quartz
222						Opal-CT
346	346	344	347		A1	Quartz
412						Opal-CT
	460	460	460	461	A1	Low quartz/moganite
	483	476	475		A1	
	501	501	501	501	A1	Moganite
782	786	786		781		Low quartz

A1= symmetric stretching-bending vibrations

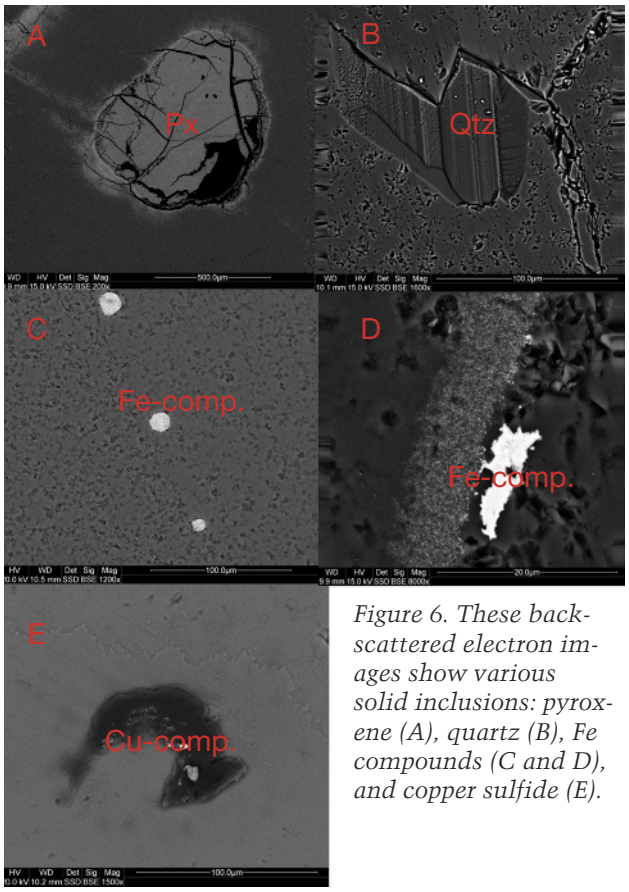

Figure 6. These backscattered electron images show various solid inclusions: pyroxene (A), quartz (B), Fe compounds (C and D), and copper sulfide (E).

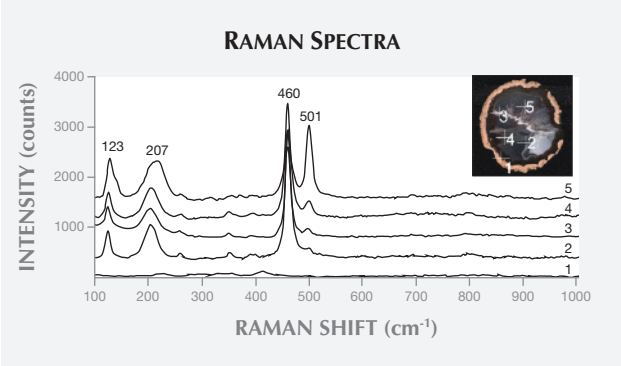

Figure 7. Raman spectra collected from various portions of agate from Sidi Rahal (points 1–5) demonstrated the presence of opal-CT (1) and low-α quartz with an admixture of moganite (2–5).

ture of these two silica polymorphs. The Raman spectrum of the external pink-orange layer revealed the presence of opal-CT with the characteristic band at 410 cm^{-1} (Pop et al., 2004). 2D mapping measurements showed that the opal-CT occurs almost exclusively in the rim, whereas the distribution of low-α quartz and moganite varies within each agate and also between samples (figure 8). The low-α quartz seems to predominate over the moganite, which occurs only in the nodules' visible white regions.

Interesting accumulations of dark brown inclusions (figure 9) were identified with Raman microspectroscopy. These complex heterogeneous inclusions consist of several different phases. Points 2–4 have very similar spectra, with the predominant band at approximately 500 cm^{-1} attributed to feldspar. Curve fitting of the wide 534 cm^{-1} band gives two components: 519 and 549 cm^{-1}, originating from anorthite and bytownite, respectively (Mernagh, 1991). In the first spectrum, the high-frequency

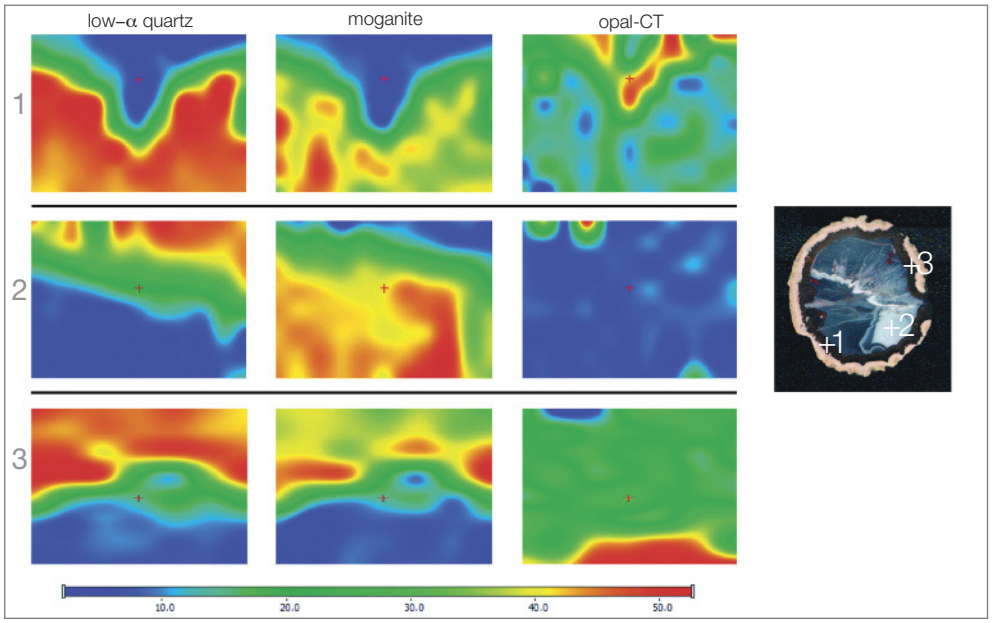

Figure 8. Non-linear Raman mapping of an agate nodule recorded in three regions shows the relative proportions of the silica polymorph. Bands characteristic of quartz (460 cm^{-1}), opal (412 cm^{-1}), and moganite (501 cm^{-1}) were chosen.

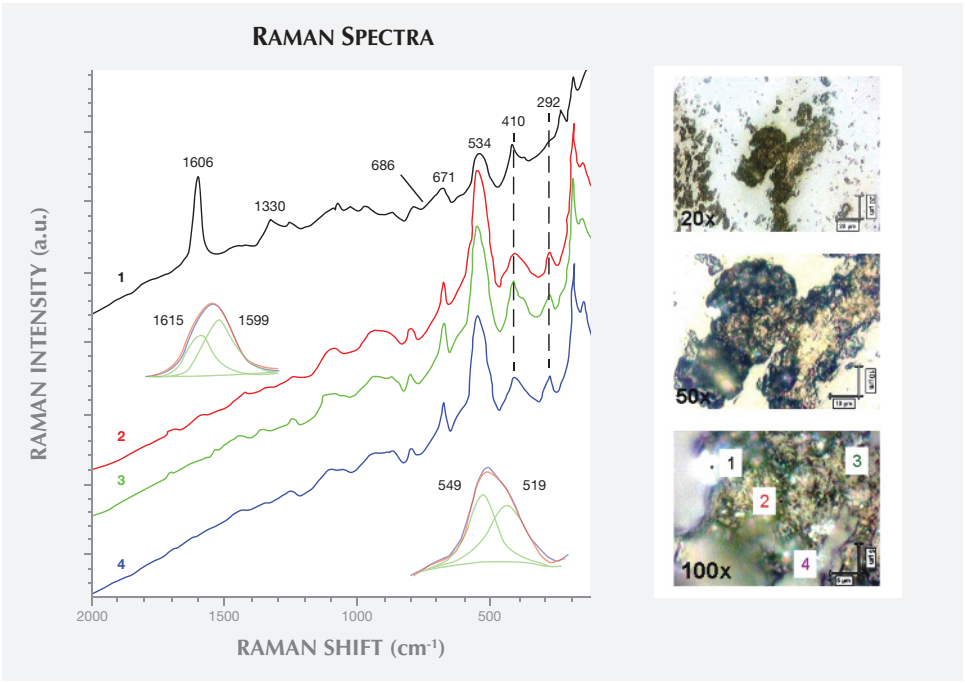

Figure 9. Photomicrographs of dark brown inclusions and Raman spectra (collected from points 1–4) in the 2000–200 cm^{-1} range show the presence of feldspars, goethite, hematite and titanium oxide.

shoulder of the 410 cm^{-1} band located at approximately 434 cm^{-1} and the broad, weak band at 686 cm^{-1} likely indicate the presence of nanocrystalline TiO_2 (figure 10).

The presence of carbonaceous matter is very clearly marked by 1330 and 1606 cm^{-1} bands (again, see figure 10). Resolving this second band gives two bands: one at 1599 cm^{-1}, the other a D1 band at 1615 cm^{-1}, forming a shoulder on the G band. These bands are characteristic for graphite and carbonaceous matter. The 1330 cm^{-1} band (called the D band) is due to disorder-induced first-order Raman mode, and the 1599 cm^{-1} band to first-order E_{2g} Raman mode (G band); the 1615 cm^{-1} band is called the D1 band (figure 10, inset, and figure 11; see Beyssac et al., 2003). The D1 band always occurs with the D band, and its intensity increases with a decreasing degree of organization. In the second-order region (2200–3400 cm^{-1}) there also appear weaker peaks, representing poorly organized carbonaceous matter, attributed to overtone or combination scattering (table 2).

Another component of this complex inclusion is goethite, indicated by the characteristic band at 387 cm^{-1} (390 cm^{-1}) observed in points 2–4. This band is caused by symmetric stretching vibrations of Fe-O-Fe-OH (Legodi and de Waal, 2006). Hematite in the agate matrix is evidenced by marker bands at 292, 410, and 610 cm^{-1} (again, see figure 10). These bands are attributed to symmetric bending vibrations of Fe-O (Legodi and de Waal, 2006).

Figure 11 presents another example of characteristic carbonaceous matter bands within an agate ma-

Figure 10. The baseline-corrected Raman spectra for points 1 and 3 (see figure 9), collected in the 2000–200 cm^{-1} range, reveal the presence of anorthite, bytownite (inset), carbonaceous matter, and titanium oxide within the dark brown complex inclusions.

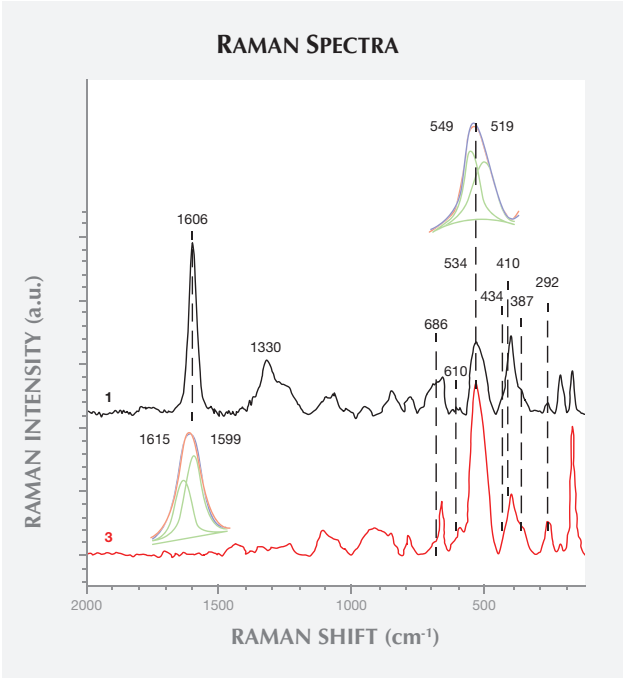

TABLE 2. Raman bands (cm^{-1}) observed in spectra shown in figures 9, 10, and 11.

Band	Assignment	References
180	Bytownite	Mernagh (1991)
225	Opal	Pop et al. (2004)
273	Goethite	Antunes et al. (2003); de Faria et al. (1997)
292	Hematite	Legodi and de Waal (2006)
387	Goethite	Legodi and de Waal (2006)
410	Opal, hematite	Pop et al. (2004); Legodi and de Waal (2006)
434	TiO_2 (nm crystallite size)	Swamy et al. (2006)
534 (519, 549)	Bytownite, anorthite, magnetite	Mernagh (1991); Antunes et al. (2003), de Faria et al. (1997)
610	Hematite	Legodi and de Waal (2006)
671	Bytownite, magnetite	Mernagh (1991); Antunes et al. (2003), de Faria et al. (1997)
686	Anorthite, TiO_2	Mernagh (1991); Swamy et al. (2006)
769	Anorthite	Mernagh (1991)
1076	Anorthite, SiO_2	Mernagh (1991); Pop et al. (2004)
1240	Anorthite	Mernagh (1991)
1330	Carbonaceous matter	Beyssac et al. (2003)
1606 (1599, 1615)	Conjugated C=C, carbonaceous matter: G and D1 mode	Beyssac et al. (2003)
2924	ν as CH_2, carbonaceous matter	Beyssac et al. (2003)
2935	ν as CH_2 in rings, carbonaceous matter	Beyssac et al. (2003)

trix (Beyssac et al., 2003). The 1585 cm^{-1} peak (E_{2g} mode) corresponding to the stretching vibration in the aromatic layers is another example of the G band. The additional band for poorly organized carbonaceous matter, the D band, appears in the first-order region around 1330 cm^{-1}. Positions and half-widths of the G and D bands in this example indicate the different degree of ordering of carbonaceous matter compared to figure 10, spectrum 1. Greater intensity of the D band (1330 cm^{-1}) with respect to the G band (1585 cm^{-1}) indicates a significant carbonaceous matter disorder in this inclusion. It is believed that organized carbonaceous matter is developed from the less homogenous organic precursors in the process of solidification of fluid inclusions (Wopenka and Pasteris, 1993). This process may lead to the formation of graphite in rocks, as we have observed in Afghan tourmalines (Wesełucha-Birczynska and Natkaniec-Nowak, 2011).

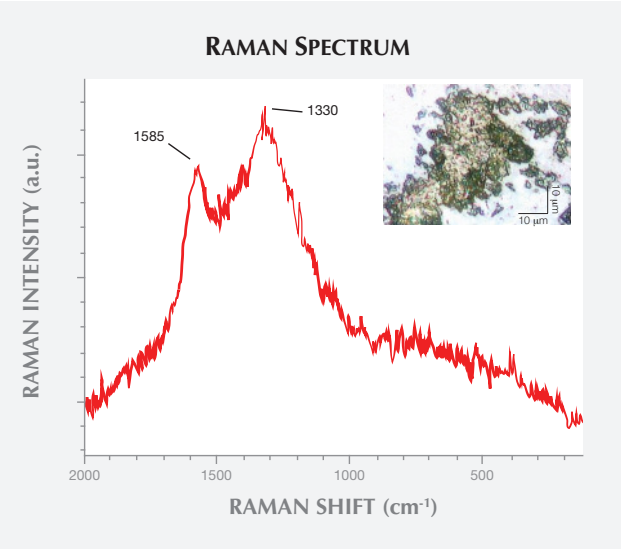

Figure 11. The Raman spectrum of the dark brown inclusions in the 2000–200 cm^{-1} is typical of carbonaceous matter. Photomicrograph by Aleksandra Wesełucha-Birczynska.

The XRF spectrum taken from sample 1 (figure 12) shows characteristic lines for Si, Cl, K, Ca, Fe, and Cu. Figures 13 and 14 present the microscopic view of the measured samples and maps of characteristic Kα X-ray intensities of Si, Ca, Cl, Cu, and Fe

Figure 12. The XRF spectrum taken from a selected area of sample 1 shows the presence of Si, Ca, Cu, Fe, and Cl.

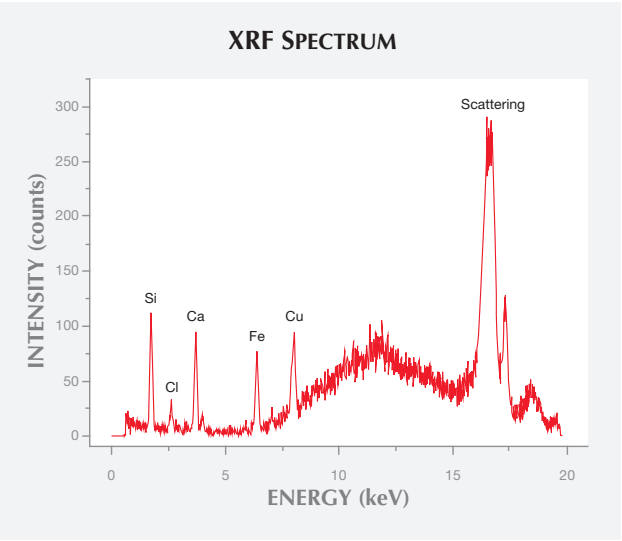

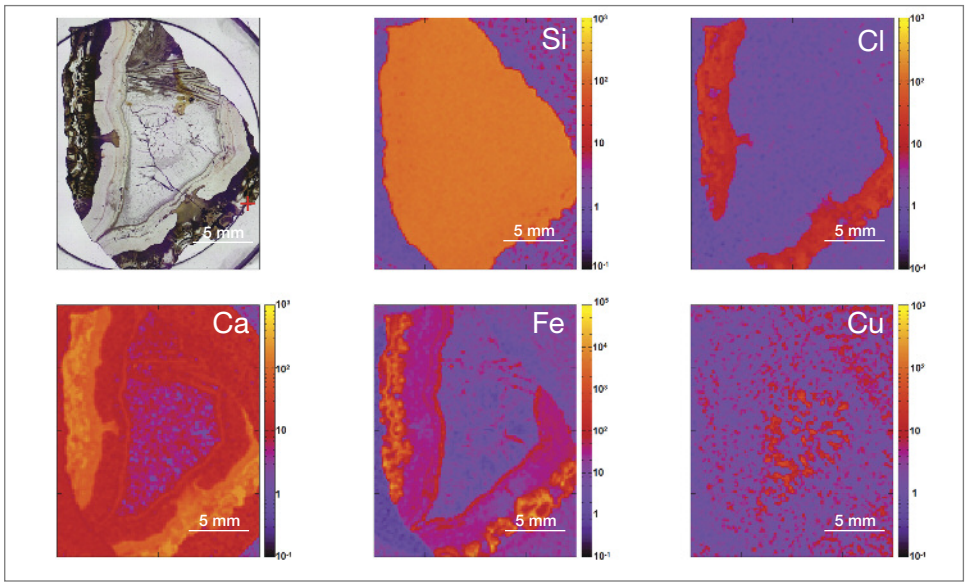

Figure 13. The microscopic view of sample 1 and maps of characteristic Kα X-ray intensities (the red cross marks the analytical point where the XRF spectrum was recorded) show the distribution of Si, Cl, Ca, Fe, and Cu.

in samples 1 and 2. As would be expected, silicon is uniformly distributed in both samples. The other elements are distributed unevenly. In both agates the highest concentrations of Cl, Ca, and Fe are distributed close to the edges. Whereas the inner part of sample 1 shows a very low abundance of Ca and Fe, these elements are evenly distributed throughout sample 2. It is worth noting that fragments containing large amounts of Cl, Ca, and Fe are quite narrow, and concentrations of these elements decrease toward the center of both samples. The varying elemental concentration within the mineral can result from the scattering of Ca, Cl, and Fe during crystal growth. Cu, on the other hand, is deposited in irregular structures measuring about 2 mm or less (sample 1) or in single points less than 0.5 mm in diameter (sample 2). For both samples, Cl and Ca show a very similar pattern; the correlations between Cl-Kα and Ca-Kα intensities are shown in figure 15. The positive correlation coefficients (R) calculated for these elements were 0.94 and 0.89 for samples 1 and 2, respectively.

DISCUSSION

Moroccan agates from Sidi Rahal occurring within Triassic basaltoids are composed mainly of low-α quartz only locally intergrown with moganite. The maturation of cryptocrystalline silica phases (the

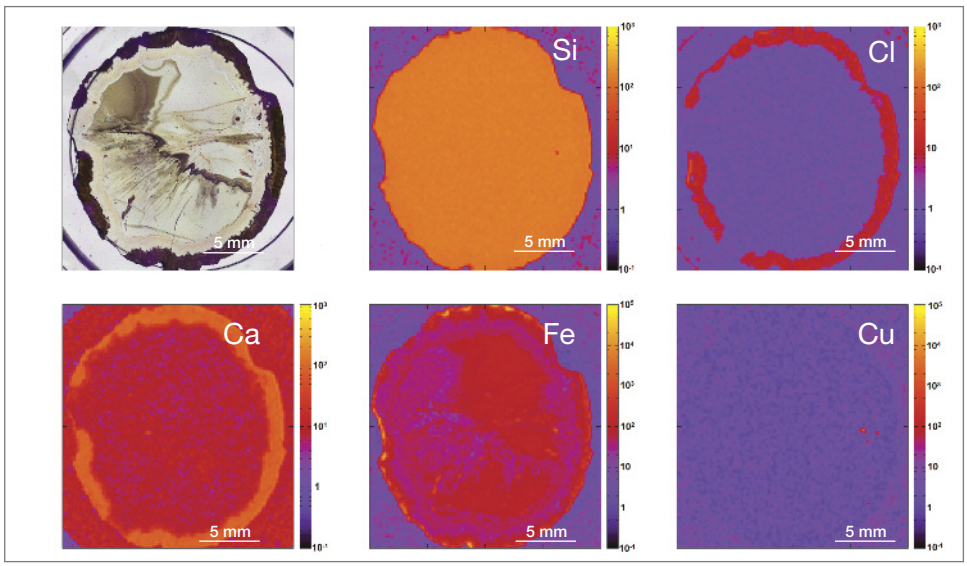

Figure 14. The microscopic view of sample 2 and the maps of characteristic Kα X-ray intensities indicate the distribution of Si, Cl, Ca, Fe, and Cu. Photomicrograph by Piotr Wróbel.

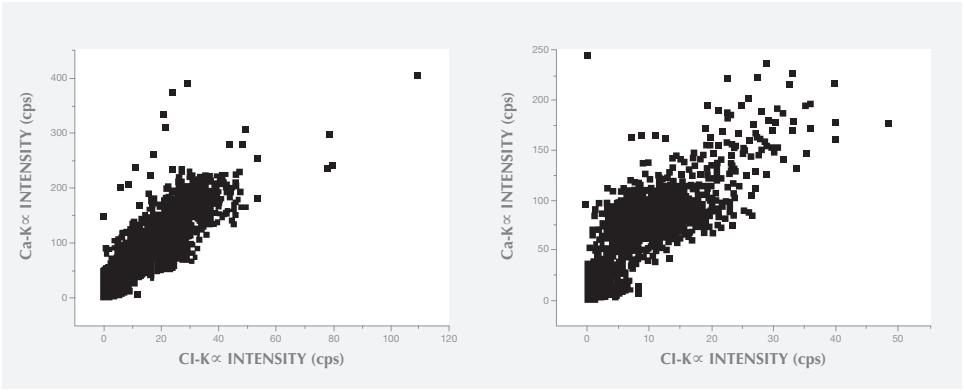

Figure 15. Positive correlations between Ca and Cl concentrations are found in agate samples 1 (R=0.94) and 2 (R=0.89).

transformation of metastable moganite into low-α quartz) generally lowers the moganite content (Moxon and Rios, 2004) over tens of millions of years (Heaney, 1995). Thus, Pop et al. (2004) proposed moganite content as a tool for age evaluation and noted no direct correlation with the geological age of the agate's host rock. Nevertheless, their investigation of the oldest (Cretaceous) microcrystalline samples showed only minor moganite content, while the youngest chalcedony had a relatively high concentration of it. Moganite has generally been identified as an indicator of evaporative sedimentation, although non-evaporitic rocks often contain 5.0–15.0 wt.% moganite (Heaney, 1995). The results of our Raman studies are consistent with these observations, as Triassic agates from Sidi Rahal contain only minor amounts of moganite (figures 7 and 8; table 1).

Pop et al. (2004) noted that moganite crystallization is favored by alkaline fluid composition combined with the high activity of ferric iron. As a result, the absence of moganite in weathered and hydrothermally altered silica samples may be a useful measure of fluid-rock interactions (Heaney, 1995). Agates from Sidi Rahal often contain thin layers with an orange-red, red, or brown-red color, and these are associated with the presence of Fe compounds. Some Fe-bearing phases form linear aggregates, suggesting a continuous supply of iron-bearing fluids to the basaltoid nodule. Hence, the occurrence of both Fe compounds strongly suggests that the crystallization of these agates was induced by Fe^{3+}-rich fluids.

The most widespread inclusions found in the samples were hematite and goethite, which probably formed during hydrothermal conditions of post-magmatic activities. The presence of Cu sulfides and Ti oxides scattered within the agate matrix might also be attributed to hydrothermal fluids. Only traces of titanium phases could have occurred, as XRF analyses did not detect their presence in the agate matrix. In a few instances, the agates' voids or some of their microfissures were filled with idiomorphic calcite crystals. The formation of this carbonate phase is associated with a *hypogenic* process (referring to a mineral deposit formed from aqueous solutions that originated at depth and ascended through the crust). Other solid inclusions occurring within the silica matrix are pyroxene, plagioclase, and an organic substance forming irregularly scattered aggregates. Pyroxene and plagioclase occur only in the outer portions, and these are typical components of the basaltoids' host rock. The organic substance was probably incorporated into the agate under late hydrothermal, hypogenic conditions by exposure to groundwater, or it might be of algal-marine origin. To determine the exact origin of the organic substance, we plan to carry out stable carbon isotope analyses in the next stage of our investigations, as we did with the "bituminous" agates from Nowy Kościół, Poland (Dumańska-Słowik et al., 2008).

In XRF maps of agate from Sidi Rahal, the location and distribution of Ca and Cl are mutually correlated (figure 15). Such a strong correlation indicates that the concentration of these elements may be related to the same mechanism. They could have been incorporated into the nodules from a marine environment. Similarly, the presence of moganite, the silica phase typical of evaporative sedimentation, and some organic components found in the agates supports the thesis that a marine environment affected the formation of these beautiful gems. Undoubtedly, the crystallization of agates from Sidi Rahal lasted millions of years and took place in stages, influenced by various geochemical processes of terrestrial and marine environments.

CONCLUDING REMARKS

Agates from Sidi Rahal are composed of three silica phases: low-α quartz, moganite, and opal-CT. The

latter occurs mainly in the nodules' pink outer zone, while the interior consists of low-α quartz and moganite. The nodules' red or brown-red layer results from linearly scattered Fe compounds (hematite). Goethite usually appears as rusty brown forms in a characteristic coarse grouping of needles.

The most common solid inclusions found within the agate matrix include pyroxene, calcium-rich plagioclase, hematite, goethite, and Ti and Cu compounds. Hydrothermal fluids seem to be responsible for the formation of iron, copper, and titanium phases within the agate's microfissures. An organic substance forms tiny irregularly scattered or zigzag-like aggregates, mainly concentrated in the external and middle zones. The substance formed under hydrothermal, hypogenic conditions and may be of algal marine origin. Similarly, the presence of calcite, mainly filling the void, is connected to hypogenic processes.

The presence of red and brown-red external nodule layers enriched with scattered Fe pigments, as well as isolated aggregates of Fe oxides and hydroxides (hematite and goethite) in the whole mass of the nodules, suggests that agate crystallization was associated with the activity of Fe^{3+} in silica-bearing fluids. The higher moganite concentration in the inner part of the agate also indicates the alkaline character of the silica fluids. The significant concentration of Ca, Cl, and Fe in the nodules suggests that the formation of agates from Sidi Rahal was affected by both marine and terrestrial geochemical processes.

Similar patterns of silica polymorph growth within banded agate were observed by French et al. (2013), who attributed these gems' formation to aqueous silica-rich fluid influxes, consistent with our observations of agates from Sidi Rahal.

REFERENCES

Antunes R.A., Costa I., De Faria D.L.A. (2003) Characterization of corrosion products formed on steels in the first months of atmospheric exposure. *Materials Research*, Vol. 6, No. 3, pp. 403–408, http://dx.doi.org/10.1590/S1516-14392003000300015.

Babault J., Teixell A., Struth L., Van Den Driessche J., Arboleya M.L., Tesón E. (2013) Shortening, structural relief and drainage evolution in inverted rifts: Insights from the Atlas Mountains, the Eastern Cordillera of Colombia and the Pyrenees. *Geological Society, London, Special Publications*, Vol. 377, http://dx.doi.org/10.1144/SP377.14.

Ball R.A., Burns R.L. (1975) Agate part 1: A review—Genesis and structure. *Australian Gemmologist*, Vol. 12, No. 5, pp. 143–150.

Beaster T.J. (2005) Agates: A literature review and electron backscatter diffraction study of Lake Superior agates. B.A. thesis, Carleton College, www.carleton.edu/departments/geol/Resources/comps/CompsPDFfiles/2005/Beaster2005.pdf

Beyssac O., Goffe B., Petitet J-P., Froigneux E., Moreau M., Rouzaud J-N. (2003) On the characterization of disordered and heterogeneous carbonaceous materials by Raman spectroscopy. *Spectrochimica Acta Part A*, Vol. 59, No. 10, pp. 2267–2276, http://dx.doi.org/10.1016/S1386-1425(03)00070-2.

Breiter K., Pasava J. (1984) Agates from Horni Halze, Czechoslovakia. *Lapidary Journal*, Vol. 37, No. 11, pp. 1556–1557.

Campos-Venuti M. (2012) *Genesis and Classification of Agates and Jaspers: A New Theory.* Published by the author, 160 pp.

Cross B.L. (2008) Classic agate deposits of northern Mexico. *Mineralogical Record*, Vol. 39, No. 6, pp. 69–88.

de Faria D. L. A., Venaüncio Silva S., de Oliveira M. T. (1997) Raman microspectroscopy of some iron oxides and oxyhydroxides. *Journal of Raman Spectroscopy*, Vol. 28, No. 11, pp. 873–878, http://dx.doi.org/10.1002/(SICI)1097-4555(199711)28:11<873::AID-JRS177>3.3.CO;2-2.

Dumańska-Słowik M., Natkaniec-Nowak L., Kotarba M., Sikorska M., Rzymełka J.A., Łoboda A., Gaweł A. (2008) Mineralogical and geochemical characterization of the "bituminous" agates from Nowy Kościół (Lower Silesia, Poland). *Neues Jahrbuch für Mineralogie Abhandlungen*, Vol. 184, No. 3, pp. 255–268, http://dx.doi.org/10.1127/0077-7757/2008/0098.

Flörke O.W., Jones J.B., *Schmicke* H-U. (1976) A new microcrystalline silica from Gran Canaria. *Zeitschrift für Kristallographie*. Vol. 143, pp. 156–165.

Flörke O.W., Flörke U., Giese U. (1984) Moganite, a new microcrystalline silica mineral. *Neues Jahrbuch für Mineralogue Abhandlungen*. Vol. 149, pp. 325–336.

French M.W., Worden R.H., Lee D.R. (2013) Electron backscatter diffraction investigation of length-fast chalcedony in agate: Implications for agate genesis and growth mechanism. *Geofluids*, Vol. 13, pp. 32–44, http://dx.doi.org/10.1111/gfl.12006.

Gottschaller S. (2012) Wichtige Mineralfundstellen in Marokko. In *Marokko*, extraLapis No. 42, Weise Verlag, Munich, pp. 76–98.

Götze J. (2000) Cathodoluminescence microscopy and spectroscopy in applied mineralogy. *Freiberger Forschungshefte*, C.485, 128 pp.

Götze J., Nasdala L., Kleeberg R., Wenzel M. (1998) Occurrence and distribution of "moganite" in agate/chalcedony: A combined micro-Raman, Rietveld, and cathodoluminescence study. *Contributions to Mineralogy and Petrology*, Vol. 133, No. 1-2, pp. 96–105, http://dx.doi.org/10.1007/s004100050440.

Götze J., Tichomirowa M., Fuchs H., Pilot J., Sharp Z.D. (2001) Geochemistry of agates: A trace element and stable isotope study. *Chemical Geology*, Vol. 175, No. 3–4, pp. 523–542, http://dx.doi.org/10.1016/S0009-2541(00)00356-9.

Götze J., Mockel R., Kempe U., Kapitonov I.,Vennemann T. (2009) Characteristics and origin of agates in sedimentary rocks from the Dryhead area, Montana, USA. *Mineralogical Magazine*, Vol. 73, No. 4, 673–690, http://dx.doi.org/10.1180/minmag.2009.073.4.673.

Graetsch H., Flörke O.W., Miehe G. (1987) Structural defects in microcrystalline silica. *Physics and Chemistry of Minerals*, Vol. 14, No. 3, pp. 249–257, http://dx.doi.org/10.1007/BF00307990.

Grice J.D., Ferraris G. (2000) New minerals approved in 1999 by the Commission on New Minerals and Mineral Names, International Mineralogical Association. *Canadian Mineralogist*,

Vol. 38, No. 1, pp. 245–250, http://dx.doi.org/10.2113/gscanmin.38.1.245.
Heaney P.J. (1993) A proposed mechanism for the growth of chalcedony. *Contributions to Mineralogy and Petrology*, Vol. 115, No. 1, pp. 66–74, http://dx.doi.org/10.1007/BF00712979.
——— (1995) Moganite as an indicator for vanished evaporates: A testament reborn? *Journal of Sedimentary Research A: Sedimentary Petrology and Processes*, Vol. 65, pp. 633–638.
Heaney P.J., Post J.E. (1992) The widespread distribution of a novel silica polymorph in microcrystalline quartz varieties. *Science*, Vol. 255, No. 5043, pp. 441–443, http://dx.doi.org/10.1126/science.255.5043.441.
Jahn S., Bode R., Lyckberg P., Medenbach O., Lierl H-J. (2003) *Marokko – Land der schönen Mineralien und Fossilien*. Bode Verlag. 536 pp.
Kingma K.J, Hemley R.J. (1994) Raman spectroscopic study of microcrystalline silica. *American Mineralogist*, Vol. 79, pp. 269–273.
Legodi M.A., de Waal D. (2006) The preparation of magnetite, goethite, hematite and maghemite of pigment quality from mill scale iron waste. *Dyes and Pigments*, Vol. 74, pp. 161–168, http://dx.doi.org/10.1016/j.dyepig.2006.01.038.
Mayer D. (2012) "Nicht nur" Achate in Marokko. In *Marokko*, extraLapis No. 42, Weise Verlag, Munich, pp. 22–25.
Mernagh T. P. (1991) Use of the laser Raman microprobe for discrimination amongst feldspar minerals. *Journal of Raman Spectroscopy*, Vol. 22, No. 8, pp. 453–457, http://dx.doi.org/10.1002/jrs.1250220806.
Mohr C. (2012) Zur aktuellen Achat-Fundsituation in Marokko. *Mineralien Welt*, Vol. 23, No. 3, pp. 82–89.
Moxon T., Rios S. (2004) Moganite and water content as a function of age in agate: an XRD and thermogravimetric study. *European Journal of Mineralogy*, Vol. 16, No. 2, pp. 269–278, http://dx.doi.org/10.1127/0935-1221/2004/0016-0269.
Moxon T., Nelson D.R. and Zhang M. (2006) Agate recrystallization: Evidence from samples found in Archaean and Proterozoic host rocks, western Australia. *Australian Journal of Earth Sciences*, Vol. 53, No. 2, pp. 235–248.
Pop D., Constantina C., Tatar D., Kiefer W. (2004) Raman spectroscopy on gem-quality microcrystalline and amorphous silica varieties from Romania. *Studia Universitatis Babes-Bolyai Geologia*, Vol. 49, No. 1, pp. 41–52.
Priester M. (1999) Der Achat- und Amethystbergbau in der Region Medio Alto Uruguai in Rio Grande do Sul, Brasilien: Eine geologische und technische Betrahtung. *Zeitschrift der Deutschen Gemmologischen Gesellschaft*, Vol. 48, No. 4, pp. 211–222.
Schwarz D. (2012) Marokko - und dieses Mal keine Achate. *Mineralien Welt*, Vol. 23, No. 2, pp. 85–88.
Strieder A.J., Heemann B. (2006) Structural considerations on Parana basalt volcanism and their implications on agate geode mineralization (Salto do Jacui, RS, Brazil). *Pesquisas em Geociencias*, Vol. 33, No. 1, pp. 37–50.
Swamy V., Muddle B.C., Dai Q. (2006) Size-dependent modifications of the Raman spectrum of rutile TiO_2. *Applied Physics Letters*, Vol. 89, No. 163118, pp. 1–3, http://dx.doi.org/10.1063/1.2364123.
Wesełucha-Birczynska A., Natkaniec-Nowak L. (2011) A Raman microspectroscopic study of organic inclusions in "watermelon" tourmaline from the Paprok mine (Nuristan, Afghanistan). *Vibrational Spectroscopy*, Vol. 57, No. 2, pp. 248–253, http://dx.doi.org/10.1016/j.vibspec.2011.08.001.
Wopenka B., Pasteris J.D. (1993) Structural characterizations of kerogens to granulite-facies graphite; applicability of Raman microprobe spectroscopy. *American Mineralogist*, Vol. 78, pp. 533–557.
Wróbel P., Czyzycki M., Furman L., Kolasiński K., Lankosz M., Mrenca A., Samek L., Wegrzynek D. (2012) LabVIEW control software for scanning micro-beam X-ray fluorescence spectrometer. *Talanta*, Vol. 93, pp. 186–192, http://dx.doi.org/10.1016/j.talanta.2012.02.010.
Verdier J. (1971) Etude géologique des basalts doléritiques du Trias du barrage de Moulay-Yussef au site des Aït-Aadel sur l'oued Tessaout, Haut Atlas. *Notes et Mémoires du Service Géologique du Maroc*, Vol. 31, No. 237, pp. 241–272.
Zenz J. (2005a) *Achat-Schätze*. Edition Mineralien Welt, Salzhemmendorf, 160 pp.
——— (2005b) *Achate*. Bode Verlag, Haltern, Germany, 656 pp. (in German).
——— (2009) *Achate II*. Bode Verlag, Haltern, Germany, 656 pp. (in German).

ABOUT THE AUTHORS

Drs. Dumańska-Słowik (dumanska@uci.agh.edu.pl) and Natkaniec-Nowak are assistant professor and associate professor, respectively, in the Faculty of Geology, Geophysics, and Environmental Protection at the AGH University of Science and Technology in Krakow, Poland. Mr. Gaweł is a researcher at the Laboratory of Phase, Structural, Textural and Geochemical Analyses at the Faculty of Geology, Geophysics and Environmental Protection at the AGH University. Prof. Lankosz is a professor, and Mr. Wróbel a Ph.D. student, in the Faculty of Physics and Applied Computer Science at the AGH University. Dr. Wesełucha-Birczyńska is an associate professor in the Faculty of Chemistry at Jagiellonian University in Krakow.

ACKNOWLEDGMENTS

The authors would like to thank Jolanta and Jacek Szczerba and Remigiusz Molenda for providing several samples. Tomasz Tobola and Małgorzata Klimek are acknowledged for their help with microscopic observations and initiation of this research, respectively. The reviewers made helpful and constructive comments on the manuscript. This work was supported by research statutory grant 11.11.140.319 from the AGH University of Science and Technology.

USEFUL VISUAL CLUE INDICATING CORUNDUM HEAT TREATMENT

John I. Koivula

The heat-induced conversion of limonitic residues to hematite in surface-reaching inclusions provides another useful clue to heat treatment in corundum. Because this alteration happens at such a low temperature, it is virtually unavoidable, during even the most routine heat treatments. The resulting difference in color between the limonitic compounds and the hematite makes this transformation obvious.

Jewelers and trade gemologists generally do not have immediate access to so-called advanced testing instruments of the type found in GIA's laboratories. Instead they rely on traditional techniques taught in gemology courses to give them the results they need. Instruments such as the gemological microscope, refractometer, and spectroscope are their first and sometimes last line of defense. Therefore, any practical means of identifying treated gems is always welcome.

One such example of a straightforward and useful observation involves the heat-induced conversion of brown to yellow hydrous ferric oxides, such as goethite, to bright red to brownish red hematite. Hydrous ferric oxides are deposited epigenetically, after the formation of the host crystal. The deposits occur when hydrous ferric oxide–enriched groundwater invades a crystal's surface-reaching features, such as partially healed secondary and pseudosecondary fractures, cleavage and parting planes, and growth tubes. The residual groundwater then dries out, leaving behind solid hydrated limonitic deposits inside the inclusions.

About the Author: Mr. Koivula (jkoivula@gia.edu) is analytical microscopist at GIA's laboratory in Carlsbad, California.

GEMS & GEMOLOGY, Vol. 49, No. 3, pp. 160–161, http://dx.doi.org/10.5741/GEMS.49.3.160.

At first it might seem simple to duplicate this natural process, but that does not appear to be the case. Under geologic time and conditions, nature deposits these residues through capillarity and varying pressure over long periods, possibly exceeding many millions of years. This depositional cycle may also be repeated many times over.

In this manner, hydrous ferric oxide particles and other particulate residues too large to enter the voids are gradually sifted out. Particles suspended in the circulating groundwater that are fine enough to enter the voids are carried by the water and deposited in the inclusions, either as amorphous solids or as crystalline minerals such as goethite.

EXPERIMENTAL RESULTS

Since a picture is often worth the proverbial thousand words, two unheated natural Sri Lankan sapphires containing typical epigenetic limonitic residues were selected for experimentation. One contained a very intricate, partially healed fracture "fingerprint" decorated with an equally intricate pattern of brownish yellow epigenetic limonite (figure 1, left). As shown in figure 2 (left), the other sapphire hosted a blocky iron sulfide inclusion with a surface-reaching crack that allowed a thin coating of epigenetic limonite to form on the surface, giving the inclusion and the crack a yellow color. In the second example (figure 2) it is not entirely clear whether the epigenetic residue resulted from surface alteration of the sulfide inclusion, groundwater deposition, or both.

As previously stated, one of the primary mineral constituents of limonite is goethite, an orthorhombic mineral with the chemical formula α-FeO(OH). When these two epigenetically stained sapphires were heated in air to the relatively low temperature of 350°C, the goethite (limonite) yielded water and converted to the trigonal mineral hematite, α-Fe_2O_3, through the chemical reaction:

$2\alpha\text{-FeO(OH)} \rightarrow \text{heat } 350°C \rightarrow \alpha\text{-}Fe_2O_3 + H_2O$

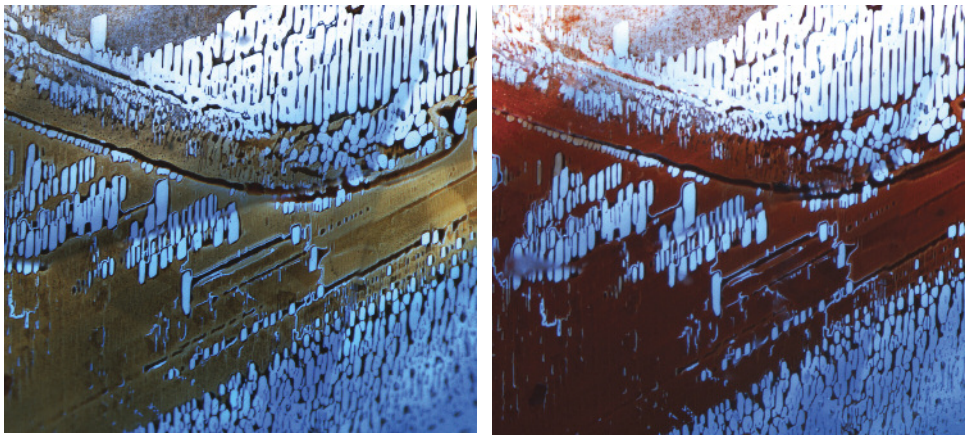

Figure 1. Left: Shown before heating, this Sri Lankan sapphire hosts an intricate partially healed fracture "fingerprint" decorated with brownish yellow epigenetic limonite. Right: After heating to just 350°C, the limonitic deposit in the fingerprint has been converted through dehydration to brownish red hematite. Photomicrographs by J.I. Koivula; magnified 60×.

Figure 2. Left: This Sri Lankan sapphire hosts a blocky iron sulfide inclusion with a surface-reaching crack, both of which are coated with yellow limonite. Right: After heating in air to 350°C, the limonite coating on both the sulfide and the related fracture changed to rust-colored hematite. Photomicrographs by J.I. Koivula; magnified 10×.

The obvious change undergone in this relatively simple heat-induced conversion is evident when comparing the pre-treatment and post-treatment images in figures 1 and 2. While the limonite is brownish yellow to yellow, the hematite has a rusty-looking brownish red color (figures 1 and 2, right).

Given the low temperature involved, it should be evident that the alteration of limonite (goethite) to hematite could happen in virtually any other gem material during routine heat treatment. Two examples include the conversion of amethyst to citrine (Koivula, 1987) and the change of color shown by limonite-stained etch ribbons in so-called rutilated topaz (Kammerling and Koivula, 1989).

CONCLUSION

The field of gemology has become highly technical, and advanced testing using an expanding variety of machines is now routine in some situations. Still, traditional non-destructive gemological testing techniques should not be ignored or forgotten. Careful microscopic observation, refractive index, calculated specific gravity, a spectrum obtained through a handheld spectroscope, or screening with UV radiation still provide enough information to answer many critical questions. Applying those methods can eliminate unnecessary advanced testing, while also serving as a guide for further analysis.

REFERENCES

Kammerling R.C., Koivula J.I. (1989) Thermal alteration of Inclusions in "rutilated" topaz. *G&G*, Vol. 25, No. 3, pp. 165–167, http://dx.doi.org/10.5741/GEMS.25.3.165.

Koivula J.I. (1987) Goethite inclusion alteration during the heat conversion of amethyst to citrine. *The Australian Gemmologist*, Vol. 16, No. 7, pp. 271–272.

THREE OCCURRENCES OF OREGON SUNSTONE

Duncan Pay, Robert Weldon, Shane McClure, and Kevin Schumacher

Figure 1. The sparsely populated high desert of eastern Oregon is home to three localities producing natural copper-bearing labradorite feldspar. In this view of Lake County's Dust Devil mine, the local source of the sunstone-bearing lavas is the group of rounded hills (Dudeck Ridge) in the background. Photo by Robert Weldon.

Over five days in late July 2013, we visited three important sources of gem-quality sunstone in eastern Oregon: the Ponderosa mine in Harney County, and the Dust Devil (figure 1) and Sunstone Butte mines, both of which are about 120 miles further south, in Lake County.

Oregon sunstone, the official state gemstone since 1987, is natural copper-bearing labradorite feldspar. Some examples exhibit red to green dichroism, and fine specimens (figure 2) larger than 5 ct can sell for more than $1,000 per carat.

Feldspars are silicate minerals that contain variable amounts of sodium (Na), potassium (K), and calcium (Ca). Labradorite belongs to the plagioclase feldspar series, which forms a solid solution between anorthite ($CaAl_2Si_2O_8$) and albite ($NaAlSi_3O_8$). Oregon sunstone, which contains substantially more calcium than sodium, has a composition of about 70% anorthite and 30% albite, or An^{70}/Ab^{30}. For more on feldspar classification and nomenclature, see box B in Rossman (2011).

No discussion of this topic would be complete without mention of the controversy surrounding treated copper-bearing feldspar; Rossman (2011) provides a chronology. In the early 2000s, Asian treaters perfected a method of diffusing copper into pale feldspar, flooding the market with low-priced, attractive red and green gems—which destabilized the market for Oregon sunstone. Promoted as "andesine" and purportedly from mines in Congo or Tibet, this material was subsequently found to be treated, but the resulting furor hindered the public's trust in natural copper-bearing feldspar. Despite this setback, Oregon sunstone miners have strived to rebuild the market, and there are signs of renewed consumer interest in their one-of-kind gem.

TRIP OBJECTIVES

This paper incorporates trip findings and previous GIA research to provide a comparative analysis of the

Figure 2. This superb 2.85 ct sunstone from Sunstone Butte displays the gem's most valued attributes: a blend of green and red bodycolor, with reflective spangles of native copper glittering in the interior. Photo by Robert Weldon.

See end of article for About the Authors and Acknowledgments.
GEMS & GEMOLOGY, Vol. 49, No. 3, pp. 162–171,
http://dx.doi.org/10.5741/GEMS.49.3.162.

gem materials and their geological context and history. We also hope to initiate research that will answer some open questions:

- Are all the eastern Oregon sunstone occurrences the same age?
- How do sunstone occurrences correlate with the local geology?
- How did the very uneven color distribution develop in fractured crystals?
- Are sunstones from each of the three mines distinguishable?

In 2006, GIA collected gems from the Ponderosa and Dust Devil mines to characterize natural Oregon sunstone and help distinguish it from treated material (McClure, 2009). For the present study, we collected representative suites of gem materials and rock samples from each mine, documenting the GPS coordinates of each find. By performing argon-argon ($^{40}Ar/^{39}Ar$) dating on basalt samples and labradorite feldspar crystals from the Ponderosa mine, we hope to confirm the age of its sunstone-bearing basalt and compare that to the Lake County mining locations. We also intend to perform petrographic analyses to characterize the gem-bearing rocks from each deposit and determine their context within the surrounding geology.

We intend to publish the results of these studies in a future *G&G* feature article and on the GIA website.

LOCATION AND ACCESS

Past stratovolcanoes of the High Cascades and across Oregon's remote High Lava Plains lie three sunstone mines (figure 3). All three produce labradorite feldspar ranging from near-colorless to pale yellow to red and green, including bicolor specimens. The sunstone often contains tiny reflective platelets of native copper, referred to as "schiller."

From Portland, we drove five hours southeast to Ponderosa, near the town of Burns. We spent three days there before driving three hours southwest to spend the next two days at the Dust Devil and Sunstone Butte mines. These deposits are referred to in the literature as the Lakeview, Lake County, Plush, or Rabbit Basin occurrences.

GEOLOGIC CONTEXT

In eastern Oregon, sunstone occurs as *phenocrysts* in highly *porphyritic* basalt flows (see figure 4). They are a minor but fascinating part of the region's recent geologic history, likely originating during an episode

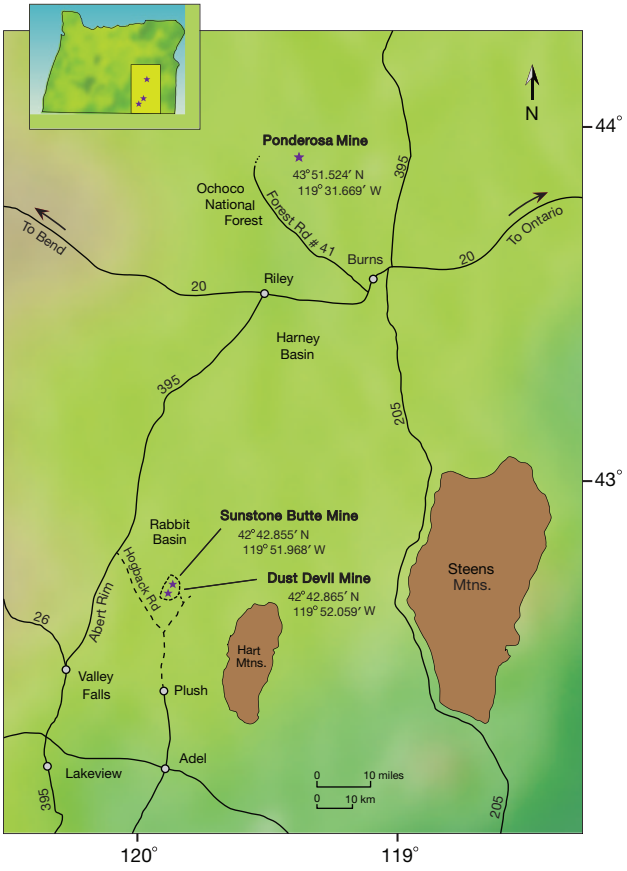

Figure 3. This map shows the location of the three mines visited in eastern Oregon. Illustration by Larry Lavitt.

of widespread basaltic volcanism that occurred 15–17 million years ago (Ma), during the Miocene epoch. Geologists debate whether the volcanic events were caused by melting of subducted oceanic crust or by a hot plume in the earth's mantle. The Steens Basalt of the Oregon Plateau (figure 5), where volcanic flow deposits can contain up to 50% large feldspar crystals (Walker, 1979), erupted around the same time as the more extensive Columbia River basalts further north. $^{40}Ar/^{39}Ar$ dating indicates the eruptions took place between 15.51 +/- 0.28 Ma and 16.59 +/- 0.10 Ma (Brueseke et al., 2007).

Considerable work has recently been done on the geology of eastern Oregon, principally under the aegis of the High Lava Plains Project, supported by the Carnegie Institute of Washington's Department of Terrestrial Magnetism (www.dtm.ciw.edu/research/HLP). This project sought to explain Oregon's recent (<20 Ma) volcanic history through the work of specialists in petrology, geochemistry, geochronology, and geophysics. Their studies provided a much better understanding of the dynamics of plate subduction and magmatism under the Pacific Northwest.

Figure 4. This specimen of basalt porphyry from Ponderosa shows a gem-quality sunstone phenocryst surrounded by smaller non-gem feldspar crystals. A porphyry *is an igneous rock consisting of large crystals (*phenocrysts*) in a finer-grained matrix or groundmass. Photo by Robert Weldon.*

According to Stewart (1966), the sunstone lavas within the Rabbit Basin are petrographically similar to plagioclase-rich flows within the Steens Basalt. They are also strikingly similar to lava flows exposed at the Abert Rim, a spectacular fault scarp some 760 meters (2,490 feet) high, located 10–15 miles southwest of the Rabbit Basin sunstone localities. Gunn and Watkins (1970) proposed that these lavas are part of the same volcanic episode, and that their feldspar phenocrysts might even have originated in the same magma chamber. In a future visit, we aim to collect representative samples from plagioclase-rich flows at Abert Rim and Steens Mountain and compare them with material from each of the three mines to see if we can confirm their relationships.

Feldspar phenocrysts that formed before eruption are surrounded by a finer-grained or glassy groundmass of the lava flow. Also contained in such groundmasses are smaller labradorite phenocrysts (An^{60}), usually just a few millimeters in size, that crystallized in the flow as it cooled. Stewart's analysis (1966) gave a composition of $An^{67.2}/Ab^{31.5}/Or^{1.3}$ for the larger feldspar phenocrysts and An^{60} for the smaller labradorite phenocrysts in the groundmass. We intend to perform Ar-Ar dating on samples of basalt and feldspar phenocrysts from all three mine locations to determine their relative ages.

The feldspar must have formed over time within a magma chamber of calcium-rich magma that cooled slowly, allowing it to reach considerable size. Stewart (1966) proposed that primary crystallization occurred at depth under relatively uniform conditions of about 1100°C. He cited a large lath-shaped

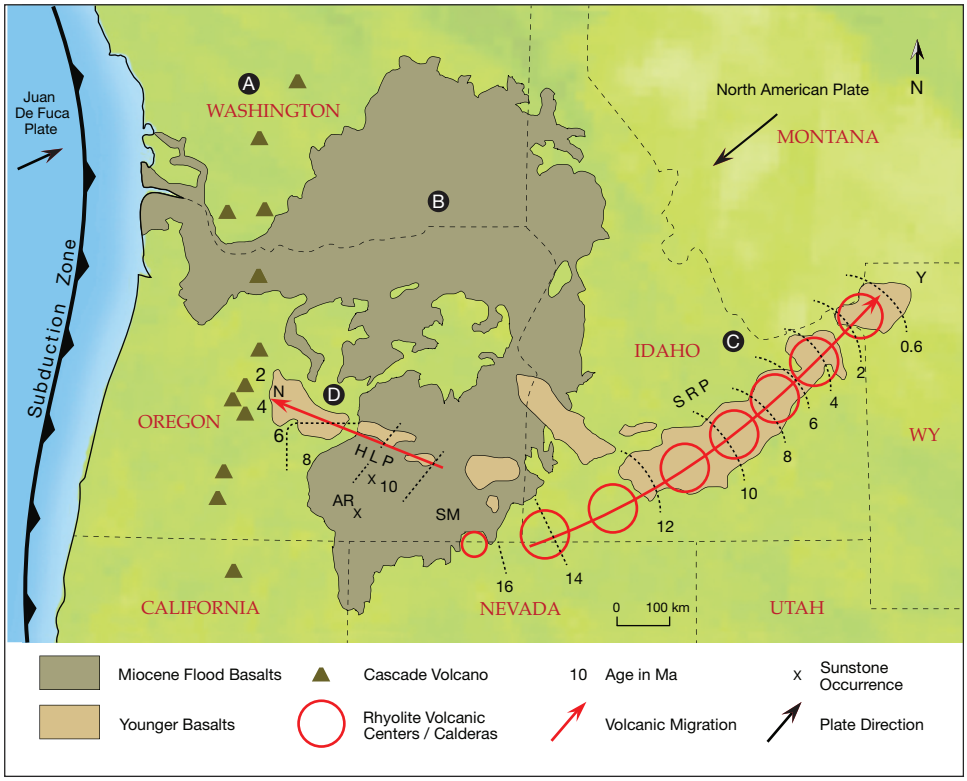

Figure 5. The High Cascade stratovolcanoes (A) are fueled by subduction under the Pacific Northwest. Flood basalts (B) inundated Oregon 15–17 million years ago. Sunstone occurrences (×) are linked to the local eruptive center of these basalts, Steens Mountain (SM) and Abert Rim (AR). As the basalts ebbed, new volcanic forces kindled a hot spot in the earth's mantle, spawning volcanic calderas (C) across Idaho's Snake River Plain (SRP) to the Yellowstone supervolcano (Y). Meanwhile, renewed activity (D) moved west across Oregon's High Lava Plains (HLP) to Newberry Caldera (N). Illustration by Larry Lavitt, adapted from Long (2009) and Grunder and Meigs (2009).

Figure 6. At a section of freshly dug pit wall in the red zone, red cores of fragmented sunstone crystals glint in the sun. Photo by Robert Weldon.

crystal measuring 8.3 × 2.6 × 0.8 cm. This is a substantial crystal by most standards, but we found larger, blockier ones at the Sunstone Butte mine. This might be because the crystals at Sunstone Butte cooled more slowly in a larger body of rock—within a cinder cone—and were not extruded in thinner lava flows, as elsewhere in the Rabbit Basin. As a result, there appears to be less fracturing due to thermal and mechanical shock, and intact crystals are recovered more frequently.

PONDEROSA MINE

The road to the Ponderosa mine gains in elevation as the scenery gradually changes from meadows to thick stands of tall ponderosa pines. It is classic volcanic highland, littered with cinder cones, extensive basalt flows, ashfall tuffs, and red cinder beds.

A map drawn by John Woodmark, Ponderosa's owner and the president of Desert Sun Mining & Gem Co., led us to the mine, where we stayed in a bunkhouse. Woodmark purchased the property in 2003. For earlier history of the Ponderosa mine, see Johnston (1991) and Sinkankas (1997).

The mine is located at an elevation of 1,753 meters (5,700 feet) on the southwest side of Donnelly Butte. The mining season runs from June to October, when the mine is free of snow. Because Woodmark owns the property, it is not subject to regulation from the Bureau of Land Management or other government agencies.

The mine site covers some 60 acres (just over 24 hectares). Although only one-fourth of an acre has been mined to a depth of 6 meters (20 feet), Woodmark said that sunstone occurs throughout the property.

Johnston (1991) reported on the Ponderosa mine and its gem materials, characterizing the labradorite as 70% anorthite and 30% albite, placing it at the labradorite/bytownite boundary.

The sunstone occurs in a localized, weathered basalt flow (figure 6). So far, this is the only one of four basalt flows examined at the site that contains sunstone. The basalt being mined is moderately to heavily weathered, reduced to reddish brown soil containing nuggets of harder basalt in sections of the pit. Currently, Woodmark is recovering higher than normal quantities of red to pink rough from a section of the pit—approximately 20% of the sunstone mined. In 2010, his estimated recovery rate of red to pink rough was around 2–4%.

The working area of the mine has more than doubled since being documented by Johnston (1991), but it still represents a relatively small area. This is because of the high concentration of feldspar in the decomposed basalt. Woodmark estimates a recovery rate of 1.5 kg of rough per cubic yard of earth moved and a possible reserve of more than a trillion carats of cuttable rough. In his opinion, this would make the Ponderosa one of the richest colored gemstone mines in the world.

Ponderosa produces 1 million carats of rough per year (figures 7–9) over the course of approximately 20 days (in three or four increments). Woodmark estimates he could mine 4–6 million carats per year, given sufficient demand. Currently there are only a handful of people to drive the loaders and operate and maintain the other equipment. The mine also employs Native

Figure 7. This loader transfers crushed basalt ore to a dry trommel, separating rock and feldspar crystals from the decomposed basalt, which is essentially dirt. Photo by Robert Weldon.

Figure 8. Pickers, including John Woodmark (foreground), load concentrate onto mesh screening tables at Ponderosa. They methodically sweep the table with a trowel, leaving "no stone unturned." Photo by Duncan Pay.

American teenagers from the nearby reservation. Woodmark pays the pickers $10 per kilogram of concentrate recovered. Each picker averages 1 kg per hour.

He personally grades the rough, first by color (red, orange, pink, yellow, colorless, green, bicolor, or schiller) and then by size. The strategy is geared toward providing a consistent supply of calibrated gems less than 7.0 mm in well-defined grades. These smaller stones are cut overseas. Woodmark does not trim or cob the rough, leading to lower yields (approximately 12% recovery, or 500–600 carats per kilogram). Larger fine-color or clear rough is supplied to designer cutters for high-priced, one-of-a-kind gems.

Woodmark stockpiles the colorless and yellow material because it is so easily treatable (Emmett and Douthit, 2009), and he is concerned it could harm the market for untreated Oregon sunstone. Woodmark is considering bead production as a source of revenue from this clear to champagne-colored rough.

Figure 9. During screening, sparks of red to pink rough sunstone glitter in the sun among pea-sized chunks of vesicular basalt. Photo by Robert Weldon.

DUST DEVIL MINE

The Rabbit Basin lies three hours south of Burns, through a desolately beautiful landscape of alkaline lakes, sand dunes, and volcanic ridges. Alt and Hyndman (1978) provide a brief summary of the roadside geology. At Hogback Road, the paved surface ends and 35 miles of gravel road begins, leading eventually to the Dust Devil mine.

Travel trailers punctuate the desert, marking the sites where miners are working claims. At 1,402 meters (4,600 feet), this is high desert country dotted with sagebrush. No permanent structures are permitted by the Bureau of Land Management, and mining activities are subject to strict environmental regulations. As with the Ponderosa mine, the weather dictates the mining season, which runs from mid-May to mid-October, when the first snows typically fall.

The sunstone-bearing basalts cover about seven square miles (18 km^2) at the northern end of the basin. They are a sequence of gray to strong reddish brown vesicular flows that form low rounded hills, reaching their highest point at Dudeck Ridge. The flows are typically only 3–6 meters (10–20 feet) thick, narrowing considerably toward the edges. The bedrock beneath the sunstone basalts is a gray-brown ashflow tuff of variable thickness. Underneath the tuff lies a vesicular black basalt (Peterson, 1972).

Figure 10. Left to right: Dust Devil employee Mark Shore, owners Terry Clarke and Don Buford, and gemologist Mariana Photiou, who works with the miners and helps market the gem. Photo by Robert Weldon.

Figure 12. Terry Clarke holds a screen up to the sun, letting transparent gems reveal themselves as glints in the light. Photo by Robert Weldon.

According to Don Buford, co-owner of the Dust Devil mine, thin flows cool rapidly, exerting pressure on crystals as they contract and causing extensive fracturing. Thicker flows cool more slowly, exerting less stress on the crystals and allowing them to retain their size. Phenocryst fracturing may also be due to movement and mechanical contact between crystals within the lava flow during emplacement (Peterson, 1972).

Buford and co-owner Terry Clarke (figure 10) have been very active in marketing untreated Oregon sunstone. Gems from Dust Devil have been used by notable artists such as Dalan Hargrave, Will Cox, Larry Winn, Larry Woods, Krista McMillan, and John Dyer to garner more than 15 American Gem Trade Association (AGTA) Cutting Edge awards. A pit operation with a modern separation plant (figures 11–14), the

Figure 11. Left: Mark Shore recovers a large sunstone crystal from its matrix as Don Buford observes. Right: Three principal stones with bodycolor or schiller totaling almost 300 carats, along with 500 carats of pale yellow stones, were recovered from this fragmented crystal; courtesy of Mark Shore, Dust Devil Mining Co. Photos by Robert Weldon.

Figure 13. Dust Devil uses heavy-duty excavators to mine the basalt ore, which is processed by a grizzly (a grille with evenly spaced bars to exclude larger rock). The basalt ore then passes through a sequence of conveyors to a shaker, a wet trommel, a hopper, and a belt for handpicking. Some of the ore goes to an optical sorting machine, depending on the mine's production needs. Photo by Robert Weldon.

mine is known for its variety of stone colors and sizes up to 1,093 ct—nearly as large as a tennis ball.

At the mine, we both witnessed and captured on video the careful recovery of crystal fragments by employee Mark Shore (figure 11, left). The fine sunstone crystal in figure 11 (right), mined from a decomposed basalt nodule, would have constituted an 841.74 ct stone if found in one piece.

This crystal is a telling example of the challenges facing the sunstone miner and the gem cutter: It is highly fractured and has the most desirable colors confined to zones in its interior, restricting the size and orientation of the gems that can be cut from it.

Figure 14. According to Don Buford, each ton of basalt from the Dust Devil mine yields one pound of sunstone rough—75% colorless or yellow, 25% red, green, bicolor, or blue, and less than 1% fine deep red. Photo by Duncan Pay.

These limit the cutter's choices and make it challenging to produce fine gems. The recovery yielded the following:

- 86.64 ct (3.5 × 3.3 × 1.7 cm): pale yellow rim with an orange-red core
- 110.99 ct (5.8 × 1.7 × 1.3 cm): pale yellow rim with an orange-red core and a touch of green on the periphery
- 101.63 ct (4.0 × 2.2 × 1.4 cm): orange-red core with intense schiller and a narrow green periphery
- The remaining pieces were pale yellow: one 45.29 ct specimen, three totaling 100.49 carats, four totaling 80.89 carats, and a bag of assorted yellow shards totaling 315.81 carats.

Rossman and Hofmeister (1985) confirmed a correlation between sunstone's copper concentration and its aventurescence and color. They proposed an excellent model for precipitation of native copper and subsequent development of red and green colors in sunstone during cooling, but their paper does not discuss color zones and distribution of schiller relative to conchoidal fractures within the gems.

Most crystals are fractured and therefore difficult to recover intact. Pough (1983) drew a correlation between sunstone's color distribution and its conchoidal fractures: Red and green colors—along with schiller—tend to be limited to the cores of phenocrysts, rarely reaching fracture surfaces (again, see figure 11, right).

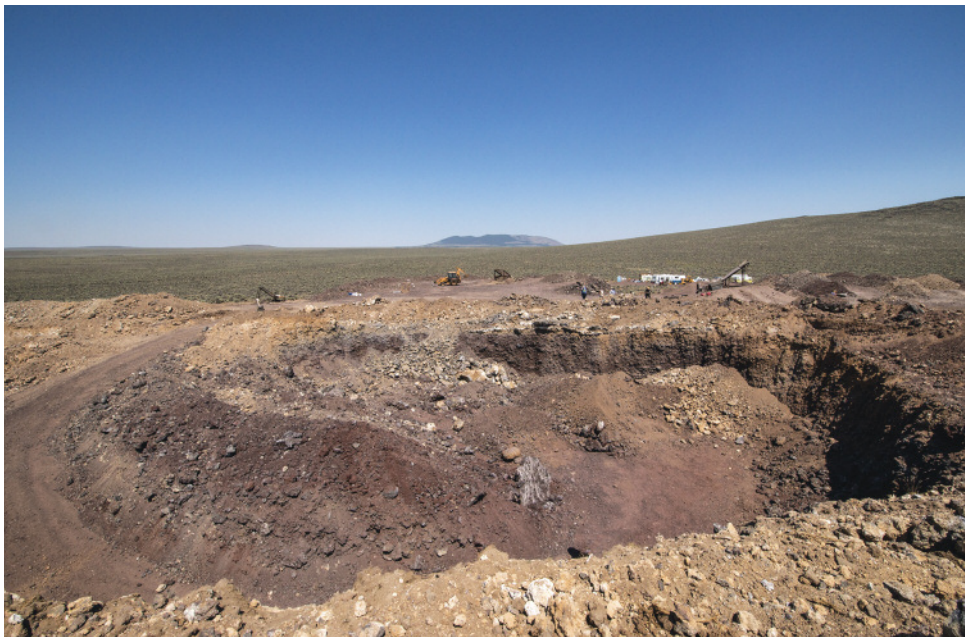

Figure 15. The main pit of the Sunstone Butte mine lies in a cinder cone that forms a small hill above the surrounding desert. Photo by Robert Weldon.

We plan to investigate whether copper can be leached from crystals after emplacement by a secondary process. The example shown in figure 11 would be ideal for chemical analysis, as we know that all its fragments came from a single crystal.

SUNSTONE BUTTE MINE

A new deposit, Sunstone Butte (figure 15), has become known among boutique jewelry designers since 2011 for its large green, red, and bicolor gems. According to mine owners Dave Wheatley and Tammy Moreau, 45–50% of the gem-bearing "ore" is volcanic cinder as opposed to the basalt flows at the other Rabbit Basin mines. They told us that the most notable aspects of the mine's production are the size of the crystals and their green colors. Crystals often reach 100 ct, and sometimes up to 500 ct (figure 16). About 75% of the sunstones have green coloration, many with bluish green "teal" hues.

The rock is far less decomposed than at the other locations we visited. The claim owners are essentially mining into the top of the cone. Possibly because it is a much thicker body of rock—which cooled more slowly than the thinner lava flows elsewhere in the basin—the crystals are much larger and often recovered whole. Some exceed 10 cm in length (figure 17),

Figure 16. This rough sunstone measures approximately 5 cm (2 inches) in length. Note how the green core follows the contours of the rough. The green core is characteristic of material from this mine. Photo by Duncan Pay.

Figure 17. This large, blocky labradorite feldspar crystal from the Sunstone Butte mine measures approximately 10 × 5 × 5 cm (4 × 2 × 2 inches). Photo by Duncan Pay.

Figure 18. Sunstone Butte co-owner Tammy Moreau taps on the back of a piece of volcanic matrix with a small hammer to release feldspar phenocrysts. Photo by Robert Weldon.

which is extraordinary for this type of deposit. Due to the slower cooling of the magma that contained them, they also seem much less internally fractured. The crystals may also have suffered less mechanical stress because they remained within the mass of the cinder cone rather than being extruded in a lava flow.

Wheatley mines the cinder cone using an excavator. Ore is transported to a separator and screened down to less than 20 cm in size and run through a small processing plant where crystals are removed from their volcanic matrix. From there, the material is reduced to fist-sized pieces with a small hammer, allowing the crystals to be handpicked (figure 18). Lastly, the miners remove any remaining volcanic residue—essentially a hard red crust—from the crystals by tumbling them in a cement mixer with water for a couple of hours.

The gems from Sunstone Butte are among the finest we have seen, notable for their size and clarity as well as their dichroic nature. In addition to exploring mining processes, we observed fashioned sunstones (figure 19) as both single pieces and suites of contemporary cuts, many featuring red, bicolor, or schiller stone pairings to maximize the appearance of yellow to colorless material. We collected more than 500 video segments and 1,500 photos, as well as several kilograms of samples for further study, including whole crystals and typical bicolor and red crystal fragments.

These samples will add to our understanding of these deposits and their unique gem materials. The emergence of new material from Sunstone Butte, adding to the consistent commercial supply from the Ponderosa and Dust Devil mines, indicates that the market for Oregon sunstone could grow.

Figure 19. These three gems from Sunstone Butte illustrate the range of colors the mine produces: a 2.40 ct green "Plush" cut, a 4.95 ct pale yellow "snowflake" cut, and a 7.95 ct "spinel-color" red gem. Photo by Robert Weldon.

REFERENCES

Alt D.D, Hyndman D.W. (1978) *Roadside Geology of Oregon*. Mountain Press Publishing Co., Missoula, MT.

Brueseke M.E., Heizler M.T., Hart W.K., Mertzman S.A. (2007) Distribution and geochronology of Oregon Plateau (U.S.A.) flood basalt volcanism: The Steens Basalt revisited. *Journal of Volcanology and Geothermal Research*, Vol. 161, No. 3, pp. 187–214, http://dx.doi.org/10.1016/j.jvolgeores.2006.12.004.

Emmett J.L., Douthit T.R. (2009) Copper diffusion in plagioclase. GIA Thailand, www.giathai.net/pdf/Red_Feldspar_2009_Emmett.pdf, August 21.

Gunn B.M., Watkins N.D. (1970) Geochemistry of the Steen Mountain Basalts, Oregon. *Geological Society of America Bulletin*, Vol. 81, No. 5, pp. 1497–1516.

Hofmeister A.M., Rossman G.R. (1985) Exsolution of metallic copper from Lake County labradorite. *Geology*, Vol. 13, No. 9, pp. 644–647, http://dx.doi.org/10.1130/0091-7613(1985)13<644:EOMCFL>2.0.CO;2.

Johnston C.L., Gunter M.E., Knowles C.R. (1991) Sunstone labradorite from the Ponderosa mine, Oregon. *G&G*, Vol. 27, No. 4, pp. 220–233, http://dx.doi.org/10.5741/GEMS.27.4.220.

McClure S.F. (2009) Observations on identification of treated feldspar. GIA Thailand, www.giathai.net/pdf/Red_Feldspar_2009_Mcclure.pdf, September 10.

Peterson N.V. (1972) Oregon sunstones. *Ore Bin*, Vol. 34, pp. 197–215.

Pough F.H. (1983) Heliolite, a transparent facetable phase of calcic labradorite. *Journal of Gemmology*, Vol. 18, No. 6, pp. 503–514.

Rossman G.R. (2011) The Chinese red feldspar controversy: Chronology of research through July 2009. *G&G*, Vol. 47, No. 1, pp. 16–30, http://dx.doi.org/10.5741/GEMS.47.1.16.

Sinkankas J. (1997) *Gemstones of North America: Volume III*. GeoScience Press Inc., Tucson, AZ.

Stewart D.B., Walker G.W., Wright T.L., Fahey J.J. (1966) Physical properties of calcic labradorite from Lake County. *The American Mineralogist*, Vol. 51, January–February, pp. 177–197.

Walker G.W. (1979) Revisions to the Cenozoic stratigraphy of Harney Basin, Southeast Oregon. *Geological Survey Bulletin 1475*, United States Department of the Interior, Washington DC, 35 pp. [see pubs.usgs.gov/bul/1475/report.pdf].

ABOUT THE AUTHORS

Mr. Pay (dpay@gia.edu) is editor-in-chief of Gems & Gemology. *Mr. Weldon is manager of photography and visual communications at GIA in Carlsbad. Mr. McClure is director of identification at GIA's Carlsbad laboratory. Mr. Schumacher is digital resources specialist at GIA in Carlsbad.*

ACKNOWLEDGMENTS

The authors would like to thank all the sunstone miners for their generosity of spirit and the time they committed to showing us every detail of their mining operations; nothing was too much trouble, and we were made to feel at home everywhere we visited. We thank John Woodmark and his crew at the Ponderosa mine; Don Buford, Terry Clarke, and Mark Shore at the Dust Devil mine; Dave Wheatley, Tammy Moreau, and David Grey at the Sunstone Butte mine; along with Nirinjan Khalsa and especially Mariana Photiou for their help liaising with the miners.

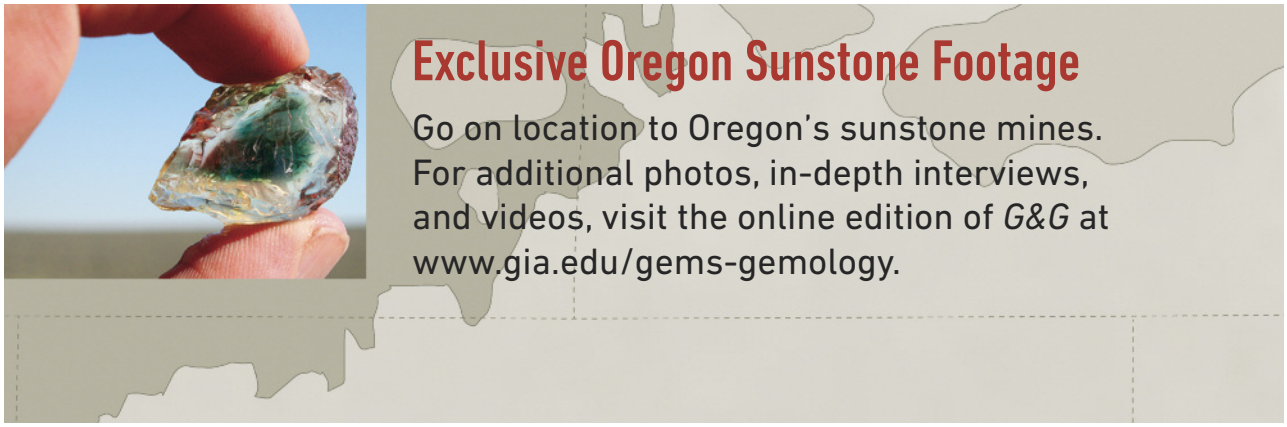

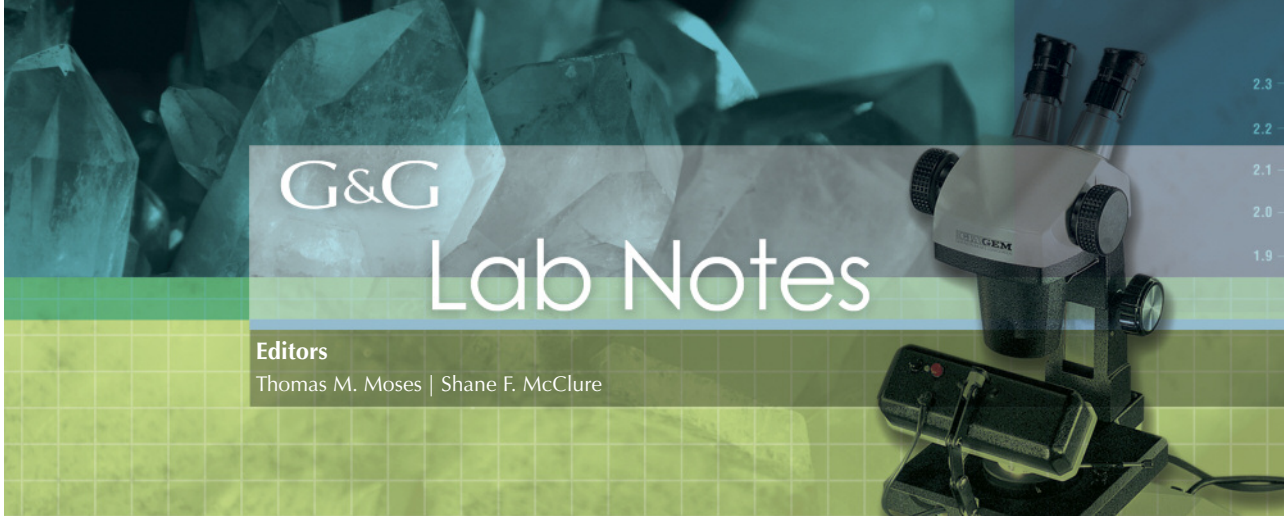

Imitation Rainbow Moonstone ASSEMBLAGE

The Carlsbad laboratory recently received for examination four semitransparent to translucent cabochons with a white bodycolor (figure 1), ranging from 1.74 to 10.57 ct. These stones appeared similar to white plagioclase feldspar with multicolor iridescence, known in the trade as "rainbow moonstone" (Summer 1997 Gem News, pp. 144–145). However, a cursory examination proved they were distinctly different: assembled materials composed of a colorless, transparent base cemented to a fibrous white top and coated with a colorless plastic. The stones also displayed an unusual iridescence.

The colorless plastic coating had an RI of 1.55, but this was not useful in identifying the substrate components. The assembled stone fluoresced medium blue to long-wave UV and weak blue to short-wave UV. In polarized light, a bull's-eye optic figure was resolved in the colorless base material, confirming rock crystal quartz; small fluid inclusions and reflective particles in the bottom sections indicated natural origin. Raman spectroscopy conclusively identified the fibrous top as gypsum.

Microscopic examination revealed an iridescent coating on the quartz section, much like that used on "Aqua Aura" quartz (Fall 1990 Gem News, pp. 234–235). Closer inspection revealed that the iridescent coating was located on the quartz in the join. The colorless plastic coating contained numerous gas bubbles and was easily deformable with a pointer probe. This plastic layer was apparently added to give a vitreous luster to the otherwise dull, waxy gypsum. Gas bubbles in the colorless cement layer made it quite easy to recognize these stones as assemblages.

Figure 1. These assembled cabochons (1.74–10.57 ct) with multicolor iridescence are a skillful imitation of rainbow moonstone. They are composed of a natural rock crystal quartz base with an iridescent coating cemented to a gypsum top, and the entire assemblage is coated in colorless plastic.

When viewed face-up, the assemblages made an attractive imitation of rainbow moonstone due to their white bodycolor, milky appearance, and rainbow iridescence. This is the second time the Carlsbad laboratory has examined an assemblage containing plastic-coated gypsum (Fall 2012 Lab Notes, pp. 210–211). Coupling a luster-enhancing coating with an iridescent layer created an interesting imitation rainbow moonstone from two common materials.

Amy Cooper, Nathan Renfro, and Tara Allen

An Enormous South Sea CULTURED PEARL Filled with Cultured Pearls

Known for their size, South Sea cultured pearls can attain a diameter of 20 mm or more. A massive baroque white South Sea cultured pearl weighing 49.55 ct and measuring 27.12 × 23.23 × 21.67 mm (figure 2) was recently submitted to the New York laboratory for identification. Besides its remarkable size, we noted a small corner section

Figure 2. The large 49.55 ct South Sea cultured pearl (left) is shown alongside a typical 13 mm South Sea cultured pearl.

Editors' note: All items were written by staff members of GIA laboratories.

GEMS & GEMOLOGY, Vol. 49, No. 3, pp. 172–177, http://dx.doi.org/10.5741/GEMS.49.3.172.

Figure 3. A small pearl was plugged into this opening in the baroque pearl.

with a circular gap highlighted by a yellowish glue-like material (figure 3). This feature suggested that a smaller pearl with similar color and luster had been used to fill an opening in the baroque cultured pearl.

Microradiography revealed that this smaller pearl was a nonbead-cultured pearl with an irregular linear dark central growth feature (figure 4, top). Both pearls originated from a salt-water environment, according to energy dispersive X-ray fluorescence (EDXRF) spectroscopy. Surprisingly, microradiography revealed three additional bead-cultured pearls within the large baroque specimen (figure 4, bottom). These three cultured pearls showed their own distinct bead demarcations and had all been drilled through. The large void was filled with an unknown substance that prevented the three pearls from moving around.

Although we occasionally see filled or plugged pearls (see D. Hargett, "Unusually large worked and plugged cultured pearl," Winter 1991 Lab Notes, p. 251), this was the first time we had encountered a South Sea cultured pearl filled with multiple bead-cultured pearls. We believe this enormous pearl was originally cultured with a single bead nucleus, but that somehow the bead emerged through an opening. To maintain the specimen's weight and durability, the three bead-cultured pearls were used to fill the void and the opening was plugged with a smaller nonbead-cultured pearl.

Surjit Dillon Wong and Joyce WingYan Ho

Figure 4. The baroque pearl's internal structure suggested a nonbead cultured pearl (top). X-radiography showed that three bead cultured pearls were used to fill the void (bottom).

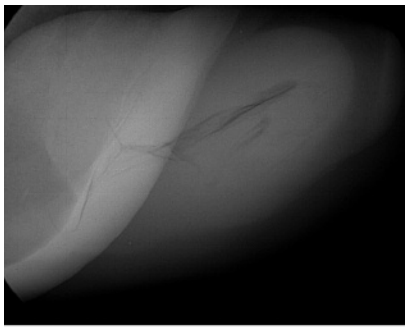

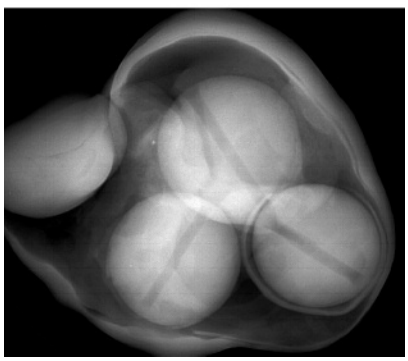

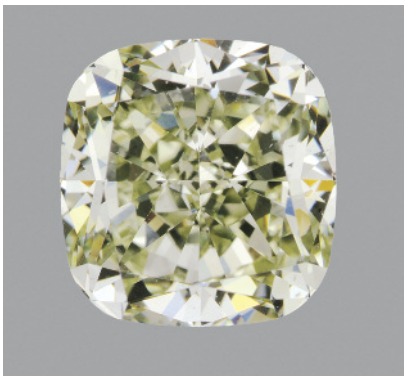

Figure 5. This 2.54 ct Fancy Light greenish yellow diamond showed a high quantity of nickel, believed to be related to its fancy color saturation.

DIAMOND

With High Concentration of Nickel

A 2.54 ct cushion-cut diamond (figure 5) was color graded as Fancy Light greenish yellow. Its UV-Vis-NIR spectrum showed a large absorbance caused by nickel-related defects (figure 6). It is unusual for a diamond to be solely colored by nickel, and more so for the diamond to be graded in the

Figure 6. This UV-Vis-NIR spectrum shows an unusually large absorption band related to nickel defects in diamond.

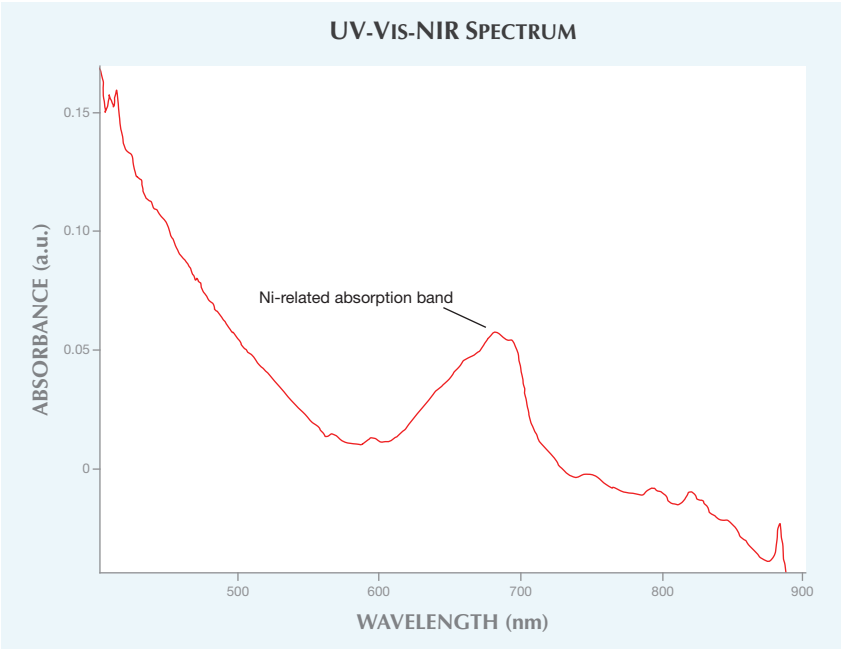

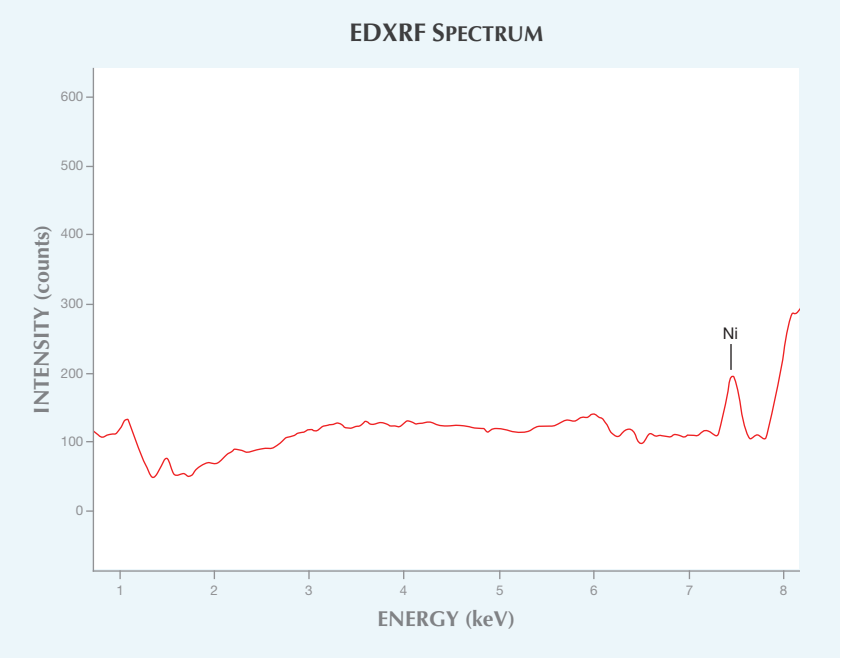

Figure 7. The greenish yellow diamond's EDXRF spectrum shows a clear peak at 7.5 keV, a characteristic peak of nickel.

fancy color range. Such diamonds have been previously reported (W. Wang et al., "Natural type Ia diamond with green-yellow color due to Ni-related defects," Fall 2007 *G&G*, pp. 240–243), but this was the first time energy-dispersive X-ray fluorescence (EDXRF) spectroscopy has been run to detect the presence of nickel. As seen on the XRF spectrum (figure 7), the nickel content was high enough to be detected. This is likely related to the diamond's fancy color saturation.

In addition to its unusual color origin, the diamond contained a mineral inclusion with a color-change effect. It appeared purple under the incandescent well light of a gemological microscope and dark blue under the fluorescent overhead light on the same microscope. We suspected the inclusion was a color-change garnet, and this was confirmed using Raman spectroscopy. The stone also contained a small cloud of oriented reflective inclusions associated with type IaA diamonds, consistent with this sample's diamond type. The diamond showed weak green transmission, which was unusual because it had no defects commonly associated with green transmission (i.e., the H3 feature). Whether the transmission is related to the nickel content is not known.

Troy Ardon

Unusual Laser Manufacturing Remnant

It is common to see laser manufacturing remnants on diamonds, especially stones in blocked form where the cut is not finished. Cutters may use lasers to show where to cut, which features to remove, or the desired shape. The remnants usually appear as straight or sinusoidal lines along the areas to be cut or removed.

Figure 8. The 0.9 mm diameter laser manufacturing remnant on this diamond showed an interesting pattern.

A 3.59 ct Fancy Light brownish greenish yellow diamond recently submitted to the Carlsbad laboratory for examination displayed an unusual laser feature.

The table of the blocked heart shape showed a laser remnant with an interesting pattern that resembled a watch face (figure 8). Unlike the typically linear remnants, this feature was circular and located directly on the table. The cutter's intentions for placing the 0.9 mm diameter circle on the table are unclear, but it makes for a striking pattern rarely seen on diamonds, especially finished stones.

Tara Allen

Purple JADEITE Rock

The Carlsbad laboratory recently took in a semi-translucent mottled purple bead for identification. Under microscopic examination, the material displayed an aggregate structure composed of fibrous lavender grains with a brownish white component (figure 9). Reddish orange minerals and small needle-like brown crystals were also observed. A spot RI reading of 1.55 was obtained on most of the stone, with a few places giving a reading of 1.66. The bead had a hydrostatic SG of 2.99 and was inert to both long- and short-wave UV radiation.

Basic gemological testing was inconclusive, but Raman spectroscopy performed on the various components of the stone confirmed the lavender and white portions were a mixture of

Figure 9. This 13.60 mm mottled purple bead consists primarily of jadeite and quartz.

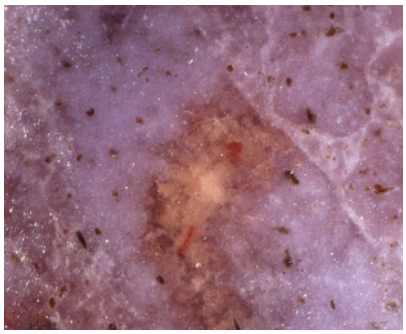

Figure 10. Upon closer examination, the jadeite rock also contains reddish orange cinnabar and brown aegerine crystals. Magnified 30×.

jadeite and quartz, while the reddish orange portions were cinnabar. Additional spots on the scattered needle-like inclusions matched aegerine, a sodic-ferric clinopyroxene (figure 10). In addition to Raman testing, an infrared (FTIR) spectrum was collected to confirm the stone was not polymer-impregnated (E. Fritsch et al., "Identification of bleached and polymer-impregnated jadeite," Fall 1992 *G&G*, pp. 176–187; Spring 1994 Lab Notes, p. 43).

Purple rock containing jadeite and quartz has been reported in the Bursa region of western Turkey (M. Hatipoğlu et al., "Gem-quality Turkish purple jade: Geological and mineralogical characteristics," *Journal of African Earth Sciences*, Vol. 63, 2012, pp. 48–61). To date, the composition of this material is unique to the area. It occurs as a metamorphic product in the contact zone between a large blueschist belt and a granodiorite stock. While neither mercury nor cinnabar (a mercury sulfide) is mentioned in the literature on purple jadeite rock, mercury mining in western Turkey has been reported (M. Yildiz and E.H. Bailey, "Mercury deposits in Turkey," *U.S. Geological Survey Bulletin 1456*, 1978).

The presence of mercury deposits in the region makes it highly likely that cinnabar or other mercury-bearing minerals would occur in the purple jadeite rock, consistent with a Turkish origin, though the origin of this sample has not been confirmed. Because jadeite and aegerine are both sodic pyroxenes, their occurrence together is understandable.

Purplish jadeite rock is being used in the jewelry trade and fashioned into beads, cabochons, and carvings.

Amy Cooper and Tara Allen

A Useful Technique to Confirm the Hydrophane Nature of OPAL

With the emergence of opal production in Wollo, Ethiopia, the supply of hydrophane opal has increased significantly. This deposit offers beautiful material at a fraction of the price of similar-looking opal from several other sources, including Australia and Brazil. However, most of the opal from Wollo is hydrophane, which simply means it is porous enough to readily absorb water, much like a sponge. This property can occasionally cause durability issues that may lead to significant cracking, depending on the porosity of the material and how included it is. In general, it is difficult to predict if this material will crack when immersed, but the potential is certainly higher in hydrophane opal than in nonporous material. In hydrophane opal with a bodycolor other than white, there is the distinct possibility of artificial coloration, since stones that absorb water also absorb dye (N. Renfro and S.F. McClure, "Dyed purple hydrophane opal," Winter 2011 *G&G*, pp. 260–270). While this ability to absorb water is not proof of dye, it calls for extra caution when examining an opal for color modification, especially if it has a bodycolor that can exist naturally, such as orange.

With white or colorless opals, checking for dye is not necessary, but the gemologist may find it valuable to determine if they are hydrophane so the client can be warned to avoid immersing them in liquid. Micro inclusions often present in these stones are sometimes the source of minute internal cracks. When these opals are saturated with water, the cracks often enlarge due to the strain and propagate through the entire stone. In these cases,

Figure 11. This Ethiopian hydrophane opal with a small crack was examined at 15× magnification in reflected light (A). The lighting environment has been changed to direct transmitted light or brightfield illumination by opening the baffle in the microscope well (B). A drop of water placed on the surface (C) and absorbed by the stone creates an optical aberration (D) that confirms the opal's hydrophane nature. Note that the water has also produced a more pronounced optical aberration in the crack.

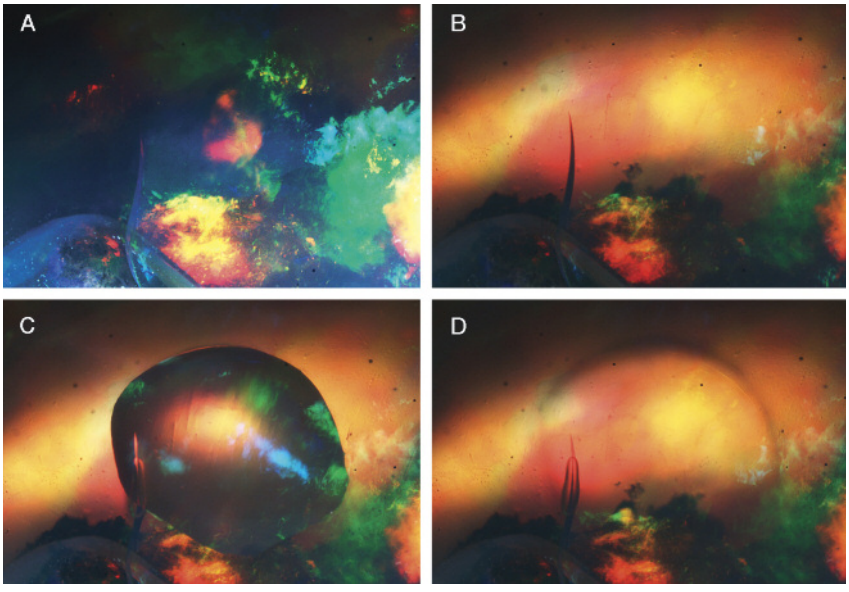

the only option is to recut several small stones from the broken fragments.

To safely determine if an opal is hydrophane and avoid further propagation of existing cracks (figure 11), the stone should be examined using a standard gemological microscope and direct transmitted light (with the microscope in brightfield mode). Simply place a single drop of water on the surface and observe how the water drop interacts with the opal. After a few seconds of allowing the water to either evaporate or soak into the stone, reexamine the appearance. If the water is absorbed into the stone, that area's refractive index will be slightly different, creating an optical aberration where the drop is placed and confirming that the stone is hydrophane. This method poses less risk of breakage than complete immersion.

Nathan Renfro

Green SAPPHIRE Filled with Glass

In recent years, one of the most problematic gem treatments has been the filling of ruby with lead glass, due to its unstable nature. In 2007, a new application for lead glass treatment in corundum began to appear in the market: sapphire filled with cobalt-colored lead glass (T. Leeawatanasuk et al., "Cobalt-doped glass-filled sapphire; an update," *The Australian Gemmologist*, Vol. 25, No. 1, 2013, pp. 14–20).

Figure 12. This 1.83 ct specimen proved to be a manufactured product consisting of lead glass and natural green sapphire.

Figure 13. Flattened gas bubbles and a blue flash effect suggest that this stone contains significant amounts of lead glass, which was confirmed by EDXRF spectroscopy. Field of view 1.57 mm.

Recently examined at the Carlsbad laboratory was a particularly unusual 1.83 ct green sapphire (figure 12) that proved to be filled with a significant amount of lead glass.

Standard gemological testing gave an RI of 1.762–1.770, a hydrostatic SG of 4.00, a prominent absorption band at 450 nm, and inert reaction to long- and short-wave UV. These properties are consistent with natural corundum. Microscopic examination, however, revealed numerous low-relief cracks throughout the stone that showed a prominent blue flash effect, as well as several flattened gas bubbles trapped within the filler (figure 13). Also observed were reflective rutile needles.

To determine if a leaded glass was used to hide the cracks in the corundum, we applied EDXRF spectroscopy, which confirmed the presence of lead. UV-visible spectroscopy was used to explore whether the color was intrinsic to the corundum (as in glass-filled ruby) or intrinsic to the filler glass (as in sapphire filled with a lead glass colored by cobalt). The UV-Vis spectrum revealed a prominent 450 nm series related to Fe^{3+} pairs responsible for the yellow component of the green color, which was consistent with the overall green bodycolor of the stone. The blue component was observed as diffuse planar color zoning unrelated to the network of fractures. This combination of natural yellow and blue components produced the overall green bodycolor.

This was the first lead glass–filled green sapphire examined at the Carlsbad laboratory. On a GIA identification report, this would be called a "manufactured product."

Phil York

Large Pinkish Brown CVD SYNTHETIC DIAMOND

Distinguishing diamonds of natural and synthetic origin is one of the most important tasks of any gemological laboratory. With the advances in technology and methodology available to manufacturers, a wider variety of synthetic diamonds has begun to emerge. Recently, a client submitted a 1.03 ct emerald-cut synthetic diamond (figure 14) to the Carlsbad laboratory. We determined it had been grown from the chemical vapor deposition (CVD) process. This was evident from the large silicon-vacancy peak at 737 nm seen in both the UV-visible and photoluminescence spectra of this type IIa synthetic diamond. A lack of tatami strain and the distinctive growth patterns observed in the DiamondView (see W. Wang et al., "Latest-generation CVD-grown synthetic diamonds from Apollo Diamond Inc." Winter 2007 *G&G*, pp. 294–312) confirmed the origin (figures 15 and 16).

As the vast majority of CVD synthetic diamonds submitted to the lab weigh less than one carat, this sample was unusual for its size, as well as its

Figure 14. This 1.03 ct CVD synthetic is notable for its size and Faint pinkish brown color.

Figure 15. Viewed under crossed polarizers, this synthetic diamond shows mottled strain, but no tatami strain, consistent with its CVD growth origin.

color grade of Faint pinkish brown. This is the first colored CVD synthetic diamond examined by GIA that did not merit a "Fancy" modifier, but instead fell in the Faint to Light range. While pink CVD-grown synthetics have been documented, in most cases the color was generated by post-growth treatment. Here the pinkish color seemed solely related to the growth process, with no subsequent treatments (HPHT annealing, irradiation, and then annealing) coming into play.

Troy Ardon and Sally Eaton-Magaña

TURQUOISE with Fingerprint Pattern

The Carlsbad laboratory recently identified a natural, untreated turquoise bead necklace with an interesting feature. The bluish green beads displayed a natural turquoise structure with thin black matrix veining (figure 17). During microscopic examination, a few of the beads showed a less-saturated greenish discoloration pattern resembling fingerprints. The bead selected for testing had a spot RI of about 1.60 and fluoresced weak bluish green under long-wave UV, with no short-wave fluorescence. To rule out polymer impregnation treatment, we collected an infrared (FTIR) spectrum. It showed no peaks in the polymer regions, ruling out polymer-impregnated turquoise (K.S. Moe et al., "Polymer-impregnated turquoise," Summer 2007 *G&G*, pp. 149–151). The unusual pattern may have been the result of glue or another contaminant present during the initial handling or drilling of the beads, preserving actual human fingerprints. With time and wear, the discoloration of the beads made the fingerprints more distinct (figure 18).

Figure 17. A few of the natural, untreated turquoise beads in this necklace display a fingerprint pattern.

Untreated turquoise is porous and often absorbs skin oils and other contaminants, making the color more greenish. As a result, turquoise is commonly treated to enhance its appearance and protect it from discoloration. Most of the product on the market, especially lower-quality material, has been wax- or polymer-impregnated to improve its durability (S.F. McClure et al., "Gemstone enhancement and its detection in the 2000s," Fall 2010 *G&G*, pp. 218–240).

This interesting piece serves as a useful example of why turquoise is routinely treated. Simply handling it can affect the color and appearance over time, as illustrated by the fingerprint pattern preserved in this piece.

Tara Allen and Amy Cooper

Figure 16. DiamondView imaging remains one of the most reliable methods for confirming a CVD synthetic diamond. This image shows distinctive growth patterns.

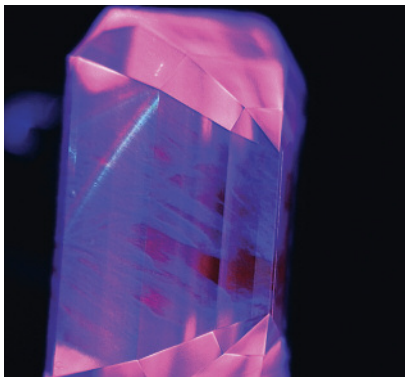

Figure 18. The light area shows a discoloration in the form of a fingerprint pattern.

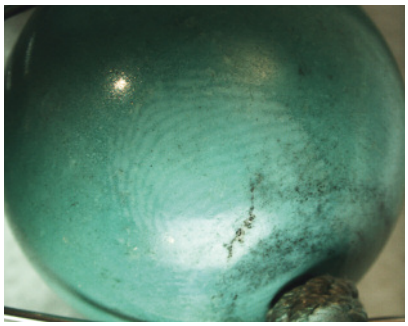

PHOTO CREDITS:
Don Mengason—1, 17; Jian Xin (Jae) Liao—2, 3; Surjit Dillon Wong—4; Robison McMurtry—5, 9, 12, 14; Troy Ardon—8, 15; Nathan Renfro—10, 11, 18; Phil York—13; Sally Eaton-Magaña—16.

G&G
Gem News International

Contributing Editors
Emmanuel Fritsch, *CNRS, Team 6502, Institut des Matériaux Jean Rouxel (IMN), University of Nantes, France* (fritsch@cnrs-imn.fr)
Franck Notari, *GGTL GemLab–GemTechLab, Geneva, Switzerland* (franck.notari@gemtechlab.ch)
Kenneth Scarratt, *GIA, Bangkok, Thailand* (ken.scarratt@gia.edu)

COLORED STONES AND ORGANIC MATERIALS

Unusual epigenetic malachite discs in quartz. When mineral-rich fluids become trapped in open cracks and evaporate, they can leave behind epigenetic mineral precipitates. These epigenetic mineral deposits are fairly common in gem materials, usually taking the form of brownish iron oxide staining in cracks. These deposits are often a nuisance, impairing the potential beauty of the finished gem, but occasionally they contribute vibrant colors with interesting geometric shapes, such as inclusions of pyrite trapped in cracks in quartz.

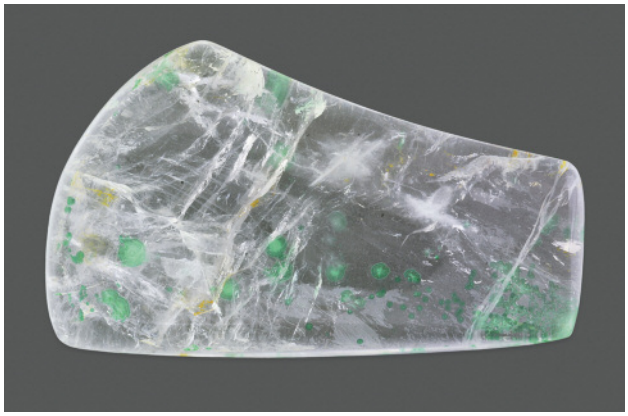

Figure 1. This 52.99 ct freeform cabochon of rock crystal quartz, reportedly from Brazil, contained several epigenetic discs of malachite. Photo by Robison McMurtry.

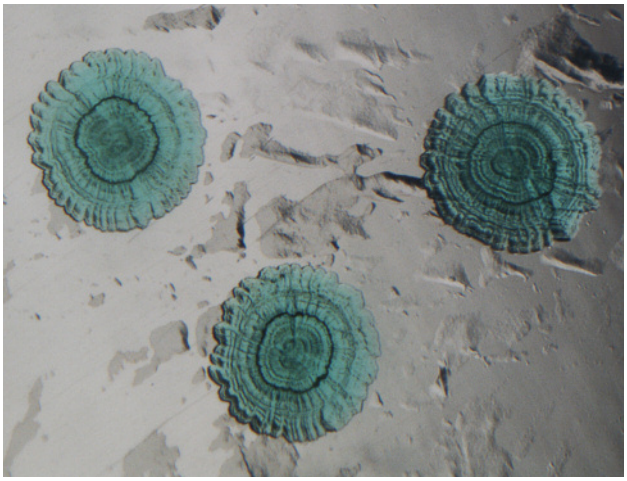

Figure 2. These radial discs of epigenetic malachite were trapped within cracks of rock crystal quartz. Photomicrograph by Nathan Renfro; shadowed illumination, field of view 2.15 mm.

An unusual freeform cabochon of rock crystal quartz (figure 1), obtained from Leonardo Silva Souto (Cosmos Gems, Teófilo Otoni, Brazil) and reportedly of Brazilian origin, was examined at GIA's Carlsbad laboratory. The 52.99 ct stone contained several interesting inclusions of malachite (figure 2). These inclusions were obviously epigenetic, as they were confined within secondary cracks in the quartz host. This planar confinement caused the inclusions to grow outward after nucleating. The flattened discs were particularly interesting due to the vibrant interference colors visible in polarized light (figure 3), as well as their uniform structure. The identification of the inclusions and the host was confirmed by Raman spectroscopy.

Malachite has been previously reported as a syngenetic inclusion in chalcedony and gypsum (e.g., E.J. Gübelin and J.I. Koivula, *Photoatlas of Inclusions in Gemstones*, ABC Edition, Zurich, 1986), but epigenetic malachite in quartz

Editors' note: Interested contributors should send information and illustrations to Justin Hunter at justin.hunter@gia.edu or GIA, The Robert Mouawad Campus, 5345 Armada Drive, Carlsbad, CA 92008.

Gems & Gemology, Vol. 49, No. 3, pp. 178–186,
http://dx.doi.org/10.5741/GEMS.49.3.178.

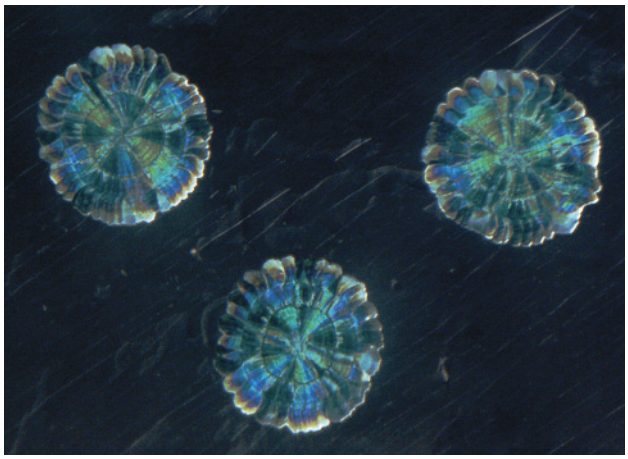

Figure 3. In polarized light, these malachite discs showed vibrant interference colors. Photomicrograph by Nathan Renfro; field of view 2.15 mm.

is rather uncommon. In this stone, the resulting vivid green color is an improvement over the otherwise ordinary, colorless quartz.

Nathan Renfro
GIA, Carlsbad

DIAMOND

Unusual dumbbell-like inclusion in diamond. The French Gemmological Laboratory (LFG) in Paris had the opportunity to grade a 0.40 ct near-colorless round brilliant diamond with a large, unusual inclusion (figure 4). Initial inspection under the loupe showed the internal feature consisted of a thin middle "bar" and two broader appendices (figure 5). Viewed from certain angles, it appeared almost metallic. This feature, which lowered the clarity grade to SI_2, was reminiscent of the metallic dumbbell inclusions observed in HPHT synthetic diamonds.

Figure 4. This 0.40 ct round brilliant diamond displayed a large, unusually shaped inclusion. Photo by Aurélien Delaunay.

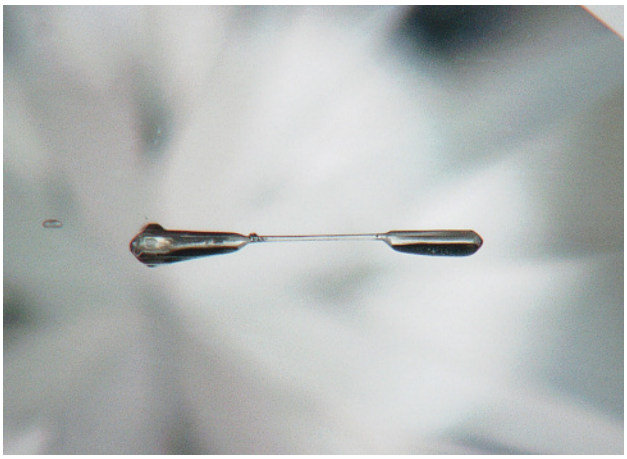

Figure 5. At first inspection, this dumbbell shape was reminiscent of the metallic flux inclusions seen in HPHT synthetic diamond. Photomicrograph by Aurélien Delaunay; magnified 120×.

DiamondView luminescence images demonstrated that the inclusion was crystallographically oriented, parallel to the edge between two octahedral faces (figure 6). Dumbbell inclusions in HPHT synthetics have a clear crystallographic orientation, often along an octahedral edge as well.

But the stone fluoresced weak blue under long-wave UV radiation and was inert in short-wave UV, a classic luminescence behavior for natural diamond and unknown in synthetic specimens. Furthermore, the infrared absorption spectrum was typical of a natural type IaAB diamond with minor hydrogen. This proved the natural origin of both the

Figure 6. DiamondView luminescence images demonstrated the diamond's natural origin, as only traces of octahedral growth were found. The inclusion is crystallographically oriented, parallel to the edge between two octahedral faces, as highlighted by the slightly more inert elongated rectangle beside it. Photomicrograph by Aurélien Delaunay, magnified approximately 60×.

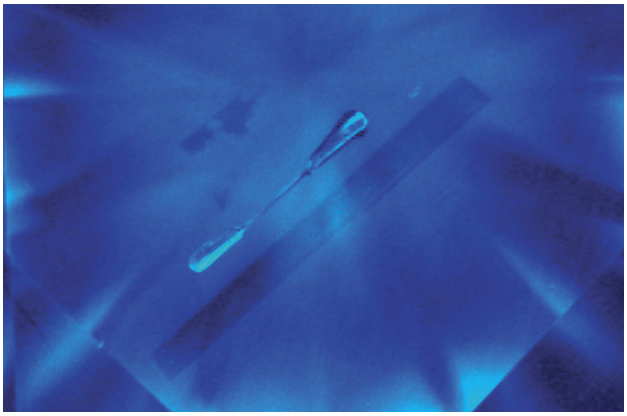

stone and its inclusion. With magnification, the inclusion appeared colorless and transparent rather than metallic and opaque, though with a high optical relief. Its morphology was not cuboctahedral—as with inclusions in synthetic diamond—but rounded octahedral. The exact nature of the crystal remains unknown, as we could not obtain a Raman spectrum due to its intense luminescence, but colorless inclusions in diamonds are often forsterite.

Emmanuel Fritsch
Aurélien Delaunay
French Gemmological Laboratory, Paris

SYNTHETICS AND SIMULANTS

Boron carbide: A new imitation of black diamond. As black diamond has gained popularity in the past few years, so have aggregates of black synthetic moissanite and crystalline silicon (Spring 2011 Lab Notes, pp. 54–55). One specimen received by the Gem Testing Laboratory in Jaipur, a 1.04 ct black submetallic round brilliant (figure 7), appeared to be synthetic black moissanite but proved otherwise. The specimen was presented to the owner as a diamond.

Due to the prevalence of black synthetic moissanite in the marketplace and gem laboratories, we immediately checked for the typical aggregate structure under the microscope. Although a granular pattern was distinctly visible in reflected light (figure 8), it was much denser and finer than the kind usually seen in black synthetic moissanite. This raised uncertainty, so additional gemological tests were performed. The specimen had an over-the-limit RI, an SG of 2.43, and a hardness above 9 on the Mohs scale. The low SG value ruled out the possibility of synthetic moissanite (3.22), but otherwise offered no clues as to the specimen's identity.

Qualitative EDXRF analysis revealed Fe, with traces of Si and K. Raman spectra taken from several points using 532 nm laser excitation showed major peaks at approximately 260, 320, 480, 532, 720, and 1088 cm^{-1}, with smaller peaks at about 800, 824, 874, 967, and 998 cm^{-1} (figure 9). This combination of features did not match anything in our database, but an extensive literature search revealed an exact match with the Raman spectra of boron carbide (V. Domnich et al., "Boron carbide: Structure, properties, and stability under stress," *Journal of the American Ceramic Society*, Vol. 94, No. 11, 2011, pp. 3605–3628, http://dx.doi.org/10.1111/j.1551-2916.2011.04865.x).

Boron carbide is an advanced ceramic material with high hardness, low density, thermal stability, and extreme abrasion resistance, making it suitable for nuclear, military, and aerospace applications. The material is typically produced by reacting and fusing carbon with boric oxide (B_2O_3) in an electric arc furnace, followed by a sintering

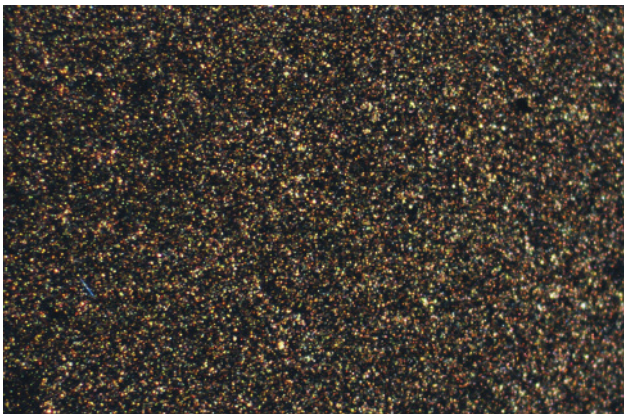

Figure 8. Under reflected light, the boron carbide specimen displayed a dense, fine granular structure typically associated with aggregates such as ceramics. Photomicrograph by Gagan Choudhary; magnified 48×.

Figure 7. This 1.04 ct black submetallic round brilliant, initially represented as diamond, was identified as boron carbide. Photo by Gagan Choudhary.

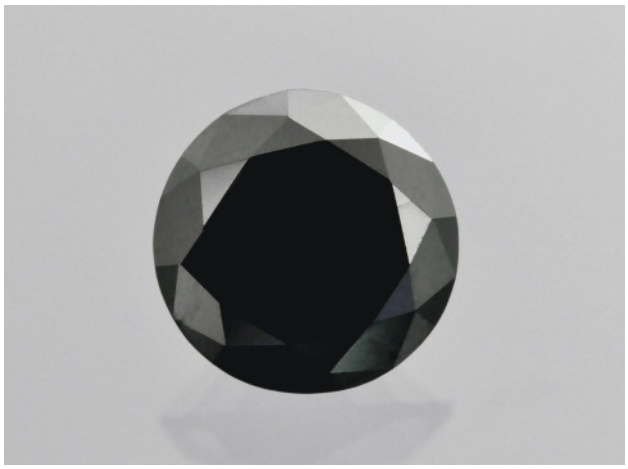

Figure 9. The boron carbide's Raman spectrum showed major peaks at approximately 260, 320, 480, 532, 720, and 1088 cm^{-1}.

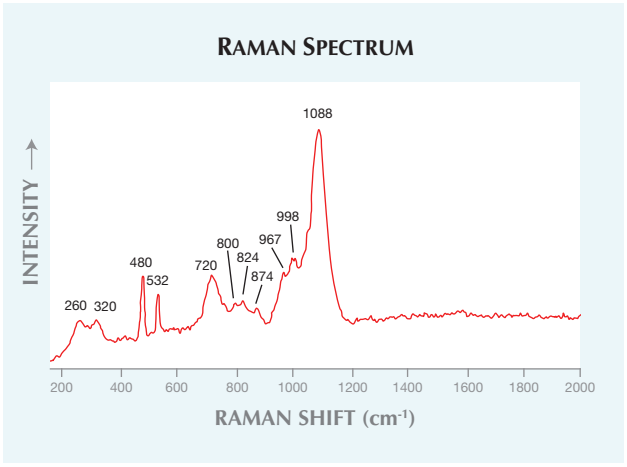

process of hot pressing in graphite dies under a vacuum or argon atmosphere at temperatures of 1900–2200°C and pressures of 0.02–0.04 GPa for 15–45 minutes (Singhal and Singh, "Sintering of boron carbide under high pressures and temperatures," *Indian Journal of Engineering and Materials Sciences*, Vol. 13, April 2006, pp. 129–134).

Although boron carbide is common in engineering and materials science—used as scratch-resistant coating and plating in tank armor, bulletproof vests, and padlocks—this was our first encounter with it as a diamond simulant. Our literature search (by Mr. Sandeep Vijay, a staff gemologist) did not reveal any gemological uses of this ceramic product. Distinguishing boron carbide from black diamond or synthetic moissanite was straightforward on the basis of SG, but Raman spectra and reference data were needed for identification. The possibility of market penetration cannot be ruled out.

Gagan Choudhary (gagan@gjepcindia.com)
Gem Testing Laboratory, Jaipur, India

Amber with insect-bearing filling. We recently tested an interesting strand of Islamic prayer beads resembling amber (figure 10). It consisted of 33 round yellow beads approximately 12 mm in diameter, two oval-shaped separators, and a fancy-shaped link. It was purchased as amber from a dealer at an annual festival in Dubai.

The round beads contained dark brown plant debris and a variety of insects: ants, flies, and spiders, all in good condition. The beads' surfaces also featured noticeable circular zones, and when exposed to long-wave UV radiation, they displayed a weak, blue fluorescence and distinctive chalky blue circular areas (figure 11). The beads were inert to short-wave UV radiation.

These features were similar to those of copal filled with plastic (Winter 2010 GNI, pp. 326–328). We obtained spot RI readings of 1.52 on the circular zones and 1.54 elsewhere. Next, we analyzed the strand using Raman spectroscopy with a 785 nm diode laser. The separator link and the main portion of the beads showed peaks between 1434 and 1644 cm^{-1}, consistent with amber. The circular areas' strong bands at 623, 807, 1100, and 1599 cm^{-1} were consistent with epoxy resin (figure 12).

Microscopic examination with immersion in water indicated that all the round beads had been cored and filled (figure 13). The beads were identified as amber filled with colorless to light yellow plastic to imitate insect-bearing amber.

Sutas Singbamroong (sssutas@dm.gov.ae),
Nazar Ahmed, and Hassan Al Marzooqi
Gemstone Unit, Dubai Central Laboratory
Dubai, United Arab Emirates

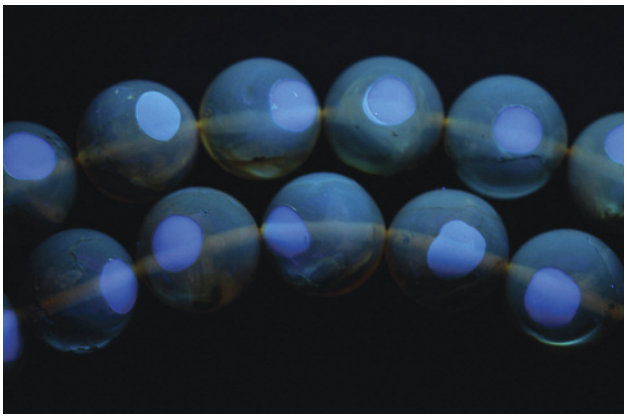

Figure 11. When exposed to long-wave UV radiation, these beads displayed weak blue fluorescence and distinct, chalky blue circular areas. Photo by Sutas Singbamroong.

Figure 10. The beads in this strand of prayer beads measure approximately 12 mm in diameter. Photo by Sutas Singbamroong.

Figure 12. Raman spectra collected from the main portion of the beads were consistent with amber, whereas the circular areas indicated an epoxy resin.

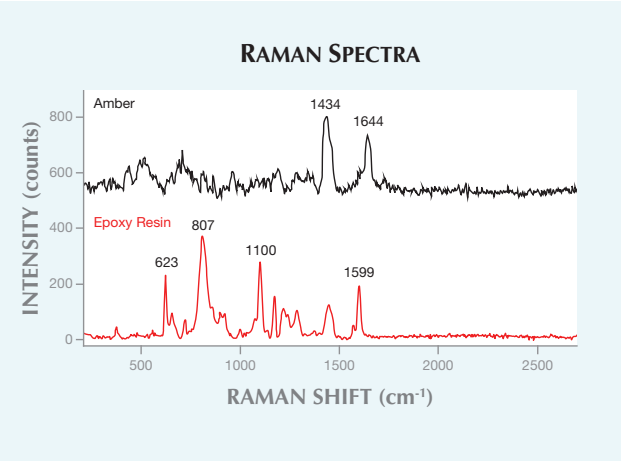

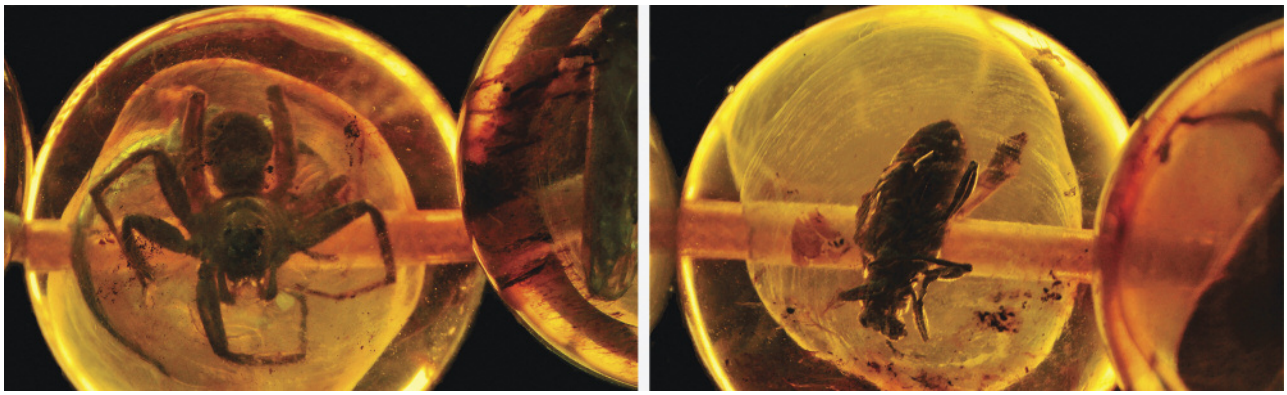

Figure 13. Microscopic observation with immersion in water clearly indicated that these amber beads had been cored and filled with a colorless to light yellow plastic containing insects. Photomicrographs by Sutas Singbamroong; magnified approximately 10×.

Phosphorescence in synthetic sapphire. A 4.89 ct colorless oval mixed-cut specimen was submitted as a sapphire to the Gem Testing Laboratory at the Indian Gemological Institute in Delhi for identification (figure 14). Standard gemological examination gave an RI of 1.760–1.768, with a uniaxial negative optic sign and a birefringence of 0.008, as well as a hydrostatic SG of 4.00. These properties were consistent with sapphire. While this specimen was eventually proven to be synthetic, its unusual characteristics—a lack of curved growth banding visible in the DTC DiamondView and very rare phosphorescence—called for instrumentation generally used in diamond identification.

Magnification showed what appeared to be long needles near the girdle, but closer examination revealed they were long cracks (figure 15). Rather than the Plato lines generally found in light-colored flame-fusion synthetic sapphires, the sample displayed two sharp planes under crossed polarizers. These planes, which had a noticeable separation in between, were visible in twinning lamellae position. Small stress knots near the table surface—but no physical inclusions—were also visible under crossed polarizers (figure 16). Such cracks, which are generally found on the surface of synthetic sapphire, may be due to stress during crystal growth.

The sample was inert to long-wave UV radiation but showed a chalky blue fluorescence in short-wave UV, a common feature of synthetic sapphires. It also produced 30 seconds of phosphorescence—the first time this contributor has observed phosphorescence in sapphire, natural or synthetic. Examination in the DiamondView also showed an uncommon blue phosphorescence (figure 17), but it did not show curved growth banding—a fluorescence pattern normally seen in synthetic sapphire grown by the flame-fusion process.

Identification could only be made on the basis of short-wave UV transmission analysis using the SSEF Diamond Spotter. When the instrument was switched on, short-wave UV radiation transmitted through the sample and the green dot glowed. The specimen's transparency under the Diamond Spotter's short-wave emission at 254 nm proved its synthetic origin, as natural sapphire does not transmit short-wave UV below 288 nm (S. Elen and E. Fritsch, "The

Figure 14. This 4.89 ct colorless synthetic sapphire was presented as a sapphire. Photo by Meenakshi Chauhan.

Figure 15. These fine, linear cracks near the girdle resemble long needles. Photomicrograph by Meenakshi Chauhan; magnified 40×.

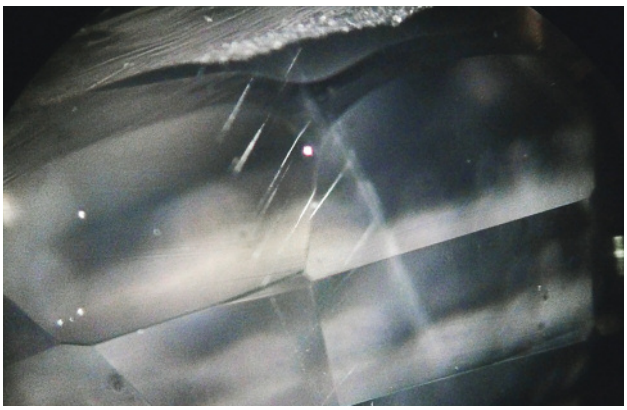

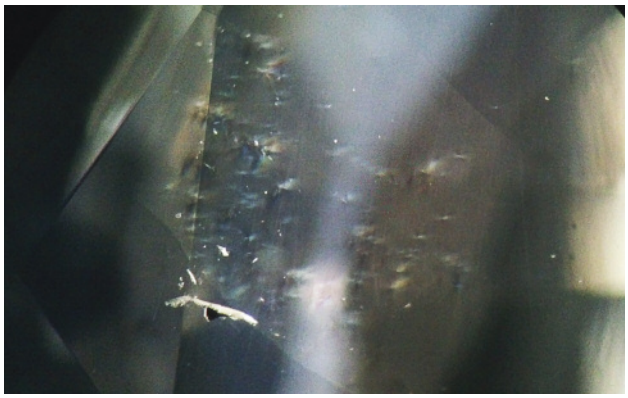

Figure 16. These small stress points, visible on the table between crossed polarizers, were confined to a small space. Photomicrograph by Meenakshi Chauhan; magnified 30×.

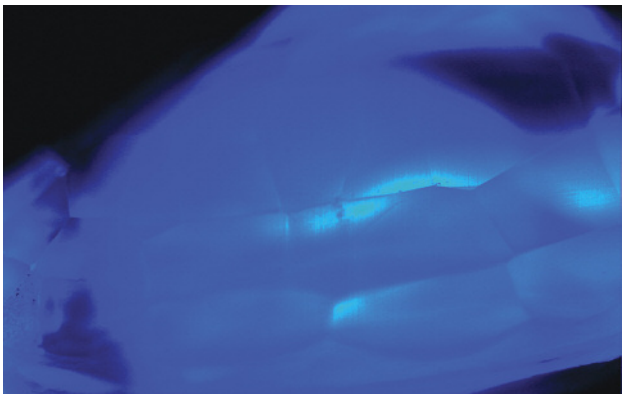

Figure 17. The colorless sample showed blue phosphorescence in the DiamondView, evidence of its synthetic origin. Image by Meenakshi Chauhan.

separation of natural from synthetic colorless sapphire," Spring 1999 *G&G*, pp. 30–41, http://dx.doi.org/10.5741/GEMS.35.1.30).

Despite the confirmation of synthetic origin, no conclusion could be made regarding the synthesis process used. Consistent with specimens grown by the Czochralski pulling method, there were no curved color bands, inclusions, or Plato lines. Conversely, the specimen's chalky blue fluorescence and twinning are indicative of flame-fusion growth. These findings present the possibility of either (1) a synthesis process not yet explored by the gemological community or (2) growth by a known process, but with near perfection. While the DiamondView and Diamond Spotter were developed to analyze diamonds, they can also play a vital role in identifying other gemstones.

Meenakshi Chauhan
Indian Gemological Institute Gem Testing Laboratory
Delhi, India

Unusual faceted massive fuchsite. French gem dealer Patrick de Koenigswarter (MinerK) recently showed us some interesting material he purchased in 2011 from an Ethiopian rough dealer. At the time of purchase, the green rough (figure 18) was presented to him as emerald from a new find near the Kenticha pegmatite zone in Ethiopia, well known for tantalite and superb amazonite crystals. However, beryl was ruled out due to the material's waxy luster and low hardness of 3 or less on the Mohs scale—it was easily scratched with a copper coin.

Routine gemological testing was done on the four samples, which consisted of three rough pieces (17–138 ct) and a 2.56 ct emerald cut. The faceted stone (figure 18, bottom right) always remained lit under crossed polarizers, indicating a polycrystalline structure. The color was unevenly distributed, from light green to intense green, sometimes close to an emerald color. The refractive index, though difficult to measure, was around 1.60. The specific gravity values were 2.80 for two of the pieces and 2.90 for the others, a difference possibly due to the presence of mineral inclusions. All four pieces were inert under both long- and short-wave UV, and red to pink under a Chelsea filter. Additional analyses were required to properly identify this material.

Qualitative and quantitative analyses were performed with a JEOL-5800LV scanning electron microscope (SEM) equipped with a PGT (Princeton Gamma Tech) energy dispersive IMIX-PTS detector. The following elements were found (in atomic %): Si = 16.1%, Al = 17.0%, K = 4.0%, and Na = 1.3%; O was calculated as 61.0%, plus traces of Ba (0.3%), Fe, and Cr. These last two elements were clearly detected on the spectrum but in concentrations too low to be measured (below 0.1%). This composition is consistent with muscovite, a member of the mica family. We ob-

Figure 18. This massive Cr-muscovite, reportedly from southern Ethiopia, is better known in the trade as fuchsite. The longest rough piece measures 53 mm, and the faceted stone weighs 2.56 ct. The material was difficult to polish because of its low hardness, 3 or less on the Mohs scale. Photo by Thierry Pradat.

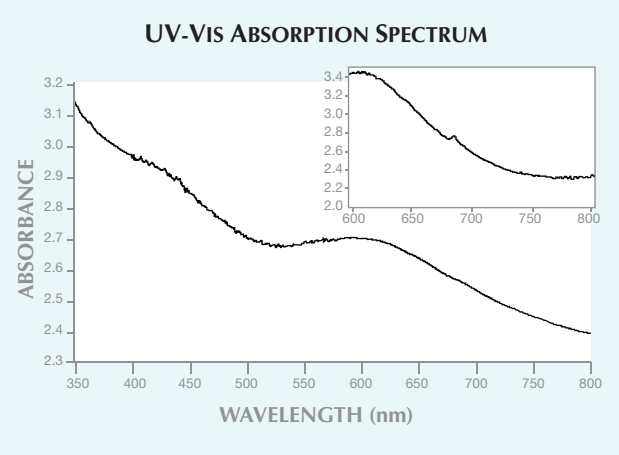

Figure 19. The UV-visible spectrum of the Ethiopian fuchsite shows a large absorption band around 600 nm, a continuum of increasing absorption toward the UV, and a weak, sharp peak at 682 nm. These features are consistent with green color produced by trivalent chromium.

served platy brown polyhedral inclusions, identified by EDS and Raman as rutile due to telltale broad bands around 611 and 443 cm^{-1}.

We also performed UV-visible absorption spectrometry using a 1 nm sampling and spectral bandwidth in the 350–800 nm range. The spectrum showed a large band centered at about 600 nm and a continuum of increasing absorption toward the UV region (figure 19). These features generated two transmission windows, one in the green around 530 nm and the other in the red to infrared. This explains both the green bodycolor and the red appearance in the Chelsea filter. The continuum is caused by the scattering of light at grain boundaries in this polycrystalline aggregate. We also observed a weak but sharp peak at 682 nm, which we attributed to "chromium lines" of the trivalent chromium (figure 19, inset).

Chemical and spectroscopic results identified Cr^{3+} as the main cause of the green color. Hence, this material was fuchsite, the chromian variety of muscovite. To the best of our knowledge, this is the first time such a massive, translucent polycrystalline fuchsite has been faceted. The gem's low hardness makes it unsuitable for jewelry, but it is adequate for collectors.

Figure 20. This 444 g dark violetish blue carving of Lord Mahaveera, submitted as sapphire, was identified as corundum coated with a blue polymer. Photo by Gagan Choudhary.

Thierry Pradat
Gems Plus, Francheville, France
Benjamin Rondeau
University of Nantes
Emmanuel Fritsch

TREATMENTS

Corundum carving coated with colored polymer. Coating, one of the traditional forms of enhancement, is still widely used on a number of gem materials. This contributor alone has reported on recent examples (e.g., Spring 2011 GNI, pp. 71–72; Summer 2012 GNI, pp. 154–155). The latest is a dark violetish blue carving of the early Jain spiritual leader Lord Mahaveera, submitted as sapphire (figure 20), that turned out

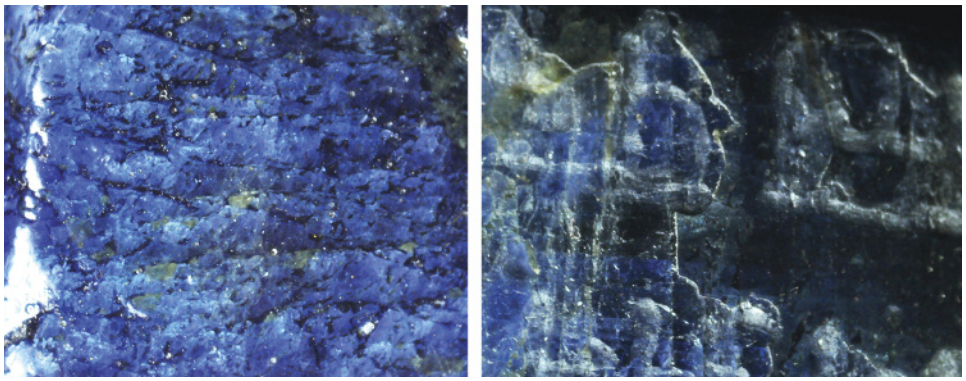

Figure 21. Color concentrations within cavities, large fractures, and twinning planes (left) confirmed the presence of a dye. The chipped layer of blue polymer (right) indicates a coating; this polymer layer was easily indented by a metal pin. Photomicrographs by Gagan Choudhary; magnified approximately 20×.

Figure 22. These fire opals, a 14.49 ct cabochon (left) and a 1.09 ct cushion cut (right), are shown prior to immersion in plain water at room temperature. Note the natural-looking color. Photos by Larry Tai-An Lai.

to be corundum coated with a blue colored polymer.

The 444 g opaque carving measured 10.00 × 8.00 × 4.50 cm. Although it had the heft of sapphire, its dull, vitreous to waxy luster (again, see figure 20) raised doubts. Examination from different directions using a fiber-optic light revealed substantial color variation in different parts of the carving; some areas appeared pale blue, others dark violetish blue. This patchy, concentrated color variation is associated with dyes. Parallel whitish crisscross lines were also observed, consistent with the twinning planes associated with corundum. Further microscopic observation revealed color concentrations within cavities, large fractures, and twinning planes, confirming the material had been dyed (figure 21, left). Finer fractures appeared whitish, however. When the carving was rotated, some areas also displayed a chipped bluish layer on the surface (figure 21, right), an attribute typically found in coated materials. This layer was easily indented with a metal pin, suggesting the presence of a polymer. In addition to these features, the carving possessed a granular texture in many places, as commonly seen in rocks. These grains were also identified as corundum on the basis of the crisscross pattern of their twinning planes, which is consistent with corundum.

Under UV light (long- and short-wave), the carving displayed patchy white and chalky green fluorescence, mainly on the surface. A desk-model spectroscope revealed weak absorptions at 540, 610, and 640 nm, confirmed with UV-Vis-NIR spectroscopy. Such bands are associated with cobalt-based dyes. RI and SG could not be measured because of the piece's large size, though visual features were sufficient to identify the carving as corundum.

Gagan Choudhary (gagan@gjepcindia.com)
Gem Testing Laboratory, Jaipur, India

Water immersion revealing dye in fire opal. Opal is often treated to enhance its play-of-color or improve its durability. Dye or impregnation methods in particular are easily applied to opals and other porous amorphous materials. A recent article on treated hydrophane opal (N. Renfro and S. McClure, "Dyed purple hydrophane opal," Winter 2011 *G&G*, pp. 260–270) noted that we could expect to see more of this material. Two years later, this appears to be the case.

The Lai Tai-An Gem Lab in Taipei received two fire opals from a local dealer for identification: a 14.49 ct oval cabochon (23.80 × 15.27 × 9.12 mm; figure 22, left) and a 1.09 ct cushion cut (7.67 × 7.64 × 4.67 mm; figure 22, right),

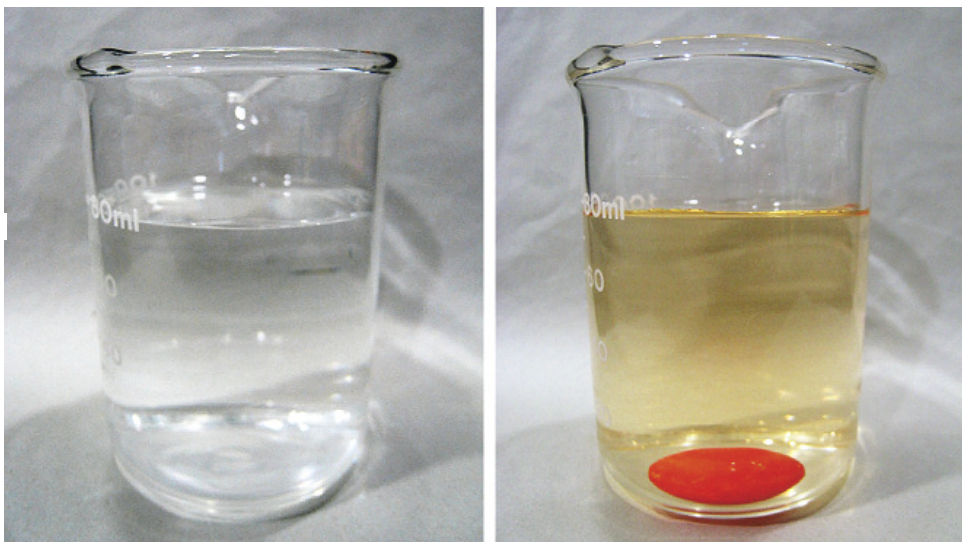

Figure 23. The clear water in this glass beaker (left) turned orange after soaking the fire opal cabochon overnight at room temperature (right). The obvious water discoloration proves the sample was dyed. Photos by Larry Tai-An Lai.

Figure 24. After removal from the water, this cabochon exhibited an obvious loss of color, indicating dye treatment. Photo by Larry Tai-An Lai.

both with pronounced play-of-color. Both gave RI readings of about 1.45. Observation with a gemological microscope and analysis with an FTIR/Raman spectrometer revealed the structure expected for natural opals. Orange color concentrations around some surface pits were also observed, indicating treatment.

But the most obvious clue was the effect caused by immersing the cabochon in water at room temperature overnight (figure 23). The water took on an orange tint, proving that the dye applied to these stones was water soluble, unlike the dye examined by Renfro and McClure (2011). The cabochon itself showed considerably less color after it was removed from the water (figure 24). This simple result reinforces the need for caution when buying fire opals, even ones with a natural-looking color. The change in color would come as a shock to any client unfortunate enough to purchase this dyed material without suitable disclosure.

Larry Tai-An Lai
Lai Tai-An Gem Laboratory, Taipei

CONFERENCE REPORTS

June 2013 Hong Kong Jewellery & Gem Fair. The former British colony of Hong Kong, now a Special Administrative Region of the People's Republic of China, is one of the world's top ten importers and exporters. Almost half of Hong Kong's trade is with mainland China, which makes it a very attractive site for global gem and jewelry trade shows. The fact that it is a free trade port with no tariffs and minimal licensing also draws suppliers and buyers. Alongside Las Vegas and Basel, Switzerland, Hong Kong's gem and jewelry shows rank among the world's most important in terms of size, trading, and industry trendsetting.

Three main Hong Kong shows are held every year, in March, June, and September. The September show is the largest, with two venues needed to accommodate all the exhibitors. The June and September events are organized by UBM, a global communications and marketing firm. This year's June show, the 26th annual Hong Kong Jewellery & Gem Fair, was held at the Hong Kong Convention and Exhibition Center (HKCEC), concurrently with Asia's Fashion Jewellery and Accessories Fair. It featured several themed pavilions, including diamonds, colored stones, jadeite, pearls, fine jewelry, antique jewelry, design, and manufacturing tools.

Approximately 40,000 buyers attended the June show, a figure that typically reaches 60,000 for the September event. While the buyers represented a truly international mix, the percentage from China has consistently increased. As the country's wealth continues to soar, the emergence of a consumer economy has led to strong gains in gemstone and jewelry purchases. As Chinese consumers become more sophisticated, they are demanding higher-quality diamonds, gemstones, and jewelry.

Western designs and brands are also popular in China, which has created opportunities for international suppliers, including diamond dealers and gold jewelry manufacturers. China is the world's largest buyer of gold. With its free trade policies, geographic location, and tradition as a gateway to China, Hong Kong is poised to remain Asia's largest trading hub for fine jewelry, as well as a top destination for international suppliers and buyers.

Tao Hsu and Andy Lucas
GIA, Carlsbad